# Modelling carbon uptake of Australian evergreen ecosystems under rising $CO_2$ concentration and water limitation

By

**Jinyan Yang**

A thesis submitted in fulfilment of the requirements for the degree of Doctor of Philosophy

**December 2018**

WESTERN SYDNEY UNIVERSITY

Hawkesbury Institute for the Environment

**For Shixin Yang, my grandfather,**

**from whom I found inspiration and courage.**

# Acknowledgements

I would like to thank my parents, Ning Yang and Haiying Li for their support over my persuasion of a career in science and their sacrifice of allowing the only child to study abroad for nearly ten years. Their dedication and kindness beyond the responsibility of parents have been leading me forward.

This work would have never been possible without my wife, Yang Li, who accompanied me through the hard periods of life. She always shows me love and courage, and gives me strength and reason to continue.

I deeply appreciate the mentoring of my supervisors Prof. Belinda Medlyn and Dr. Martin De Kauwe. They shared their knowledge and wisdom with patience but no reserve. I am also grateful for the advice and support from my previous supervisor Dr. Remko Duursma.

This thesis uses data collected by many researchers from Hawkesbury Institute for the Environment. I thank them for their kindness of sharing the data. I am also thankful to the administrative and technical staff who created an enjoyable working environment.

# Declaration of Authenticity

The work presented in this thesis is, to the best of my knowledge and belief, original except as acknowledged in the text. I hereby declare that I have not submitted this material, either in full or in part, for a degree at this or any other institution.

# Table of Contents

# List of Figures

# List of Tables

**Abstract**

The current rise in the atmospheric $CO_2$ concentration ($C_a$) provides both challenges and opportunities to terrestrial plant communities. Higher $C_a$ provides a benefit to plants by allowing them to achieve higher photosynthetic rates at lower stomatal conductance ($g_s$). On the other hand, the negative impact of rising $C_a$ is global warming. Rising temperatures directly affect plants but also increase the dryness (vapour pressure deficit, $D$) of the air. Higher $D$ could reduce $g_s$ and thus photosynthesis, leading to a loss of plant fitness. Terrestrial vegetation models can be used to quantify the combined impact of these environmental changes but need to be evaluated for their performance against observations.

This thesis focuses on evaluating $C_a$ responses of Australian ecosystems, which feature evergreen trees adapted to frequent water deficits. In the following chapters, I focus on three major components of terrestrial vegetation models: leaf area index (LAI); the response of $g_s$ to $D$; and the response of $g_s$ and photosynthesis to elevated $C_a$. These three components are particularly important for the modelling of rising $C_a$ because the leaf scale response is captured by the responses of $g_s$ and photosynthesis to water deficit and $C_a$, while LAI is particularly important for the up-scaling of leaf level carbon and water fluxes to the whole ecosystem. Improvements in these components are thus likely to reduce the uncertainties in current terrestrial vegetation models.

In Chapter 2, I test the concept of ecohydrological equilibrium for its ability to predict key traits of Australian evergreen ecosystems. This theory posits that long-term equilibrium LAI ($L_{equ}$) is determined by water availability. The predicted LAI values and the response to $C_a$ both compared well to those of satellite-derived data. These results indicate that $L_{equ}$ could be a useful alternative to satellite-derived data to terrestrial vegetation models to guide foliage carbon allocation.

In the second research chapter (Chapter 3), I compared existing $g_s$ models and commonly used assumptions (i.e., hydraulic and non-stomatal limitations) for their ability to predict leaf and canopy-scale carbon and water fluxes under high $D$. I found that incorporating an empirical non-stomatal limitation of apparent photosynthetic capacity with increasing $D$ improved model performance against data and outperformed models incorporating hydraulic limitation . The results suggest that future models should consider non-stomatal limitations to photosynthesis, especially in high-$D$ environments.

The Chapter 4 of this thesis aimed to determine the gross primary productivity (GPP) under ambient and elevated $C_a$ (+38%; 150 µmol mol$^{-1}$) at the *Eucalyptus* Free Air $CO_2$ Enrichment (EucFACE) experiment. I parameterised the process-based model, MAESTRA, with a suite of *in situ* measurements of canopy structure and plant physiology shared with me by the EucFACE scientific community. I also conducted an attribution analysis to explore the determinants of the response of GPP to elevated $C_a$. My findings indicate a relatively small elevated $C_a$ response of GPP (+8%) in the evergreen woodland. My results are key to understanding the response of this ecosystem to elevated $C_a$.

In summary, the findings from this thesis provide some key insights into current gaps in the modelling of terrestrial vegetation. The results show viable options to improve the leaf gas exchange and LAI submodels that are used by terrestrial vegetation models. Overall, this thesis suggests ways for future terrestrial vegetation models to address these gaps for more realistic predictions under changing climate and rising $C_a$.

## Chapter 1. Introduction

### 1.1 Climate change in Australia

The climate to which Australian plants are adapted is under change. The atmospheric carbon dioxide concentration ($C_a$) has increased significantly since the beginning of the industrial era (Joos and Spahni, 2008) and is projected to increase by 1.5-8 (μmol $mol^{-1}$ $yr^{-1}$) in future (IPCC, 2014). Although this increase in $C_a$ could potentially stimulate plant growth (Swann et al., 2016; Roy et al., 2016), the benefit could be offset by the accompanied increase in temperature. Since 1910, Australia's climate has warmed by around 1°C and is further projected to increase by 2.8–5.1°C by 2090 (Representative Concentration Pathways 8.5; Dey et al., 2019). Since temperature controls the saturating vapour pressure via the Clausius-Clapeyron relationship, a change of temperature translates into a change in *D* with constant actual vapour pressure. The increase in *D* thus might result in increase of atmospheric demand of water which is already much higher than the supply (precipitation) in most regions in Australia (Figure 1.1). The mean annual temperature is predicted to increase by 0.5-5 ºC by 2090 resulting in an increase of potential evapotranspiration by up to 18% (IPCC, 2014).

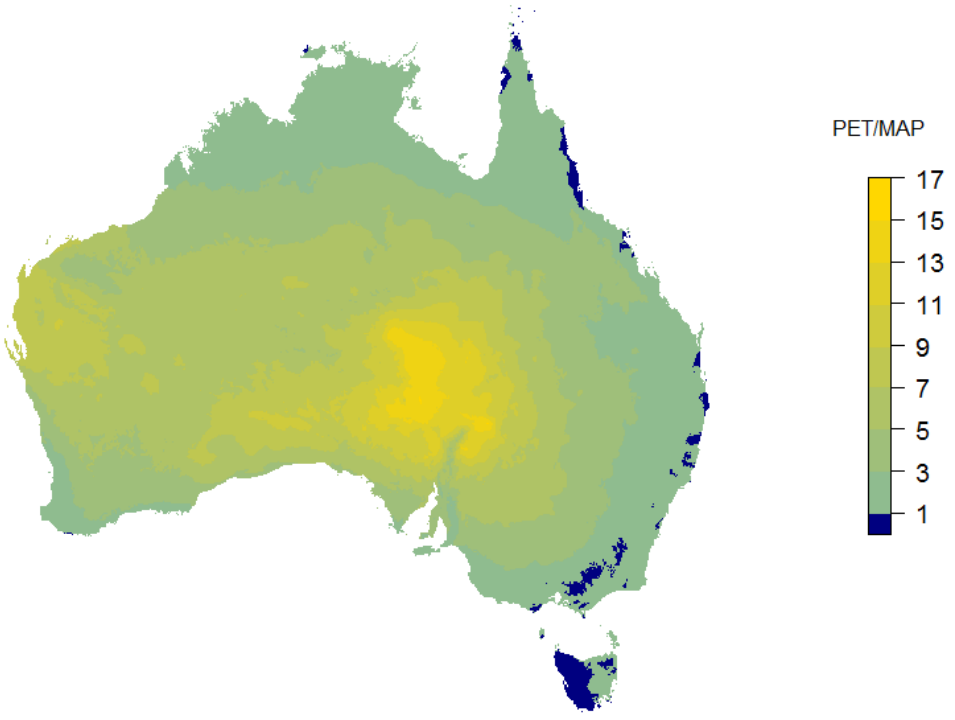


*Figure 1.1. The aridity of Australia shown as the ratio of potential evapotranspiration (PET) to mean annual precipitation (MAP). Data obtained from eMAST (Ecosystem Modelling and*

*Scaling Infrastructure; Whitley et al., 2014) from 1991 to 2011. Only the regions coloured in blue have MAP higher than PET.*

Rainfall over Australia shows large spatial and temporal variation (Smith, 2004; Nicholls, 2006; Risbey, 2011; Dey et al., 2019). In southwest Australia, annual rainfall has been reduced by 17% since the 1960's, with most of the reduction in winter (Smith, 2004; Timbal, 2004). A similar but weaker trend has also been reported in central and eastern Australia (Smith 2004; Risbey, 2011). The only region experiencing an increase in mean annual rainfall is northwest Australia, where rainfall has mainly increased during the summer (the wet season). Projections of future rainfall in Australian remain uncertain (CSIRO and Bureau of Meteorology, 2015; Dey et al., 2019). However, even if rainfall does not decrease in the future, the increase of temperature alone would pose challenges for plants in Australia.

### 1.2 Observed ecosystem responses to climate change

The increase in *D* and variable rainfall expose plants to water scarcity (increasing aridity and/or more frequent drought). Water scarcity has been identified as a major cause of loss of ecosystem productivity (Phillips et al., 2009; Wright et al., 2013; Huang et al., 2016; Humphrey et al., 2018) and even mortality globally (Allen et al, 2010; Choat et al., 2012; Choat et al., 2018). Within Australia, a recent drought in southeast Australia (i.e., the 'Millennium Drought' during 2001–2009) reduced the crop yield by ~20% (van Dijk et al., 2013). Ma et al. (2016) analysed the satellite-based enhanced vegetation index and showed that the carbon uptake declined with decreasing precipitation in semi-arid Australia. At the moment of writing this thesis, Australia, particularly Queensland and New South Wales, are going through one of the worst droughts on record (High resolution monthly and multi-monthly rainfall gridded datasets from 1900 onwards; Bureau of Meteorology).

The impacts of water scarcity, on the other hand, might be mitigated by higher $C_a$ (Swann et al., 2016; Roy et al., 2016). Increasing $C_a$ enhances plant water use efficiency (WUE; i.e., carbon gain per unit water loss) due to the stimulation of photosynthesis (Kimball et al. 1993) and the reduction of stomatal conductance (Morison, 1985). Data from tree rings and decadal-scale eddy-covariance studies show a consistent increase of WUE that has been attributed to rising $C_a$ (Peñuelas et al., 2011; Knauer et al., 2017). Satellite-based Earth Observation data are also available for a sufficiently long period to allow analysis of trends over time. Since 1980s there has been a general greening trend over most parts of the world

(Zhu et al., 2016; Yang et al., 2016) as well as Australia (Donohue et al., 2009), indicating a potential increase of leaf area index (LAI; single-sided leaf area per unit ground; $m^2$ $m^{-2}$). These findings indicate that, under high $C_a$, plants may reduce water use per unit leaf area in exchange for a higher LAI. Indeed, Ukkola et al. (2015) show that plants in dry regions increased LAI during 1982 to 2010 based on satellite-derived vegetation index and ground-based evapotranspiration measurements from 190 river basins in Australia. Increasing water scarcity and $C_a$ thus have opposing effects on plants and need to be modelled to better understand how their effects will combine to determine plant behaviour under future conditions.

The size of the atmospheric carbon stock is the result of the global carbon cycle as well as anthropogenic emissions. Future $C_a$ will be determined by the release of carbon from sources and the uptake by sinks. Terrestrial vegetation is a key component of the global carbon cycle. It contributed to a carbon sink of 2.5 PgC $yr^{-1}$ (Pan et al., 2011) compared to an ocean sink of 2.2 PgC $yr^{-1}$ and an anthropogenic source of -8.7 Pg C yr−1 (Le Quéré et al., 2017). Moreover, large temporal and spatial fluctuations (up to 4 PgC $yr^{-1}$) have been observed in the land carbon sink and attributed to changes in plant productivity (Battle et al., 2000; Schimel et al., 2001). The semi-arid region covering most of Australia has a profound influence on the inter-annual variability of terrestrial carbon sink (Ahlstrom et al. 2015). Predicting the productivity of terrestrial vegetation is important not only to examine the health of the plants but also to forecast future $C_a$, because of the interactions between plant productivity and $C_a$. The net impact of rising $C_a$ thus depends on the magnitude of increase of $C_a$ as well as the response of terrestrial vegetation.

### 1.3 Field studies of ecosystems under future conditions

Pioneering studies using open-top chambers to expose whole trees to elevated $C_a$ reported a stimulation of photosynthesis of up to 51% (Eamus and Jarvis, 1989; Curtis and Wang 1998; Saxe et al. 1998; Medlyn et al., 1999). Later, Free Air Carbon Enrichment (FACE) was applied to explore the response of whole ecosystems to elevated $C_a$ under field conditions around the world. It has been shown that, on average, an increase of $C_a$ from 360 to 560 μmol $mol^{-1}$ results in a 22% reduction in stomatal conductance ($g_s$) and a 31% increase in photosynthesis (Norby et al., 1999; Ainsworth and Rogers, 2007; Norby and Zak, 2011). However, the responses of $g_s$ and photosynthesis to $C_a$ vary among plant functional types.

The effect of rising $C_a$ also depends on water limitation. However, plants respond differently to air and soil dryness. Eamus et al. (1995) showed that photosynthesis and its response to elevated $C_a$ were insensitive to $D$ in *Eucalyptus tetrodonta* saplings. Ainsworth and Rogers (2007) reported that the combined impact of dry soil and high $D$ tended to diminish the $C_a$ effect. Dry soil alone may also have a large impact on plant responses to $C_a$. The response of desert shrubs to elevated $C_a$ was only observable during wet periods (Hamerlynck et al., 2002; Naumburg et al., 2003). Duan et al. (2014) showed that the benefits of rising $C_a$ did not ameliorate drought-induced mortality in *Eucalyptus* seedlings. Kelly et al. (2015) reported that the plants reduced LAI but maintained $g_s$ under prolonged drought and that elevated $C_a$ reduced the impact of drought. The impact of water limitation on the plant responses to elevated $C_a$ might be large and might vary with species and environments. These observations pose challenges to our knowledge of plant response to rising $C_a$ under changing climate. It is thus important to test whether current theories and models can explain and capture the observed response of LAI and leaf gas exchange to increasing dryness and $C_a$.

### 1.4 Terrestrial biosphere models (TBMs)

TBMs are numerical representations of terrestrial vegetation function. TBMs all use environmental and physiological data to predict carbon, water, energy, and nutrient fluxes but early TBMs started with separate developments for different purposes. There are land surface models, which focus on the water and energy balance of the atmosphere-soil system with plants being a constant modifier (e.g., Bonan, 1995). However, these models ignore the impact of the change of vegetation under varying environments. On the other hand, terrestrial biogeochemistry models (e.g., Parton et al., 1993; Foley, 1994) focus on the flow of carbon and nutrients between plants and soil. These models do not allow feedbacks between vegetation and atmosphere. To address these issue, dynamic global vegetation models were proposed (e.g., Foley et al. 1996). This newer thread of models incorporates both atmosphere-plant-soil feedbacks and dynamic vegetation distribution constrained by the environment. More recent model developments have assimilated the strength of the previous approaches and diminished the differences among the types of models (e.g., LPJ in Sitch et al., 2003; CABLE in Kowalczyk et al., 2006; DAYCENT in Parton et al., 2010).

The atmosphere-plant-soil feedback in TBMs plays a key role in forecasting the trajectories of future climate, $C_a$, and vegetation productivity (e.g., Cox et al., 2000; Pitman, 2003; Scholze et al., 2006; IPCC, 2014). However, evaluations of TBMs show that there are still large uncertainties in their predictions. Arora et al. (2013) reported large differences in the

predicted response of terrestrial carbon budget to rising $C_a$ in the models in CMIP5 (phase 5 of the Coupled Model Intercomparison Project). Piao et al. (2013) evaluated 10 TBMs and showed models being overly sensitive to $C_a$ and rainfall. Zaehle et al. (2014) compared 11 TBMs with data from two FACE sites and illustrated a large discrepancy in the predicted productivity and its response to elevated $C_a$ among the models. This result is supported by Medlyn et al. (2016) who applied the same evaluation to a FACE site in Australia. The discrepancy can be attributed to the differences in the formulation of key processes in TBMs: the photosynthesis and stomatal conductance models (Medlyn et al., 2016); the scaling from leaf gas exchange to canopy (Jarvis, 1995); the carbon allocation to leaf (Li et al., 2018); and the impacts of dry air (De Kauwe et al., 2015) and soil (Zhou et al., 2013; Drake et al., 2017) on plants.

### 1.5 Identified gaps

I identified three major gaps where models currently do not represent $C_a$ and dryness effects well. Although this thesis focused on Australian ecosystems, existing evidence across the world suggest that these gaps apply to other continents and ecosystems. First, there is a large divergence between the predicted leaf area index (LAI; $m^2\ m^{-2}$) among TBMs, and between model predictions and *in situ* and satellite-derived observations (e.g., De Kauwe et al. 2014; Medlyn et al., 2016). Studies also show that the models over-estimate the response of LAI to elevated $C_a$ because LAI in the models depends on the predicted GPP and carbon allocation (De Kauwe et al. 2014; Mahowald et al. 2016). The result of this inter-dependence likely leads to the unrealistic predictions of LAI (Anav et al. 2013; Murray-Tortarolo et al., 2013; Mahowald et al. 2016) and exaggerated effects of $C_a$ on LAI (De Kauwe et al. 2014; Mahowald et al. 2016; Medlyn et al., 2016). It is thus critically needed to improve mechanisms in TBMs to constrain LAI predictions. The ecohydrological equilibrium theory proposed by Eagleson (1982) added water balance as a constraint on LAI (i.e., LAI comes into equilibrium with the water availability). However, only a few early attempts tried to incorporate the ecohydrological equilibrium theory into vegetation models (Woodward, 1987; Nemani and Running, 1989; Haxeltine et al. 1996; Kergoat et al., 2002; Woodward and Lomas, 2004). None of these earlier attempts were incorporated into TBMs, despite an attempt in SDGVM by Woodward and Lomas (2004) which surprisingly did not successfully improve the predictions.

Second, at the leaf scale, stomatal regulation is directly related to the dryness of the air (Cowan and Farquhar, 1977; Ball et al., 1987; Mott and Parkhurst, 1991). The leaf gas

exchange models in the TBMs, however, predict divergent stomatal behaviour with increasing *D* (De Kauwe et al., 2015; Knauer et al., 2015; Franks et al., 2017). This difference among models highlights the lack of mechanistic understanding of stomatal regulation in dry air. One plausible hypothesis is that plants regulate $g_s$ to ensure hydraulic safety: when the air is dry the plant water supply might be insufficient to match the demand; the plants thus reduce $g_s$ to avoid hydraulic failure (e.g., Buckley, 2005; Eamus et al., 2008). Alternatively, stomatal regulation at high *D* could be the result of the down-regulation of photosynthesis (i.e., the 'Midday depression'; Huang et al., 2006): when photosynthesis reduced, the demand of $CO_2$ decreased, thereby leading to a closure of stoma to save water (Tezara et al., 1999; Lawlor and Cornic, 2002). Neither of these hypotheses have been widely tested or incorporated in TBMs.

Third, the response of canopy carbon flux is crucial to determining the ecosystem carbon budget in the future. Nevertheless, current models predicted a divergence of responses of carbon flux to rising $C_a$ at ecosystem (De Kauwe et al., 2014; Zaehle et al., 2014; Medlyn et al., 2016) and global (Ciais et al., 2013; Piao et al., 2013) scales. The observations are also showing discrepancy at leaf and canopy scales. The observations of leaf gas exchange to elevated $C_a$ consistently showed increase (Ainsworth and Rogers; 2007) and could be captured by models (e.g., Leuning, 1995; Medlyn et al., 2011). At whole-tree scale, however, mature forest growth did not show observable response to elevated $C_a$ (e.g., Finzi et al., 2002; Körner et al., 2005; Ellsworth et al., 2017). The inconsistency between leaf and canopy responses indicates issues how models scale fluxes from the leaf to the canopy. Quantifying photosynthesis at the canopy scale is thus important to resolve the scaling issue in TBMs.

### 1.6 Research targets

The previous sections synthesised the current knowledge and identified the gaps in the understanding of the impacts of elevated $C_a$ and water limitation on ecosystem carbon uptake. The overall aim of this thesis was to use a modelling framework, combined with data, to address these gaps. Specifically, this thesis aimed to improve three components of TBMs: prediction of LAI; leaf gas exchange responses to increasing *D*; and scaling of $C_a$ effects from leaf to the whole-canopy. The first goal of this thesis is thus to explore the capacity of ecohydrological equilibrium theory to predict LAI at large scales. The second goal is to improve the modelling of photosynthesis and $g_s$ responses to rising *D* using nonstomatal limitation. The last goal is to quantify the responses of canopy carbon flux to elevated $C_a$ and to partition the response to individual drivers.

The potential to use ecohydrological equilibrium theory as a parsimonious solution to calculate long-term steady-state LAI can be further explored. Following McMurtrie et al. (2008), I took the approach of implementing the theory as simply as possible, applying a minimal set of equations to predict the long-term equilibrium. This approach allowed me to focus on evaluating the performance of the theory independent of other model assumptions. I tested several alternative implementations of the theory, identified the best-performing model, and evaluated the predictions against *in situ* data and satellite-derived estimates for Australia. To test its capacity to predict LAI in future environmental conditions, I also used the model to predict the recent trend in LAI with the increase in $C_a$ and compared the predictions to satellite-derived observations. The outcome from this study should indicate whether incorporation of this theory is a potential avenue to improve the foliage carbon allocation schemes in existing TBMs.

There is also a need to resolve the cause of divergence of leaf gas exchange at high *D* and to identify the most appropriate approach to inform the TBMs. I thus evaluated current models and a range of hypotheses in a woodland site where *D* reaches high levels every summer (mean daily maximum = 2.7 kPa; maximum overall = 8 kPa). Previous studies in and around this site provided the opportunity to evaluate the models and hypotheses on different scales. On leaf scale, the models were parameterized with and evaluated against leaf gas exchange data. The best model was then selected and implemented into a process-based stand scale model, MAESTRA (Duursma and Medlyn, 2012), to explore whether improvements could also be made at the canopy scale. These findings would inform TBMs with the key limitation(s) of leaf gas exchange under high *D*.

The last study aimed to improve the prediction of the response of canopy carbon flux to rising $C_a$. I used MAESTRA to assess the ambient of carbon flux and the response to elevated $C_a$. I first parameterised the model with *in situ* physiological and meteorological measurements taken during the course of the four-year experiment (2013-2016), and then predicted the ecosystem carbon flux under ambient and elevated $C_a$ and evaluated the predicted transpiration against estimates from sap flow data. The aims of this study were thus to: determine the upscaled GPP and transpiration of a mature evergreen woodland; quantify the $CO_2$ response of GPP and transpiration; partition the impacts of each limiting factor.

The following chapters thus explored these questions:

i. Could consideration of water balance help predict long-term steady-state LAI? (Chapter 2)
ii. How is leaf water use (regulated by $g_s$) balanced with canopy water use (related to both LAI and $g_s$) and how is the relationship affected by climate change? (Chapter 2)
iii. Under high *D*, could any existing model capture the observations? If not, is the issue with the photosynthesis or the $g_s$ modelling? (Chapter 3)
iv. What is the baseline carbon flux of Australian evergreen woodlands? How does it change with rising $C_a$? (Chapter 4)

### 1.7 Candidate contributions

Chapter 2 is published as Yang, J., Medlyn, B. E., De Kauwe, M. G. and Duursma, R. A.: Applying the Concept of Ecohydrological Equilibrium to Predict Steady State Leaf Area Index, J. Adv. Model. Earth Syst., 10(8), 1740–1758, doi:10.1029/2017MS001169, 2018.

In Chapter 2, the candidate conceived and designed the model and obtained data for the simulation. The candidate also drafted the manuscript. B.E.M., M.G.DK, and R.A.D. provided comments on the daft.

Chapters 3 and 4 are in preparation for submission as journal articles. It is anticipated that the publication associated with Chapter 3 will have the following co-authors: B. E. Medlyn, R. A. Duursma, M. G. De Kauwe, D. Kumarathunge, T. E. Gimeno, K. Y. Crous, D. S. Ellsworth, K. Mahmud, J. Peters, B. Choat, D. Eamus, M. Jiang. The anticipated co-authors of Chapter 4 are: B. E. Medlyn, R. A. Duursma, M. G. De Kauwe, M. Jiang, D. Kumarathunge, T. E. Gimeno, K. Y. Crous, D. S. Ellsworth.

In Chapter 3 and 4, the candidate designed the study, developed the codes for analyses, modified the original MAESTRA model, compiled the meteorological and physiological data sets used in both simulations, analysed the results and wrote the chapters. The rest of the co-authors contributed their data, except for B.E.M., M.G.DK, R.A.D., and M.J., who provided supervisory advice and helped revise the manuscripts.

## Chapter 2. Applying the concept of ecohydrological equilibrium to predict steady-state leaf area index

### 2.1 Abstract

Leaf Area Index (LAI) is a key variable in modelling terrestrial vegetation, because it has a major impact on carbon and water fluxes. However, several recent inter-comparisons have shown that modelled LAI differs significantly among models, and between models and satellite-derived estimates. Empirical studies show that LAI is strongly related to precipitation. This observation is predicted by the ecohydrological equilibrium theory, which provides an alternative means to predict steady-state LAI.

We implemented this theory in a simple optimization model. We hypothesized that, when water availability is limited, plants should adjust steady-state LAI and stomatal behaviour to maximize net canopy carbon export, under the constraint that canopy transpiration is a fixed fraction of total precipitation.

We evaluated the predicted LAI ($L_{opt}$) for Australia against ground-based observations of LAI at 135 sites, and continental-scale satellite-derived estimates. For the site-level data, the root mean square error (RMSE) of predicted $L_{opt}$ was 1.07 $m^2$ $m^{-2}$, similar to the RMSE of a comparison of the data against nine-year mean satellite-derived LAI ($L_{sat}$) at those sites. Continentally, $L_{opt}$ had a $R^2$ of 0.7 when compared to $L_{sat}$. The predicted $L_{opt}$ increased continental-wide with rising atmospheric $CO_2$ concentration over 1982-2010, which agreed with satellite-derived estimations, while the predicted stomatal behaviour responded differently in dry and wet regions.

Our results indicate that long-term equilibrium LAI can be successfully predicted from a simple application of ecohydrological theory. We suggest that this theory could be usefully incorporated into terrestrial vegetation models to improve their predictions of LAI.

## 2.2 Introduction

Leaf Area Index (LAI; or $L$ in equations) is a key biophysical variable in terrestrial biosphere models (TBMs), as it determines the exchange of carbon and water between the vegetation and the atmosphere. However, current TBMs systematically overestimate LAI when compared to satellite-derived estimates (Anav et al. 2013; Murray-Tortarolo et al., 2013; Mahowald et al. 2016). At individual sites, recent model inter-comparisons have shown that there is a sizeable spread amongst models (>4 $m^2$ $m^{-2}$) in predicted maximum LAI (Walker et al. 2014; Medlyn et al. 2016). Models also disagree about the size of the projected change in LAI in response to warming and increasing atmospheric carbon dioxide ($C_a$; De Kauwe et al. 2014; Mahowald et al. 2016). Typically, these models predict LAI as the outcome of leaf growth (dependent on net primary productivity, its allocation to leaves, and leaf mass per area) and turnover processes (usually constant input parameters). Uncertainty across models arises from differences in the way these processes are implemented, reflecting a lack of mechanistic understanding of the controls of these processes (De Kauwe et al. 2014).

An alternative approach that could be used to predict LAI is based on the idea of ecohydrological equilibrium: that the LAI comes into equilibrium with the water availability at a given location (Eagleson, 1982). There is strong empirical support for a relationship between LAI and water availability especially in evergreen ecosystems. In *Eucalyptus*-dominated ecosystems in Australia, Specht and Specht (1989) found a strong ($R^2$ = 0.8) relationship between LAI and an evapourative coefficient, represented as relative evapotranspiration / precipitation. Similarly, Ellis and Hatton (2008) reported a linear relationship between LAI and precipitation ($R^2$ = 0.8) across eucalypt woodlands in southern Australia. Donohue et al. (2013) demonstrated a strong correlation between precipitation and satellite-derived maximum foliage coverage in dry regions of Australia. Across rainfall gradients of California, USA, Jin and Goulden (2014) analyzed precipitation and satellite-derived absorbed photosynthetically active radiation ($Q_{APAR}$; generally assumed to be proportional to LAI), and found a saturating relationship, with the sensitivity of $Q_{APAR}$ to precipitation being higher in drier regions. Globally, Iio et al. (2014) reported a strong LAI correlation with wetness index (precipitation/potential evapotranspiration) in dry regions, although the relationships varied with plant functional types (R varying from 0.13 to 0.57).

There have been relatively few attempts to incorporate this well-understood control on LAI into vegetation models. Woodward (1987) was the first to apply the idea of ecohydrological equilibrium in a large-scale model, predicting equilibrium LAI ($L_{equ}$) from considerations of

water and energy balance. In his approach, transpiration was calculated using the Penman-Monteith equation, in which increasing LAI was assumed to increase both canopy absorbed radiation and surface conductance. $L_{equ}$ was given by the maximum value of LAI for which transpiration is less than incoming precipitation. Thus, $L_{equ}$ maximized the absorbed radiation subject to the constraint of water availability. Since this calculation was based only on energy and water balance, it did not predict any change in $L_{equ}$ with rising $C_a$.

Nemani and Running (1989) also used this theory to predict $L_{equ}$ at stand scale. These authors used the FOREST-BGC model and empirical data to estimate the baseline transpiration and associated $L_{equ}$ in one experimental pine stand in Montana, USA. They then modelled transpiration for 20 other similar stands and, by assuming the $L_{equ}$-transpiration relationship is constant, predicted $L_{equ}$ for each stand. They found a strong correlation with the observed LAI ($R^2 = 0.87$). However, this approach cannot be applied more broadly, since the relationship between transpiration and $L_{equ}$ will vary with ecosystem type.

Kergoat (1998) suggested that a combination of water and carbon limitations would predict more realistic $L_{equ}$ than consideration of water limitation alone and included two constraints on $L_{equ}$: (i) plant transpiration (a function of both stomatal conductance ($g_s$) and LAI) must not deplete soil moisture below a critical point; and (ii) the bottom layer of the canopy must have a positive carbon balance. $L_{equ}$ was then predicted as the maximum LAI that satisfies these constraints. The predicted $L_{\mathrm{equ}}$ captured the LAI variation by biome globally, and the associated runoff matched observations in 28 sites. Kergoat et al. (2002) expanded the model in Kergoat (1998) by additionally accounting for the construction cost of leaves and reported improved accuracy as compared to satellite-derived LAI. The approach proposed by Kergoat et al. (2002) has not been widely adopted, possibly because of computational demands of a daily optimization.

Beerling and Woodward (2001) incorporated $L_{equ}$ as a component of Sheffield Dynamic Global Vegetation Model (SDGVM). The $L_{equ}$ in SDGVM was based on similar carbon constraints as Kergoat et al. (2002) but differed in the water balance constraint: they assumed that plant transpiration should be less than the precipitation reaching the ground. They also avoided the need to iterate by calculating LAI from the water and carbon balances of the previous year in a multi-year simulation. Woodward and Lomas (2004) validated the LAI predicted by SDGVM against optical measurements from the FLUXNET network and found a strong correlation ($R^2 = 0.8$) across 52 sites. The $L_{equ}$ model in SDGVM is more practical than the Kergoat models because of the simplification of water balance calculation. The

goodness of fit of SDGVM $L_{equ}$ to observations suggested that such a simplification may be reasonable and necessary considering the limitation in computational capacity. However, some recent applications of the SDGVM model have found it to significantly overestimate LAI at specific sites (Medlyn et al. 2016, De Kauwe et al. 2017).

One feature common to all the models described above is that the $g_s$ response to drying soil is a fixed function of soil moisture. However, there is increasing empirical evidence to suggest that there are important differences in plant stomatal behaviour across ecosystems and climatic zones (Lin et al. 2015). We take an alternative approach to predicting the ecohydrological equilibrium, based on the MATEY (Model Any Terrestrial Ecosystem – Yearly) model proposed by McMurtrie et al. (2008). In the original MATEY model, plants are assumed to maximize net carbon export by regulating both $g_s$ and LAI, subject to the constraint that evapotranspiration cannot exceed a given fraction of incoming precipitation. The MATEY model thus optimizes both LAI and $g_s$ at the same time. McMurtrie et al. (2008) evaluated their model at two forest stands but not on larger scales. We identified that a potential issue of optimizing both $g_s$ and LAI is that the variabilities of $g_s$ and LAI are on different temporal scales (minutes versus weeks). Hence, we characterized the variability of $g_s$ using a model of stomatal behaviour in which variation is represented by the stomatal slope parameter $g_1$ (Eqn. 11; Medlyn et al., 2011; Prentice et al. 2014). The term $g_1$ is related to the water cost per unit carbon gain introduced by Cowan and Farquhar (1977) and is similar to the fitted slope in the widely-used Ball-Berry model (Ball et al., 1987).

Here, we investigate whether this optimality theory can successfully predict LAI across the Australian continent. Following McMurtrie et al. (2008) we take the approach of implementing the theory as simply as possible, applying a minimal set of equations to predict the long-term equilibrium. This approach allows us to focus on evaluating the performance of the theory independent of other model assumptions. Success of this simple parsimonious approach would indicate that the theory could usefully be incorporated into TBMs as an alternative to existing foliage carbon allocation schemes. We chose Australia as an example to evaluate the applicability of the concept of ecohydrological equilibrium because abundant and high-quality data are available for model construction (i.e., plant physiology and meteorology) and evaluation (i.e., $g_1$ and LAI data). In addition, Australia is dominated by evergreen ecosystems, for which the steady-state approach is more easily interpreted. Utilizing the theory to predict LAI of deciduous ecosystems would require an additional set of assumptions regarding phenology (e.g., Caldararu et al., 2014).

The goal of this research is thus to explore the capacity of ecohydrological equilibrium theory to predict LAI at large scales. The outcome from this study should indicate whether incorporation of this theory is a potential avenue to improve the foliage carbon allocation schemes in existing TBMs. We tested several alternative implementations of the theory, identified the best-performing model, and evaluated the predictions against in situ data and satellite-derived estimates for Australia. To test its capacity to predict LAI in novel environmental conditions, we also used the model to predict the recent trend in LAI with the increase in atmospheric carbon dioxide and compared the predictions to satellite-derived observations.

## 2.3 Materials and Methods

### 2.3.1 Model

The model, named EELS (Ecohydrological Equilibrium Leaf-area-index Simulator; Version 1.0), is a variant of the MATEY model (McMurtrie et al. 2008). It optimizes canopy net carbon export ($P_{net}$; g C $m^{-2}$ $yr^{-1}$), the difference between canopy production and leaf construction and respiration costs, for a given long-term climate, which is specified by the atmospheric $CO_2$ concentration ($C_a$; μmol $mol^{-1}$), mean annual precipitation ($W_{MAP}$; mm $yr^{-1}$), vapour pressure deficit ($D$; kPa), and annual total photosynthetically active radiation ($Q_{PAR}$; MJ PAR $m^{-2}$ $yr^{-1}$). $P_{net}$ is optimized based on a trade-off between leaf area index (LAI; $m^2$ $m^{-2}$) and water use per unit leaf area, here represented by $g_1$ ($kPa^{0.5}$), the stomatal slope parameter (Medlyn et al., 2011). In the original MATEY model (McMurtrie et al. 2008), the optimization was a trade-off between LAI and stomatal conductance ($g_s$; mol $H_2O$ $m^{-2}$ $s^{-1}$). Here, instead of using $g_s$ directly, we model $g_s$ as a function of the carbon assimilation rate, $g_1$, $D$, and $C_a$, with the optimal stomatal behaviour model of Medlyn et al. (2011). We chose to use $g_1$ because: (i) $g_1$ is related to plant water cost per unit carbon gain (Cowan and Farquhar, 1977; Medlyn et al., 2011) and thus combines the impacts of plant physiology, genetics, and prior environmental conditions; (ii) $g_1$ is less temporally variable than $g_s$ (Lin et al., 2015). A further difference from the original MATEY model is that our model considers the cost of foliage (both construction and maintenance), modelled as a function of LAI instead of being a fixed fraction of production (McMurtrie et al. 2008).

The trade-off between LAI and $g_1$ in the model is represented by the responses of light use efficiency ($\varepsilon_l$; g C $MJ^{-1}$), water use efficiency ($\varepsilon_w$; g C $mm^{-1}$), the foliage cost per unit ground area ($C_{total}$; g C $m^{-2}$ ground), and the absorbed photosynthetically active radiation ($Q_{APAR}$; MJ PAR $m^{-2}$ $yr^{-1}$). Increasing LAI increases the fraction of absorbed $Q_{PAR}$ and the transpiration fraction but also adds to $C_{total}$, while increasing $g_1$ enhances $\varepsilon_l$ but reduces $\varepsilon_w$. The total possible transpiration is set by $W_{MAP}$ and the transpiration fraction, leading to a negative relationship between LAI and $g_1$. As a result, there are optimal values of LAI and $g_1$ ($L_{opt}$ and $g_{1.opt}$) that maximize $P_{net}$ under a given $W_{MAP}$ (Figure 2.1 and 2.2). This $L_{opt}$ is different from the $L_{equ}$, which is based on eco-hydrological equilibrium, by incorporating optimization. All symbols are defined at first use and again in Table 2.1. Equations are defined in the following paragraphs and Text S1. The model assumes the same equations and parameters for all plant functional types. Alternative assumptions were tested in developing the model

(Supplementary Material for Chapter 2) but showed little improvement of the prediction and were thus not incorporated for parsimony.

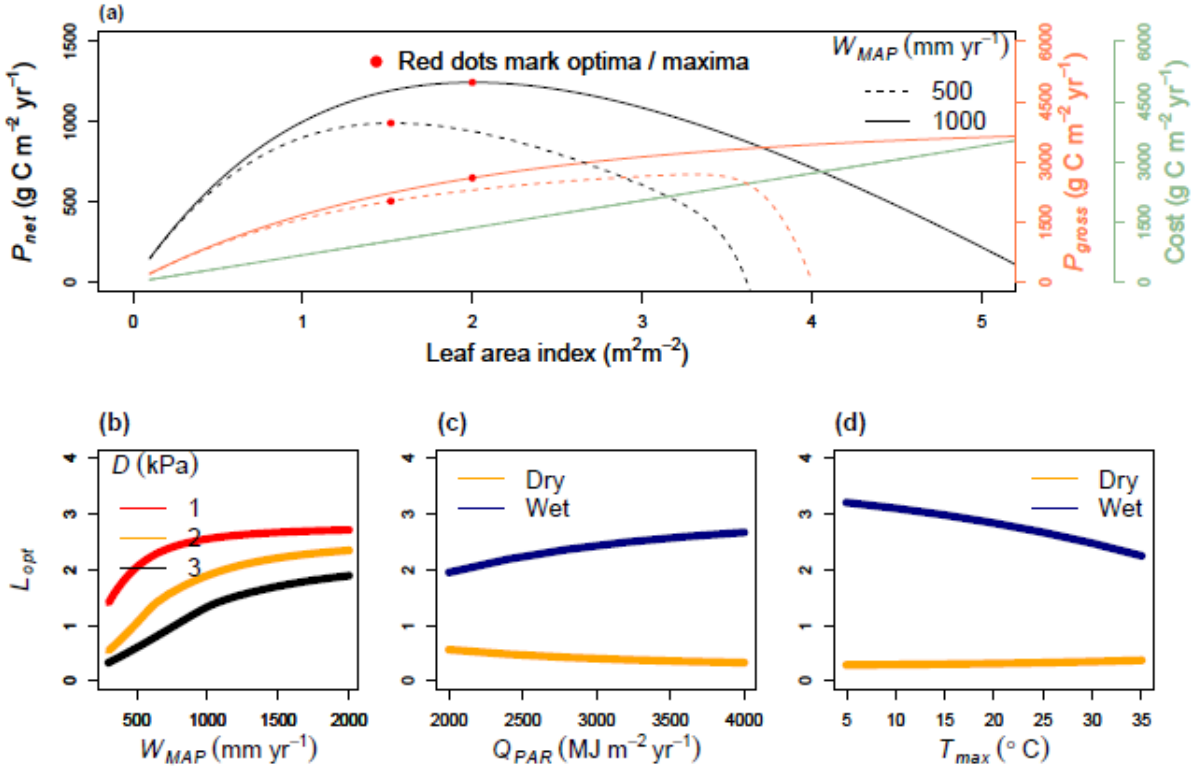


*Figure 2.1. Model behaviour and sensitivity. Panel (a) shows two examples of how model optima are obtained for two mean annual precipitation scenarios, $W_{MAP}$ (500 and 1000 mm; solid and dashed lines, respectively). Other inputs are set to D = 1.5 kPa, $Q_{PAR}$ = 3000 MJ PAR m$^{-2}$ yr$^{-1}$, and $T_{max}$ = 25 ºC. Orange lines indicate gross primary production ($P_{gross}$, scale on right-hand axis); green lines indicate foliage cost (scale on right-hand axis); black lines indicate canopy net carbon export ($P_{net}$), which equals $P_{gross}$ - $C_{total}$ (Eqn. 8). Panel (b-d) show sensitivity of predicted $L_{opt}$ to climate factors for two scenarios: dry ($W_{MAP}$=300 mm yr$^{-1}$; D=3 kPa) and wet ($W_{MAP}$=1500 mm yr$^{-1}$; D=1 kPa). Panel (b) shows the relationship of $L_{opt}$ to mean annual precipitation ($W_{MAP}$) for three values of vapour pressure deficit (D). Mean annual photosynthetically active radiation ($Q_{PAR}$) and mean annual maximum temperature of each month ($T_{max}$) were fixed to 4000 MJ m$^{-2}$ yr$^{-1}$ and 25 °C, respectively. Panels (c) and (d) shows the impact of $Q_{PAR}$ and $T_{max}$ in conditions, respectively.*

The water constraint in the model is represented by $W_T$ (plant transpiration; mm yr$^{-1}$), which was assumed to be a fraction of evapotranspiration following (Wang et al., 2014):

$$W_T = a_T \cdot L^{b_T} \cdot W_{ET} \quad (1)$$

where $a_T$ and $b_T$ are fitted parameters from Wang et al. (2014), with values of 0.77 and 0.1, respectively; $L$ is leaf area index ($m^2$ $m^{-2}$). $W_{ET}$ is evapotranspiration (mm $yr^{-1}$), which is related to mean annual precipitation following Zhang et al. (2001):

$$W_{ET} = \frac{W_{MAP} + 2 \cdot c_w}{1 + \frac{2 \cdot c_w}{W_{MAP}} + \frac{W_{MAP}}{c_w}} \quad (2)$$

where $W_{MAP}$ is the mean annual precipitation (mm $yr^{-1}$) and $c_w$ is an empirical constant (fitted potential evapotranspiration) in Zhang et al. (2001), with data for forest ecosystems. Our model here differs from McMurtrie et al. (2008), who assumed a constant fraction (0.8) of rainfall was used by the plant. We used the more complicated calculation of transpiration because: (i) Transpiration can be less than half of total evapotranspiration (Yepez et al., 2005; Wang et al., 2010; Sutanto et al., 2012; Wang and Dickinson, 2012; Kool et al., 2014); (ii) and the fraction of transpiration in evapotranspiration is related to vegetation cover (Liu et al. 2017). The impacts of using these functions on the prediction are shown in the Supplementary Material for Chapter 2.

The canopy carbon uptake is related to transpiration by the water use efficiency:

$$P_{gross} = \varepsilon_w \cdot W_T \quad (3)$$

where $P_{gross}$ is gross primary production (g C $m^{-2}$ $yr^{-1}$); $\varepsilon_w$ is the transpiration efficiency (g C $kg^{-1}$), calculated following Medlyn et al. (2011; Eqn. S1). $P_{gross}$ calculated with water limitation has to equal to that calculated with absorbed radiation:

$$P_{gross} = \varepsilon_l \cdot Q_{APAR} \quad (4)$$

where $\varepsilon_l$ is light use efficiency (g C $MJ^{-1}$ PAR), estimated with the model of Sands (1995 and 1996) and $Q_{APAR}$ (absorbed photosynthetically active radiation; MJ PAR $m^{-2}$ $yr^{-1}$) of the canopy is related to LAI by the Beer-Lambert law (Eqn S8). This $Q_{APAR}$ is the long-term average value: the model does not consider inter- and intra-annual variation of climate conditions or of LAI. The responses of $\varepsilon_l$ to $T_{max}$ and $D$ follows following Bernacchi et al. (2001), Medlyn et al. (2007), and Medlyn et al. (2011).

The equations for $\varepsilon_w$ (transpiration efficiency; Eqn. 3), $\varepsilon_l$ (light use efficiency; Eqn. 4), and $Q_{APAR}$ (absorbed photosynthetically active radiation; Eqn. 4) are as follows. $\varepsilon_w$ (g C $mm^{-1}$; Eqn. 3) is defined following Medlyn et al. (2011),

$$\varepsilon_w = c_1 \cdot C_a \cdot \frac{P_{atm}}{D+g_1\cdot\sqrt{D}} \qquad (5)$$

where $c_1$ converts from μmol C mol$^{-1}$ $H_2O$ to g C mm$^{-1}$ $H_2O$; $P_{atm}$ is the atmospheric pressure (kPa); $g_1$ is the optimal stomatal conductance parameter (kPa$^{0.5}$); $D$ is vapour pressure deficit (kPa). Substituting the parameters in Eqn. 3 with Eqn. 5, $P_{gross}$ (gross primary production) can be expressed as a function of $g_1$ from the water-limiting perspective.

The light use efficiency ($\varepsilon_l$; g C MJ$^{-1}$ PAR; Eqn. 4) calculation is based on Sands (1995, 1996),

$$\varepsilon_l = \mathrm{c}_2 \cdot \alpha \cdot \int_0^{\pi/2} \frac{\sin x}{(1+\mathrm{q}\cdot\sin x+\sqrt{(1+\mathrm{q}\cdot\sin x)^2-4\cdot\theta\cdot q\cdot\sin x})}\,dx) \qquad (6)$$

where $c_2$ converts from μmol C to g C; $\theta$ is the curvature of photosynthetic light response curve; $x$ is solar elevation angle; and $q$ is defined as,

$$q = \pi \cdot k \cdot Q \cdot \mathrm{c}_3 \cdot \frac{\alpha}{2\cdot h\cdot(1-m)\cdot Ax} \qquad (7)$$

where $k$ is the light extinction coefficient. Although the value of $k$ varies among the plant functional types (Zhang et al., 2014), we used a constant value of 0.5, which is the reported value for *Eucalyptus* forest (Sands, 1995) and grassland (Zhang et al., 2014). $Q$ is the daily irradiance (MJ m$^{-2}$ d$^{-1}$) calculated with $Q_{PAR}$; $c_3$ converts from MJ PAR to μmol; $h$ is the total daylight length in hours; $\alpha$ is the quantum yield of photosynthesis calculated following McMurtrie and Wang (1993),

$$\alpha = \frac{\alpha_J}{4} \cdot \frac{C_a - \Gamma^*}{C_a + 2\cdot\Gamma^*} \qquad (8)$$

where $\alpha_J$ is the quantum yield of electron transport (mol mol$^{-1}$); $C_a$ is atmospheric $CO_2$ concentration (μmol mol$^{-1}$); and $\Gamma^*$ is the compensation point (μmol mol$^{-1}$) calculated based on Bernacchi et al. (2001),

$$\Gamma^* = \exp(\mathrm{c}_4 - \frac{\Delta\mathrm{H}}{\mathrm{R}\cdot T_k}) \qquad (9)$$

where $c_4$ is a scaling constant; $\Delta H$ is the activation energy; $R$ is the molar gas constant; $T_k$ is the leaf temperature (K), which is assumed to be $T_{max}$, the annual mean of monthly maximum temperature (ºC), plus 273.15; $A_x$, is the light-saturated photosynthetic rate at the top of canopy (μmol m$^{-2}$ s$^{-1}$), given by,

$$A_x = \frac{Jmax}{4} \cdot \frac{C_i - \Gamma^*}{C_i + 2\cdot\Gamma^*} \qquad (10)$$

where $J_{max}$ is the maximum electron transport rate at the top of the canopy (μmol $m^{-2}$ $s^{-1}$); and $C_i$ (intercellular $CO_2$ concentration; μmol $mol^{-1}$) is defined by the unified stomatal optimisation model (Medlyn et al., 2011),

$$C_i = C_a \cdot \frac{g_1}{g_1 + \sqrt{D}} \qquad (11)$$

Substituting the parameters in Eqn. 5 with Eqn. 6-11, $\varepsilon_l$ can be expressed as a function of $g_1$ ($kPa^{0.5}$).

$Q_{APAR}$ (absorbed photosynthetically active radiation; MJ PAR $m^{-2}$ $yr^{-1}$; Eqn. 4) of the canopy is related to leaf area index (*LAI*; $m^2$ $m^{-2}$) by the Beer-Lambert Law,

$$f_{APAR} = 1 - e^{-k \cdot L} \qquad (12)$$

$$Q_{APAR} = Q_{PAR} \cdot f_{APAR} \qquad (13)$$

where $f_{APAR}$ is the fraction of absorbed photosynthetically active radiation. Substituting the parameters in Eqn. 4 with Eqn. 12 and 13, $P_{gross}$ can be expressed as a function of LAI (leaf area index). Since light-limited and water-limited $P_{gross}$ must equal (combining Eqn. 3 and Eqn. 4), $g_1$ can be solved as a function of LAI by iteration.

Eqn. 3 and 4 are the key equations describing the water and light constraints in the model and the trade-off between $g_1$ and LAI. Combining Eqn. 3 and 4, $g_1$ can be solved as a function of LAI. As a result, $P_{gross}$ can be calculated as an implicit function of LAI, which is solved by iteration. The carbon cost of building leaves is given by $C_{total}$, which includes the maintenance respiration, construction respiration and construction cost per unit ground area (g C $m^{-2}$ $yr^{-1}$), defined as a function of LAI:

$$C_{total} = c_r \cdot R_m \cdot L + C_{cost} \cdot L \qquad (14)$$

where $c_r$ converts μmol C $m^{-2}$ $s^{-1}$ to g C $m^{-2}$ $yr^{-1}$; $R_m$ is maintenance respiration per unit leaf area (μmol $m^{-2}$ $s^{-1}$); $C_{cost}$ is the carbon cost of construction, including construction respiration per unit leaf area (g C $m^{-2}$ leaf). To estimate $R_m$, we used the Australian subset of the GLOBRESP data set (Atkin et al. 2015) and took the mean across available data. We assumed that the rate of respiration acclimates to the prevailing mean temperature and thus the value for $R_m$ is taken to be a constant. We also considered two alternative assumptions for $R_m$, namely a relationship with $W_{MAP}$ or a relationship with leaf mass per area. The effects of these alternative assumptions are shown in the Supplementary Material for Chapter 2.

The construction cost, $C_{cost}$, is calculated as:

$$C_{cost} = c_c \cdot b_c \cdot \frac{M_{area}}{t_f} \quad (15)$$

where $c_c$ is the assumed proportion of carbon in dry mass (0.5 g C $g^{-1}$ DM), $b_c$ is the construction respiration ratio (g C $g^{-1}$ C). Villar and Merino (2001) reported a mean cost of 1.66 g of glucose per gram of dry mass for xeric forest. Assuming half of the dry mass is carbon and 40% of the glucose is carbon, we calculated the fraction of construction respiration ($b_c$) to be 1.3 (g C $g^{-1}$ C). $M_{area}$ is leaf mass per area (g DM $m^{-2}$ leaf), and $t_f$ is the leaf lifespan (yr). Values of $M_{area}$ and $t_f$ were taken as the mean from the GLOPNET data set (Wright et al., 2004; values are given in Table 2.1).

The model also relies on $J_{max}$, the maximum electron transport rate. We compiled a data set of Australian observations from the literature (Walker et al., 2014; Ali et al., 2015; De Kauwe et al., 2016; Data available in the Table S1) and tested for relationships with climate. $J_{max}$ was not correlated with any climate factor used in the model (Figure S.5). Thus, we used the mean of the measurements from the data set. Similar to $R_m$, the temperature dependence of $J_{max}$ is not included in the model.

The optimization target of the model, canopy net carbon export ($P_{net}$; g C $m^{-2}$ $yr^{-1}$), is then defined as the difference between production and cost:

$$P_{net} = P_{gross} - C_{total} \quad (8)$$

Hence, for the given driving conditions, the solution, $L_{opt}$, is the $L$ value that maximizes $P_{net}$.

*Table 2.1. List of values and definitions of inputs (the first four rows; marked by dashed line), parameters, constants, and outputs in the model.*

| Symbols | Definition | Value/Type | Unit | Source |
|---|---|---|---|---|
| $W_{MAP}$ | Mean annual precipitation | Input | mm $yr^{-1}$ | Whitley et al., 2014 |
| $D$ | Mean monthly maximum vapour pressure deficit | Input | kPa | Whitley et al., 2014 |
| $Q_{PAR}$ | Incident photosynthetically active radiation | Input | MJ PAR $m^{-2}$ $yr^{-1}$ | Whitley et al., 2014 |
| $T_{MAX}$ | Mean maximum temperature of each month | Input | ºC | Whitley et al., 2014 |
| $A_x$ | Light-saturated photosynthetic rate at the top of canopy | - | µmol $m^{-2}$ $s^{-1}$ | - |
| $a_l$ | Slope of relationship between $t_f$ and $M_{area}$ | 1.14 | yr $m^2$ leaf $g^{-1}$ DM | - |
| $\alpha_J$ | Quantum yield of electron transport | 0.26 | mol $mol^{-1}$ | Medlyn et al. 2007 |
| $a_m$ | Slope of relationship between $M_{area}$ and $W_{MAP}$ | -0.36 | g DM $m^{-2}$ leaf $W^{-1}$ | - |
| $a_r$ | Slope of relationship between $R_m$ and $W_{MAP}$ | -0.59 | µmol C $m^{-2}$ leaf $mm^{-1}$ | - |
| $a_{rm}$ | Slope of relationship between $R_m$ and $M_{area}$ | 0.63 | µmol C $g^{-1}$ | - |
| $a_T$ | Slope of relationship between $W_T$ and LAI | 0.77 | Dimensionless | - |
| $b_c$ | Construction respiration ratio | 1.3 | g C $g^{-1}$ C | Villar and Merino, 2001 |
| $b_l$ | Interceptor of relationship between $t_f$ and $M_{area}$ | -5.64 | yr | - |
| $b_m$ | Interceptor of relationship between $M_{area}$ and $W_{MAP}$ | 7.52 | g DM $m^{-2}$ leaf | - |

| | | | | |
|---|---|---|---|---|
| $b_r$ | Interceptor of relationship between $R_m$ and $W_{MAP}$ | 4.235 | µmol C $m^{-2}$ leaf | - |
| $b_{rm}$ | Interceptor of relationship between $R_m$ and $M_{area}$ | -2.94 | µmol C $m^{-2}$ $s^{-1}$ | - |
| $b_T$ | Power of relationship between $W_T$ and LAI | 0.1 | Dimensionless | - |
| $c_1$ | µmol C $mol^{-1}$ $H_2O$ to g C $mm^{-1}$ $H_2O$ | 4.17E-5 | g C $\mu mol^{-1}$ C mol $H_2O$ $mm^{-1}$ $H_2O$ | - |
| $c_2$ | µmol to g of C | 1.2E-5 | g C $\mu mol^{-1}$ | - |
| $c_3$ | MJ of PAR to µmol | 2E6 | MJ PAR $\mu mol^{-1}$ | Sands 1996 |
| $c_4$ | Scaling constant | 19.02 | - | Bernacchi et al. 2001 |
| $C_a$ | Atmospheric $CO_2$ concentration | 375 | µmol $mol^{-1}$ | McMurtrie et al. 2008 |
| $c_c$ | proportion of carbon in dry mass | 0.5 | g C $g^{-1}$ DM | - |
| $C_{cost}$ | Construction respiration and cost per unit leaf area | - | g C $m^{-2}$ leaf | - |
| $C_i$ | Intercellular $CO_2$ concentration | - | µmol $mol^{-1}$ | - |
| $c_r$ | µmol C $s^{-1}$ to g C $yr^{-1}$ | 378.69 | g C $yr^{-1}$ $\mu mol^{-1}$ C s | - |
| $c_w$ | fitted constant potential evapotranspiration | 1410 | mm | Zhang et al. 2001 |
| $\Delta H$ | Activation energy | 37.83 | kJ $mol^{-1}$ | Bernacchi et al. 2001 |
| $\varepsilon_l$ | Light use efficiency | - | g C $MJ^{-1}$ PAR | - |
| $\varepsilon_w$ | Intrinsic transpiration efficiency | - | g C $mm^{-1}$ $H_2O$ | - |
| $g_1$ | Stomatal slope parameter | - | $kPa^{0.5}$ | - |
| $g_{1.max}$ | Maximum $g_1$ value for optimisation | 20 | $kPa^{0.5}$ | - |

| | | | | |
|---|---|---|---|---|
| $g_{1.opt}$ | Optimal $g_1$ corresponding to $L_{opt}$ | - | $kPa^{0.5}$ | - |
| $\theta$ | Curvature of photosynthetic light response curve | 0.7 | - | Medlyn et al. 2007 |
| $J_{max\ 25}$ | Maximum electron-transport rate at the top of the canopy at 25 ºC | 160 | µmol $m^{-2}$ $s^{-1}$ | - |
| $k$ | Light extinction coefficient | 0.5 | - | Sands 1995 |
| LAI or $L$ | Leaf area index | - | $m^2$ $m^{-2}$ | - |
| $L_{equ}$ | LAI at equilibrium | - | $m^2$ $m^{-2}$ | - |
| $L_{opt}$ | Optimization modified LAI at equilibrium | - | $m^2$ $m^{-2}$ | - |
| $t_f$ | Leaf lifespan | 1.4 | yr | Wright et al., 2006 |
| $m$ | Leaf transmittance coefficient | 0 | - | McMurtrie et al. 2008 |
| $M_{area}$ | Leaf mass per area | 169.44 | g Dry mass $m^{-2}$ leaf | Wright et al., 2006 |
| $P_{atm}$ | Atmospheric pressure | 100 | kPa | - |
| $P_{gross}$ | Gross primary production | - | g C $m^{-2}$ $yr^{-1}$ | - |
| $P_{net}$ | Net carbon export from foliage | - | g C $m^{-2}$ $yr^{-1}$ | - |
| $Q$ | Daily irradiance | - | MJ $m^{-2}$ $day^{-1}$ | - |
| $Q_{APAR}$ | Absorbed PAR | - | MJ PAR $m^{-2}$ $yr^{-1}$ | - |
| $R$ | Molar gas constant | 8.314E-3 | J $mol^{-1}$ $K^{-1}$ | |
| $R_m$ | Leaf maintenance respiration | 1.59 | µmol $m^{-2}$ $s^{-1}$ | - |
| $t$ | Growing season length | 365.25 | Day | - |
| $W_{ET}$ | Evapotranspiration | - | mm $yr^{-1}$ | - |

| | | | | |
|---|---|---|---|---|
| $W_T$ | Transpiration | - | mm $yr^{-1}$ | - |

### 2.3.2 Data

The model was applied to predict $L_{opt}$ and $g_{1.opt}$ using gridded climate data, and was evaluated against ground-based measurements (stand level) as well as satellite-derived estimates (0.06-degree grid) on decadal time scale. $L_{opt}$ and $g_{1.opt}$ were evaluated together for ten sites where both measurements were available. To minimize anthropogenic effects, evaluation of the model at the continental scale were constrained to natural reserves.

The parameter values in the model were derived directly from observations. We did not try to parameterize the model by fitting the model to data. Our approach allowed the evaluation of the processes (i.e., process-based modelling) instead of obtaining the best model performing model parameters (i.e., statistical modelling).

#### 2.3.2.1 Climate inputs

Potential evapotranspiration (PET; mm $yr^{-1}$), $W_{MAP}$, actual vapour pressure, $Q_{PAR}$, and $T_{max}$ are obtained from eMAST (Ecosystem Modelling and Scaling Infrastructure; Whitley et al. 2014). We selected a 21-year period, 1991-2011, matching the satellite record (2000-2011). For computational efficiency, the climate data (0.01° native resolution) were aggregated to 0.06°. $D$ was calculated as the difference of saturation vapour pressure and actual vapour pressure with the former being a function of $T_{max}$. We also calculated an aridity index (AI), defined as PET/$W_{MAP}$. All the other gridded datasets in the following sections were aggregated to match the climate grids (0.06°). We used the long-term (21-year) mean of the four inputs for each grid cell. Plots of $W_{MAP}$, $D$, $Q_{PAR}$, and $T_{max}$ are shown in Figure S1. The model predicted a paired $L_{opt}$ and $g_{1.opt}$ for each grid cell with no temporal variation.

#### 2.3.2.2 Ground-based data

Ground-based LAI and $g_1$ data were used for evaluation. Ground-based LAI measurements were taken from four sources: Ellis and Hatton 2008 (37 sites), Iio et al. 2014 (134 sites), Duursma et al. 2016 (one site), and eight sites from the Terrestrial Ecosystem Research Network (TERN; Prober and Macfarlane, 2013; Beringer and McHugh, 2015 a and b; Bradford, 2015; Eamus and Cleverly, 2015 a and b; Liddell and Laurance, 2015; Prober and Macfarlane, 2015; Rowlings and Grace, 2015; van Gorsel, 2015). For sites that are close together (< 0.01 degree), the mean of the reported LAI values was taken, giving a total of 135

sites. Both Duursma et al. (2016) and the data from TERN used the estimated gap fraction to estimate the LAI of the canopy. As a result, both data sets are plant area index. The data from Ellis and Hatton (2008) were a synthesis and thus the methods used to estimate LAI varied by source. Iio et al. (2014) synthesized a similar data set with various methods to estimate LAI but reported ecosystem LAI (sum of understory and canopy) instead of canopy when possible. Notably, the understory LAI could be as high as canopy and thus these LAI measurements were likely underestimates. There are some notable inconsistencies among sources regarding their methodology: plant versus leaf area index; different methods to correct leaf clumping; canopy versus ecosystem LAI. Moreover, the measurements are on stand level and are not scaled to the spatial resolution of satellite-derivatives and the modelled LAI. These LAI data were mostly one-time measurements and thus could not represent intra- and inter-annual LAI variations. Corresponding ground-based $g_1$ values were estimated from in situ leaf gas exchange measurements at the top of the canopy, which were available for ten of these sites (Table 2.2). Values were estimated from data using the "fitBB" routine (R package "plantecophys"; Duursma, 2015), which uses the nonlinear least squares method to fit $g_1$ to measurements of stomatal conductance, photosynthesis, and environmental variables.

*Table 2.2. List of ground measurements of $g_1$ and LAI, ordered by aridity index (AI). The abbreviations in "Site" column are defined as follows (with site name and state): DTR— Daintree rainforest, QLD; TSM— Tumbarumba Snowy Mountains, NSW; HWS— Howard Springs, NT; ADR— Adelaide River, NT; DLR— Daly River, NT; CWS— Castlereagh Western Sydney, NSW; RWS— Richmond Western Sydney, NSW; DRR— Dry River, NT; STP— Sturt Plains, NT; CWR— Corrigin Water Reserve, WA. States: NSW—New South Wales; NT—Northern Territory; QLD—Queensland; WA—Western Australia.*

| Site | $g_{1.opt}$ | $g_{1,meas}$ | $L_{opt}$ | $L_{meas}$ | AI | Lat. | Lon. | $g_1$ References | LAI References |
|---|---|---|---|---|---|---|---|---|---|
| DTR | 3.34 | 3.45 | 2.33 | 2.65 | 0.42 | -16.1 | 145.45 | Kelly (2013) | Liddell and Laurance (2015) |
| TSM | 1.34 | 3.23 | 2.46 | 1.35 | 0.77 | -35.63 | 148.16 | Medlyn et al. (2007) | van Gorsel (2015) |
| HWS | 2.34 | 3.38 | 1.84 | 1.00 | 1.08 | -12.5 | 131.15 | Cernusak et al. (2011) | Iio et al. (2014) |
| ADR | 2.15 | 3.36 | 1.68 | 0.60 | 1.21 | -13.08 | 131.12 | Cernusak et al. (2011) | Iio et al. (2014) |

| | | | | | | | | | |
|---|---|---|---|---|---|---|---|---|---|
| DLR | 1.98 | 6.06 | 1.43 | 1.00 | 1.64 | -14.16 | 131.39 | Cernusak et al. (2011) | Iio et al. (2014) |
| CWS | 1.01 | 4.49 | 1.44 | 1.50 | 1.82 | -33.69 | 150.67 | Zeppel et al. (2008) | Zeppel et al. (2008) |
| RWS | 0.92 | 4.21 | 1.36 | 1.70 | 1.93 | -33.62 | 150.73 | Gimeno et al. (2015) | Duursma et al. (2016) |
| DRR | 1.71 | 2.94 | 1.13 | 0.90 | 2.07 | -15.18 | 132.37 | Cernusak et al. (2011) | Iio et al. (2014) |
| STP | 1.65 | 3.38 | 0.75 | 0.20 | 3.16 | -17.15 | 133.35 | Cernusak et al. (2011) | Iio et al. (2014) |
| CWR | 0.95 | 2.01 | 0.49 | 0.66 | 4.19 | -32.32 | 117.87 | Mitchell et al. (2009) | Mitchell et al. (2009) |

#### 2.3.2.3 Satellite-derived LAI data

To evaluate the model's performance at large spatiotemporal scales, we used the satellite-derived LAI product, MODIS (moderate resolution digital imaging spectroradiometer; Knyazikhin et al., 1999). The 8-day MODIS LAI (collection 5; MOD15A2) tiles for Australia were mosaicked and reprojected from their native sinusoidal projection to a regular latitude-longitude grid (GDA94) (see Paget and King, 2008). The LAI estimates were averaged for the period 2000 to 2011. Only LAI data estimated from the main radiative transfer algorithm and deemed to be of the best quality (i.e., no cloud contamination or saturation data used; quality assurance flag = 0) were used.

#### 2.3.2.4 Land cover, soil attribute~~,~~ and digital elevation maps

The model used land cover type information taken from Australian Bureau of Agricultural and Resource Economics and Sciences product, National scale land use version 4 (2005-2006; http://www.agriculture.gov.au/abares/aclump/Pages/land-use/data-download.aspx). The soil attribute maps with total Nitrogen ($N_{soil}$; %) and Phosphorus ($P_{soil}$; %) of the top layer (0-5cm) were obtained from CSIRO (Viscarra Rossel et al., 2014 a and b). The $N_{soil}$ and $P_{soil}$ data represented the total N and P in the soil and were aggregated from a native resolution (0.00083°) to 0.06°. The soil attributes were used for the statistical analysis of the importance of soil nutrients for LAI. We used the Digital Elevation Model Version 3 and Flow Direction Grid 2008 obtained from Geoscience Australia (http://www.ga.gov.au/metadata-gateway/metadata/record/66006/).

#### 2.3.2.5 Statistical benchmark and model evaluation

We derived a statistical benchmark (Abramowitz, 2005) for the model by a generalized additive model (GAM) fitting LAI measurements as a function of climate. The fitting used a

cubic spline basis with no interaction. This benchmarking is important because it quantifies the explanatory power of climate for LAI. We compared the model performance to this benchmark in order to determine how much of the information contained in the inputs is captured by the model.

We evaluated the model first at site level with measurements of both LAI and $g_1$. Then, we compared predicted $L_{opt}$ to satellite-derivatives at the scale of the whole continent, and for a sample region in the Northern Territory where there is a natural rainfall gradient spanning ~1700 to ~300 mm (1 mm $km^{-1}$; Cernusak et al., 2011). The predictions should be linearly related to the observations if the model captures the key processes. Assessment of observed increase of LAI in response to rising $C_a$ was done using Advanced Very High Resolution Radiometer (AVHRR) *NDVI* (1982-2010; cf. Donohue et al, 2013). We applied the model to predict the response of $L_{opt}$ and $g_{1.opt}$ to this increase in $C_a$ (holding long-term mean climate constant) and evaluated the predicted response of $L_{opt}$ against these observations.

## 2.4 Results

### 2.4.1 $L_{opt}$ sensitivity to climate

Predicted $L_{opt}$ was driven primarily by $W_{MAP}$ and $D$, with $Q_{PAR}$ and $T_{max}$ modifying the results to a lesser extent. The impact of $W_{MAP}$ was explained by the fact that the rainfall gradient (more than 20-fold) across Australia is much larger than that of $D$, $Q_{PAR}$, or $T_{max}$ (see Figure S1). The influence of $D$ is the result of the sensitivity of light use efficiency to $D$. Assuming fixed $D$, $Q_{PAR}$ and $T_{max}$, and at a given $W_{MAP}$, $P_{gross}$ showed a humped relationship with LAI due to the trade-off with $g_1$; the peak occurred much earlier at lower $W_{MAP}$ (orange lines in Figure 2.1a). Cost increases linearly with increasing LAI and does not vary with $W_{MAP}$ (green line in Figure 2.1a). The optimum $P_{net}$ is reached when the difference between $P_{gross}$ and Cost is maximized (shown as red dots). The predicted sensitivity (slope) of $L_{opt}$ to $W_{MAP}$ was stronger at low $W_{MAP}$ and at low $D$, both of which suggested more severe water limitation (Figure 2.1b). $Q_{PAR}$ increased $L_{opt}$ when water was abundant but slightly decreased $L_{opt}$ as water became limiting (Figure 2.1c; and see Eqn. 4 and S3). $T_{max}$ reduced $L_{opt}$ when water was abundant but slightly increased $L_{opt}$ under water limitation (Figure 2.1d; and see Eqn. S5).

### 2.4.2 Site-scale evaluation of $L_{opt}$

Figure 2.2a shows $L_{opt}$ for Australia and locations of site-scale LAI measurements. $L_{opt}$ was predicted to decrease with increasing aridity index (AI; Figure 2.2b). This response to water

availability was consistent with both ground-based and satellite-derived (MODIS) estimates. Both predicted $L_{opt}$ and MODIS were evaluated against ground-based measurements. $L_{opt}$ had equivalent RMSE (root mean squared error; 1.066 vs. 1.170 $m^2$ $m^{-2}$) but more negative bias (mean of the difference between model and observations; -0.158 vs 0.016 $m^2$ $m^{-2}$) than MODIS, suggesting that the model tended to under-predict in situ estimates, while MODIS was both higher and lower than ground data. Overall, $L_{opt}$ values were of a similar accuracy to satellite estimates when compared to in situ measurements. $L_{opt}$ correlated well with in situ LAI (Figure 2.2c; $R^2 = 0.33$), suggesting that despite the difference in scales between measurements and predictions, in situ LAI may not deviate much from the long-term equilibrium. $L_{opt}$ predictions were also consistent with satellite-derived values (Figure 2.2d; $R^2 = 0.6$). $L_{opt}$ had a non-linear relationship with both sets of measurements, showing that the model performance is close to measurements at low values of LAI but it tends to under-predict at high values of LAI. The model had comparable $R^2$ values to statistical benchmark (GAM fits) of MODIS LAI for the sites (0.6 compared to 0.77; Table 2.3) but worse to that of the situ measurements and climate (0.33 compared to 0.68; Table 2.3). This better agreement with satellite-derived values than with in-situ measurements is most likely to be due to a more consistent spatial sampling footprint between satellite and modelled data (0.06° or ~6 km).

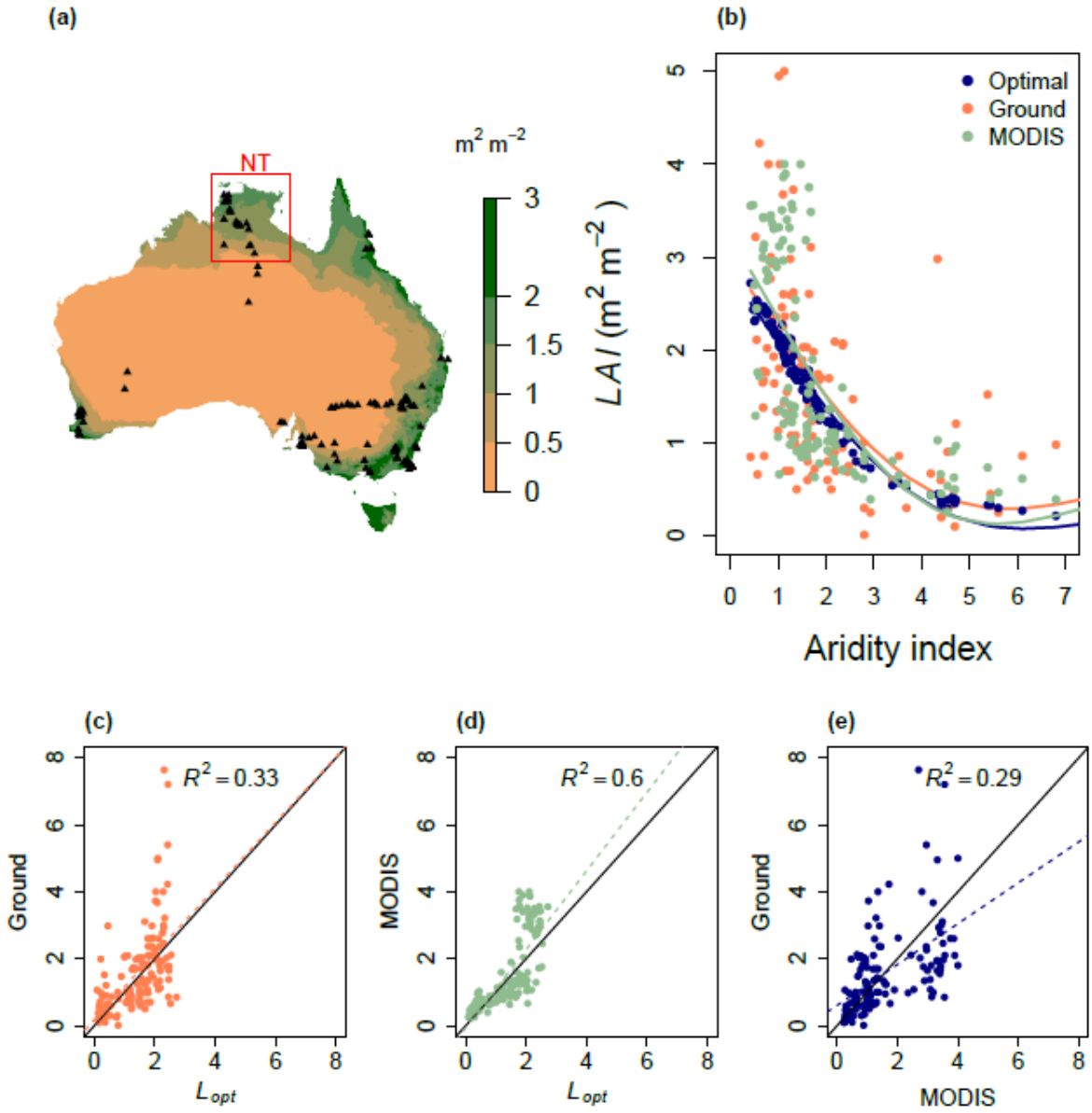


*Figure 2.2. Optimal equilibrium LAI ($L_{opt}$) plotted against AI (aridity index; potential evapotranspiration over mean annual precipitation). Panel (a) shows $L_{opt}$ for Australia, with site locations marked by triangles. Red square marks NT region discussed in section 4.3 and shown in Figure 2.4. Panel (b) shows the mean of optimal, ground, and MODIS LAI of each site (n=135) plotted against AI. Smooth lines are generalized additive model fits. Linear regressions are shown for ground versus $L_{opt}$ (c), MODIS versus $L_{opt}$ (d), and ground versus MODIS (e) with $R^2$. The 1:1 line is shown by a solid line while the colored, dashed lines are regression fits.*

On both site and continent level and in both ground-based measurements and MODIS LAI, four climate inputs already explain most of the variation of LAI ($R^2$ ~0.7) with very little benefits of incorporating soil Nitrogen ($N_{soil}$) and Phosphorus ($P_{soil;}$ Table 2.3). Furthermore, both $N_{soil}$ and $P_{soil}$ correlate with climate data (Table 2.4). However, this is not to argue that soil nutrient is not significant for LAI predictions. Instead, this finding suggests that the impacts of $N_{soil}$ and $P_{soil}$ can be very complicated and unless represented properly, cannot directly benefit the modelling of canopy carbon and water balance.

*Table 2.3. GAM fit to LAI, climate variables, and soil nutrient ($N_{soil}$ and $P_{soil}$). $L_{site}$ means in situ LAI measurements. $MODIS_{site}$ means the nine-year average MODIS LAI for the sites. $MODIS_{cont}$ means the nine-year average MODIS LAI for the Australia.*

| Dependent Variable | Independent Variable | $R^2$ | n |
|---|---|---|---|
| $L_{site}$ | $D$, $W_{MAP}$, $Q_{PAR}$, $T_{max}$ | 0.68 | 134 |
| $L_{site}$ | $D$, $W_{MAP}$, $Q_{PAR}$, $T_{max}$, $N_{soil}$, $P_{soil}$ | 0.71 | 133 |
| $MODIS_{site}$ | $D$, $W_{MAP}$, $Q_{PAR}$, $T_{max}$ | 0.77 | 133 |
| $MODIS_{cont}$ | $D$, $W_{MAP}$, $Q_{PAR}$, $T_{max}$ | 0.81 | 70007 |
| $MODIS_{cont}$ | $D$, $W_{MAP}$, $Q_{PAR}$, $T_{max}$, $N_{soil}$, $P_{soil}$ | 0.83 | 69867 |

*Table 2.4. GAM fit to soil nutrient ($N_{soil}$ and $P_{soil}$) and climate variables over Australia.*

| Dependent Variable | Independent Variable | $R^2$ | n |
|---|---|---|---|
| $N_{soil}$ | $D$, $W_{MAP}$, $Q_{PAR}$, $T_{max}$ | 0.88 | 70488 |
| $P_{soil}$ | $D$, $W_{MAP}$ , $Q_{PAR}$, $T_{max}$ | 0.34 | 70488 |

Since the prediction of $L_{opt}$ is balanced with $g_1$ in the model, we also examined the optimal $g_1$ ($g_{1.opt}$) and in situ estimates to probe our results further (Figure 2.3; site details in Table 2.2). Measured LAI and $g_1$ both declined with increasing AI. Predicted $L_{opt}$ and $g_{1.opt}$ tracked this decline in measured values. The model tended to over-predict LAI but systematically under-predict $g_1$.

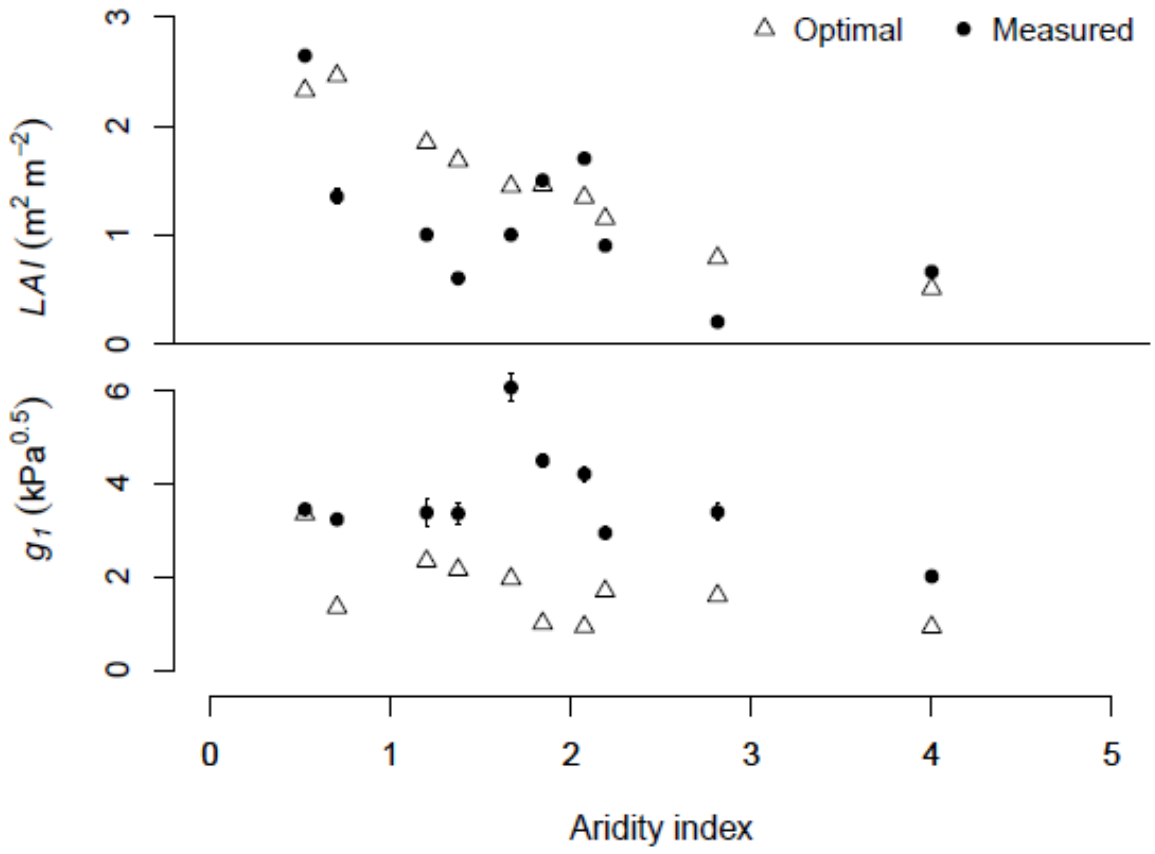


*Figure 2.3. Optimal steady-state LAI ($L_{opt}$) and $g_1$ ($g_{1.opt}$) compared with data from sites across Australia. The error bars show standard errors of measurements.*

### 2.4.3 Continental evaluation

To evaluate model behaviour at larger scales, we compared $L_{opt}$ to satellite-derived estimates across Australian natural reserves (Figure 2.4a). Predicted $L_{opt}$ captured the nine-year average from MODIS with a $R^2$ of 0.7, a bias of -0.022 ($m^2$ $m^{-2}$), and a RMSE of 0.370 ($m^2$ $m^{-2}$). The model tended to slight over-predict LAI in most regions relative to the satellite-derived estimates and under-predict only at extreme wet coastal spots and at extreme dry center (Figure 2.4a). Again, the model had comparable $R^2$ values to the statistical benchmark of MODIS LAI and climate (0.7 versus 0.81; Table 2.3). The non-linear relationship in Figure 2.4b was consistent with the site-scale evaluation (Figure 2.2). Similar to the continental-wide pattern, $L_{opt}$ was lower than MODIS at the extreme dry and wet sites in Northern Territory (Figure 2.4c). However, at the same MODIS LAI, the relative difference was smaller in the drier regions (higher AI; red vs. blue dots in Figure 2.4d).

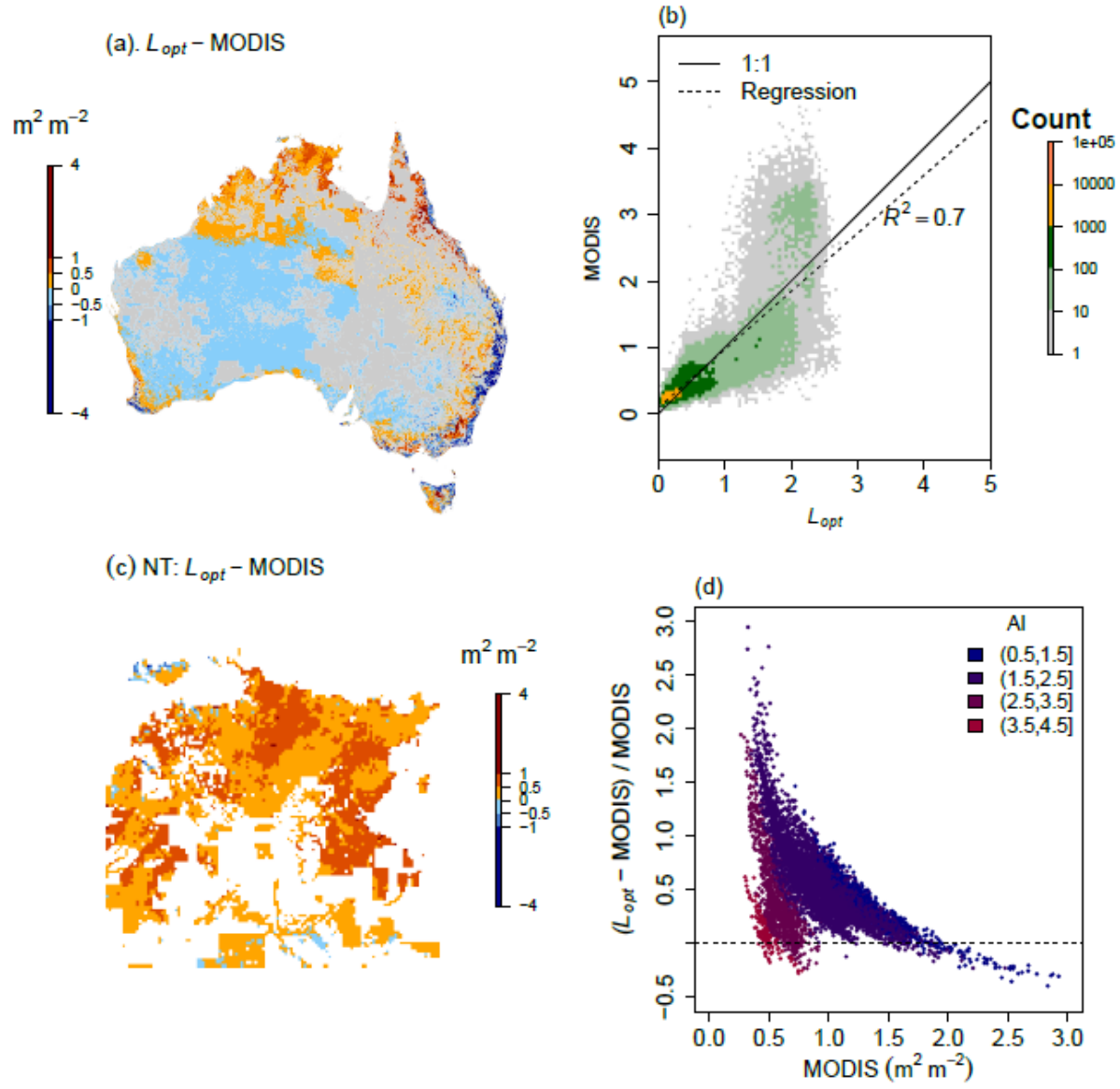


*Figure 2.4. $L_{opt}$ for Australian natural reserves compared to satellite products. Panel (a) $L_{opt}$ for natural reserves across Australia (grey indicates non-reserves). Panel (b) MODIS versus $L_{opt}$ with color-marked density. Panel (c) shows the difference between $L_{opt}$ and MODIS LAI for NT natural reserves. (d) Relative difference between $L_{opt}$ and MODIS LAI of Northern Territory, as function of MODIS LAI, with colors indicating AI.*

### 2.4.4 Change in $L_{opt}$ with elevated $C_a$

To evaluate the modelled LAI response to the recent increase in $C_a$ (340 to 389 µmol mol$^{-1}$), we compared the predictions against Donohue et al. (2013), who calculated the change of the slope of *LAI* against $W_{MAP}$ in the driest areas ($W_{MAP}$ <400 mm yr$^{-1}$) and found a 11.3% increase. We followed the same methodology and found the model predicted a 14.8%

increase of slope. The predicted $L_{opt}$ responses depended on water availability: $L_{opt}$ remained relatively insensitive to $C_a$ in wet areas while it increased by up to 20% in dry areas (Figure 2.5a). We then used the model to predict the response to future changes (a doubling of $C_a$ from 340 to 680 µmol mol$^{-1}$). The impact of future $CO_2$ fertilization on model predictions was also determined by water availability: in the mesic regions (e.g. $W_{MAP}$ = 1200 mm; $D$ = 0.5 kPa), a doubling of $C_a$ (340 to 680 µmol mol$^{-1}$) raised $L_{opt}$ by ~20% compared to a >100% increase in xeric regions (e.g. $W_{MAP}$ = 400 mm; $D$ = 3 kPa; Figure 2.5b).

We also examined how $g_{1.opt}$ is predicted to change with increased $C_a$ (340 to 389). On average, $g_{1.opt}$ was predicted to be reduced by ~7.98% (change of geometric mean) across Australia (Figure 2.5c), but the direction of change differed in dry versus wet areas. In dry areas, elevated $C_a$ reduced $g_{1.opt}$ (blue region in Fig 3c and orange lines in Fig 3d) while in wet areas, $g_{1.opt}$ was predicted to increase (~20%) increased with rising $C_a$ (red region in Fig 3c and blue lines in Fig 3d). Since the predicted percentage increase of LAI and $g_1$ to elevated $C_a$ was nearly linear in both dry and wet conditions (Figure 2.5 b and d dashed lines), responses of LAI and $g_1$ to rising $C_a$ should follow the current trajectories at least to $C_a$ ~ 680 µmol mol$^{-1}$.

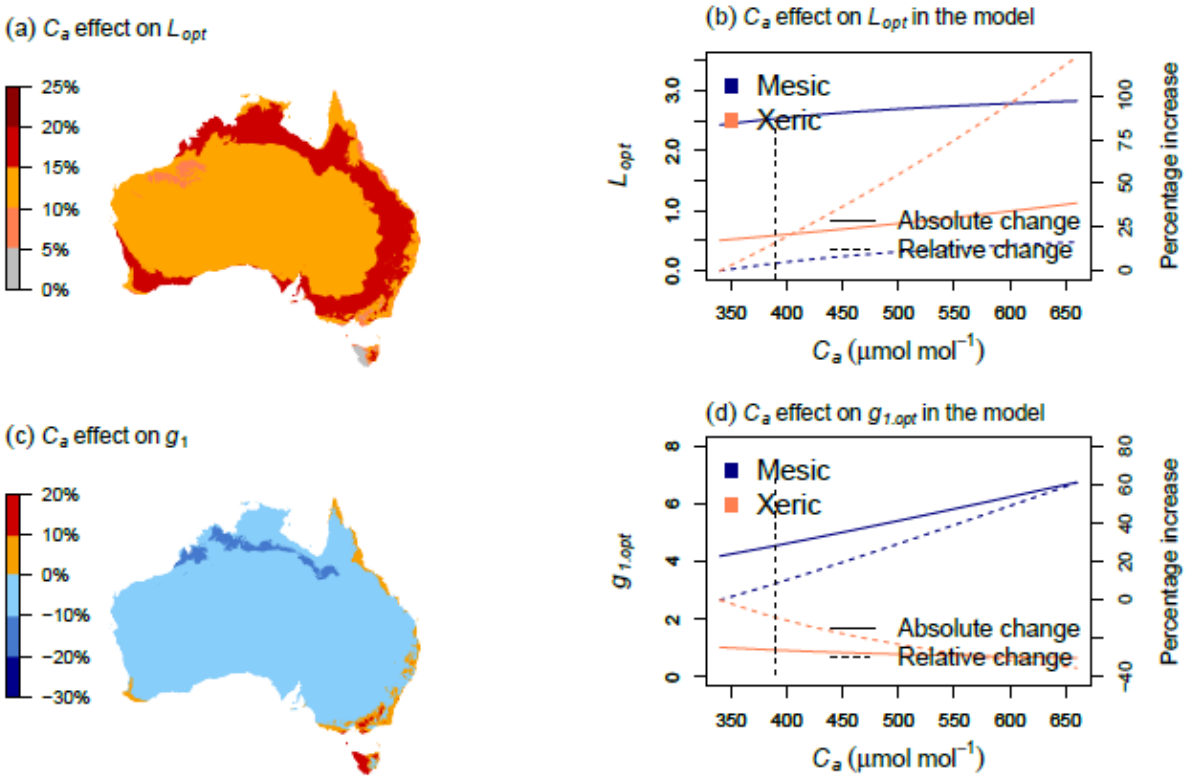


*Figure 2.5. (a) Predicted effect of the 1980-2012 increase in $C_a$ (from 340 to 389 µmol mol$^{-1}$) on $L_{opt}$ in Australia. Panel (b) shows that doubling $C_a$ (340 to 680 µmol mol$^{-1}$) stimulates $L_{opt}$ in the xeric regions by over 100% (orange dashed line) while ~20% in mesic regions (blue dashed line). The dotted vertical lines mark 389 µmol mol$^{-1}$corresponding to (a). (c) Predicted response of $g_1$.opt to the 1980-2012 increase in $C_a$. Panel (d) shows that doubling $C_a$ (340 to 680 µmol mol$^{-1}$) has different effects on $g_1$ depending on water availability.*

The effect of rise in $C_a$ may compensate the negative impacts of rise in $D$ in the model (Figure 2.6). At a $C_a$ of 350 µmol mol$^{-1}$, the model predicted that $L_{opt}$ could maintain above 2 m$^2$ m$^{-2}$ when $D$ remains below 1.5 kPa (Figure 2.6a). If the $C_a$ rises to 650 µmol mol$^{-1}$, to have the same $L_{opt}$ above 2 m$^2$ m$^{-2}$, $D$ could be >3 kPa. However, the contour lines became thinner at high $C_a$, suggesting that the sensitivity of $L_{opt}$ to $C_a$ is diminishing (right to left in Figure 2.6a). The same compensating effect is also predicted for $g_{1.opt}$, but the contour lines became denser at high $C_a$, highlighting an increasing sensitivity of $g_{1.opt}$ to $C_a$ (right to left in Figure 2.6b). Overall, the model predicted that plants would shift strategy from LAI regulation to stomatal regulation with rise in $C_a$.

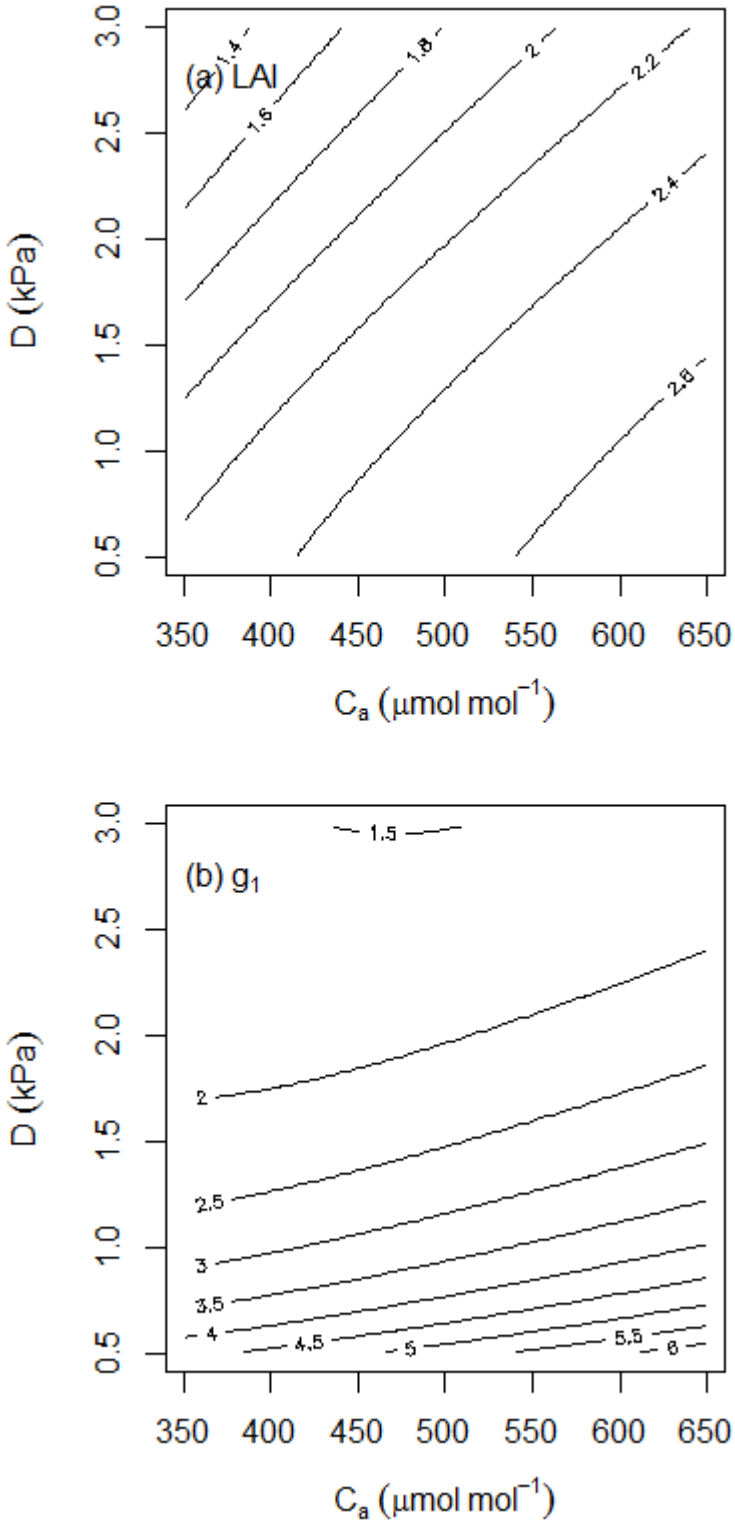


*Figure 2.6. Contour plot of change of optimal LAI and $g_1$ with atmospheric $CO_2$ concentration ($C_a$) and vapour pressure deficit (D) but constant mean annual precipitation (1000 mm yr$^{-1}$), maximum temperature (30°C), and photosynthetically active radiation (3000 MJ m$^{-2}$ s$^{-1}$).*

## 2.5 Discussion

### 2.5.1 Model performance

Predicting LAI is an important yet challenging step in the simulation of carbon and water fluxes, especially under climate change and rising $C_a$. We found that a parsimonious optimality model incorporating the concept of ecohydrological equilibrium could successfully predict long-term average LAI across the Australian continent. This theory is thus a promising approach to incorporate into existing terrestrial biosphere models (TBMs) to improve predictions of foliage carbon allocation and LAI.

The optimality model showed good agreement with ground-based and satellite measurements. Previous assessments of satellite-derived products suggested a $R^2$ of 0.56-0.85 among products (Hill et al., 2006; Garrigues et al., 2008; Yuan et al., 2011; Fang et al., 2012 and 2013). The model thus had a $R^2$ comparable to that of satellite inter-product assessments. Our results suggested that LAI could be adequately predicted from consideration of the ecohydrological equilibrium. Since $L_{opt}$ captured long-term mean MODIS, it should be possible to use $L_{opt}$ in TBMs to reduce the current differences among models and satellite-derived products. The $L_{opt}$ could, for example, be used as a target LAI for allocation routines, around which modelled LAI would vary dynamically according to phenology. Phenological variation of LAI could potentially be accounted for with a satellite-derived climatology (e.g., Broxton et al., 2014) or linked to existing process-based or optimization phenology models (e.g., Caldararu et al., 2014).

Although the model performed well overall, there was a discrepancy for high-LAI systems (Fig. 2.4b). The predicted $L_{opt}$ saturated at ca. 3 $m^2$ $m^{-2}$ while the observed values continued to increase. There are several potential causes for the discrepancy between our parsimonious model and observations at high LAI. Firstly, $R_m$, which is assumed to be a constant, might be lower in higher-rainfall regions (Supplementary Material for Chapter 2). However, there is relatively little evidence to support such a variation in $R_m$ and the mechanism which would cause reduced $R_m$ with higher water availability is not clear. In addition, nutrient limitation may be more important in regions with high LAI, and thus consideration of nutrient availability may be necessary in these areas (McMurtrie and Dewar, 2013). Furthermore, the model does not take into account the decoupling between the vegetation and boundary layer, which may be significant in high-LAI systems (De Kauwe et al., 2017). These limitations of

our simple, parsimonious approach could potentially be overcome if the theory were implemented in a TBM which treats these processes in more detail.

One key reason why our model improves LAI predictions is that it allows for variation in $g_1$ (via $g_s$) strategies in different climates. Lin et al. (2015) found, based on an analysis of a large database of leaf gas exchange measurements, that $g_1$ varies with climate and plant functional type. Previous optimal LAI models either fixed stomatal behaviour (Kergoat et al., 2002; Woodward and Lomas, 2004) or considered trade-offs between $g_s$ and LAI (McMurtrie et al., 2008). Our approach optimized $g_1$ simultaneously with LAI and thus represented a more realistic tradeoff between the canopy (LAI) and leaf-level ($g_1$) water use strategies. These predictions also potentially provide a means to inform TBMs parameterization of $g_1$ – currently using fixed parameters.

The pattern of $g_{1.opt}$ agreed well with measurements, although there was a tendency to under-predict. There may be several reasons for this under-prediction. First, $g_{1.opt}$ is the ecosystem average $g_1$ instead of only upper-canopy values. Consequently, one potential reason for overprediction of $g_1$ at site scale is that measurements focus on the upper canopy. $g_1$ varies with light availability and thus should be higher under light limitation (Campany et al., 2016). Another potential reason is the disagreement between $g_1$ estimates on different scales: plant water use efficiency (a function of $g_1$; Eqn S1.) measured on leaf and canopy scales were statistically different (Knauer et al., 2017; Medlyn et al., 2017). Moreover, the under-prediction of $g_1$ suggests that there may be potentially other trait-related costs (e.g. stem and root respiration and construction) that are currently unaccounted for in the model. The temporal distribution of rainfall may also add to the difference between observed and modelled $g_1$ as stomatal conductance should respond not only to the amount of rainfall but also to the frequency (Lu et al., 2016).

An important benefit of this model is the ability to provide climate-constrained estimates of long-term changes in LAI with respect to increasing $C_a$. The increase of $L_{opt}$ predicted by the model to rising $C_a$ was consistent with satellite-derived observations. This evaluation focused on the effect of increased $C_a$ alone; we assumed no change in long-term mean climate with rising $C_a$. The change of $C_a$ during the evaluation period was accompanied by an average +7% of $M_{MAP}$ (Donohue et al., 2009) and +8% $D$ (Donohue et al., 2013). We did not consider these changes here because the impact of the $M_{MAP}$ and $D$ roughly canceled. However, in future, rising $C_a$ could be accompanied by larger changes in $M_{MAP}$. The sensitivity of $L_{opt}$ to water availability in Australia suggests that the uncertainty in climate

predictions of rainfall for Australia (e.g. ±100% with large inter-model variations (Mehran et al. 2014)) could very likely transfer into uncertain vegetation feedbacks through changes in LAI.

The model also provides insights into the trade-off between LAI and $g_1$ in the context of rising $C_a$. Previous studies of stomatal behaviour (Manzoni et al., 2013; Lu et al., 2016; Wolf et al., 2016; Prentice et al., 2014) have examined leaf-scale optimization but generally do not consider whole-plant trade-offs such as the balance between stomatal conductance and LAI (but see Kelly et al., 2015). Leaf-scale optimization models generally predict no change in $g_1$ under elevated $C_a$. As a result, larger scale studies have also assumed constant $g_1$ with increasing $C_a$ when assessing LAI responses (e.g. Yang et al., 2016; Cheng et al., 2017; Donohue et al., 2017). Here, the predicted $g_{1.opt}$ had distinct responses to rising $C_a$ under different water availability scenarios. Under dry conditions, the model predicted reduced $g_{1.opt}$ and increased $L_{opt}$ with elevated $C_a$, suggesting that it is beneficial for the plant to use the increased available C to grow leaves. Increased LAI in water-limited areas brings a double benefit to the plant because it increases both the transpiration fraction (Eqn. 1) and PAR interception (Eqn. S8 a and b). Reduced $g_1$ also indicates a decrease in the marginal carbon cost of water (Cowan and Farquhar, 1977), which suggests that elevated $C_a$ releases water stress to some extent. Under wetter conditions, both $g_{1.opt}$ and $L_{opt}$ and predicted to increase slowly with rising $C_a$, indicating the diminishing return from increasing $C_a$ with increasing water availability. Both the direction and the magnitude of $g_1$ responses to $C_a$ under different water availability are consistent with the findings in Schymanski et al. (2015), who predicted that marginal carbon cost of water would reduce by ~14% in a dry site but increase ~13% in a wet site with 20% increase of $C_a$. The predicted change in $g_{1.opt}$ with $C_a$ adds to our general understanding of marginal carbon cost of water use: Previous meta-analyses of elevated $C_a$ experiments found overall no change in $g_1$ with increasing $C_a$ (e.g., Medlyn et al. 2001; Ainsworth & Rogers 2007; but see Keenan et al, 2013), but also indicated variation across experiments. Our model specifically predicts that $g_1$ would increase with increased $C_a$ in wet conditions, and decrease in dry conditions— a testable hypothesis.

### 2.5.2 Alternative model assumptions

Our optimality model included two important empirical assumptions: (1) plant transpiration is constrained to be a function of mean annual precipitation and leaf area index (Eqn. 1 and 2); and (2) maintenance respiration, leaf mass per area, and life lifespan do not vary with

climate. We tested alternative assumptions in each of these two areas, but none led to better model performance (Supplementary Material for Chapter 2). The model prioritized parsimony and did not incorporate assumptions that did not improve model performance. However, these parameters are inputs to the model and thus can be changed upon the emergence of new theories and evidence.

Water availability to the plant, or transpiration in the model, is crucial to model predictions. The model showed that $L_{opt}$ was sensitive to water input and thus the uncertainty in water availability contributed to the errors in the predictions. Water resources such as ground water and surface flow are not included in the model but can be used for transpiration in certain regions (Evaristo et al., 2015; Liu et al., 2017). Topography has impacts on local water availability and thus plant water use strategies (Méndez-Toribio et al., 2017). Incorporation of the ecohydrological equilibrium theory into a more detailed TBM which accounts for topography and soil type would allow these effects to be incorporated in LAI predictions.

The temporal variation of water availability is also important to determine equilibrium LAI. In extreme cases such as tropical savanna in the Northern Territory, the majority of rainfall falls during the wet half of the year (Cernusak et al., 2011). The equilibrium LAI for average rainfall in dry and wet seasons would be very different. Indeed, the model agreed more with the long-term average MODIS LAI estimates than ground-based LAI, which are typically one-off measurements (Figure 2), suggesting the potential importance of variability of water availability and other parameters (e.g., respiration). Here, we used an annual time step for simplicity. However, in strongly seasonal rainfall environments, it may be more appropriate to evaluate $L_{opt}$ on sub-annual time-scales. Hence, we aim to predict optimal seasonality along with $L_{opt}$ in future developments of the model.

Existing models could yield high quality soil moisture predictions and thus help improve the prediction of LAI seasonality. For instance, Tian et al. (2019) used soil moisture to predict the near-future (months) vegetation greenness in global dry lands. This new development suggests potential to incorporate the optimality modelling framework and realistic soil moisture models to capture the feedback between soil water and vegetation in the future.

Empirical studies have suggested variation in the four plant traits used in the model ($R_m$, $J_{max}$, $M_{area}$, and $t_f$) with climate (Wright et al., 2004; Ali et al., 2015; Atkin et al., 2015; Dong et al., 2017). This variation is potentially important to modelling carbon and water (Pappas et al., 2016). We examined existing data sets for these relationships but only found weak

correlations, which when implemented into the model did not improve model performance nor substantially modify model behaviour (Supplementary Material for Chapter 2). We also did not discover any relationship between our literature-compiled values of $J_{max}$ across Australia and climate (Figure S.5). Consequently, we assumed here that $R_m$, $J_{max}$, $M_{area}$, and $t_f$ were independent of climate. However, including empirical relationships between these parameters and $W_{MAP}$ tends to increase predicted LAI where high LAI is observed (Figures A2, A3). As a result, including variable parameters may help reduce the discrepancy between the modelled and observed LAI at high LAI (Figure 2.4d). New datasets and theories for variation in traits with climate are emerging: the correlation between plant traits and climate could be explained by physiological trade-offs (Onoda et al., 2017) and thus should be predictable by optimality models (e.g. Xu et al., 2017). The model is flexible enough to incorporate these new theories.

There is substantial evidence that leaf photosynthesis and respiration rates depend on leaf nitrogen content (Ryan, 1991; Norby et al., 2016). Nitrogen and phosphorus limitation have been suggested to be particularly common in Australian ecosystems due to the old, weathered soils (Wild 1958; Chapin et al., 1986; Elser et al., 2007; Ellsworth et al., 2017). The lack of representation of nutrient limitation may contribute to the under-prediction at high LAI seen in Fig.4d. McMurtrie et al. (2008) included a dependence of photosynthetic rate on leaf nitrogen content, and considered the three-way trade-off between leaf nitrogen, stomatal conductance and LAI. However, their approach requires knowledge of the canopy nitrogen uptake rate, which precludes application at the continental scale. To determine whether omitting nutrient availability impacts model success, we fitted GAMs to observed LAI and climate, with and without soil nitrogen and phosphorus as predictor variables. We found that including soil nutrients in the GAM did not capture more variation of measured LAI (Table 2.3). We also found that the water and carbon constrained $L_{opt}$ agreed with existing data well, despite not incorporating the impacts of nutrient limitation. However, this result does not invalidate the importance of nutrient limitation, due to correlations between soil nutrient availability and water availability (Table 2.4). The impacts of nutrient limitations thus may already be incorporated in the water limitation.

$J_{max}$ and $R_m$ are known to be sensitive to temperature in the short-term, but here we ignored this temperature dependence because both $J_{max}$ and $R_m$ have been reported to acclimate to growth temperature (Smith et al., 2015; Aspinwall et al., 2016; Reich et al., 2016). We found no correlation between $J_{max}$ and $R_m$ with temperature (Text S.2. Maintenance respiration;

Figure S.5). As a result, we decided to use constant values of $J_{max}$ and $R_m$. Temperature dependence could be explored further in future; the model is flexible and could adopt a temperature dependence if necessary.

## 2.6 Conclusion

We showed that a parsimonious optimization model incorporating ecohydrological theory can accurately predict long-term average LAI in Australian ecosystems. The inputs (i.e., climate) and outputs (i.e., LAI and $g_1$) of the model are all being measured and thus enable convenient application and evaluation. Although set to be constant or calculated via empirical equations, all the parameters used in the model can be taken as inputs enabling accommodation to different purposes of studies. This approach could readily be incorporated into vegetation models to set a target long-term LAI, with the short-term variation modified as a function of water balance dynamics and phenology. Although the evaluation is limited to Australia, these findings may also apply to other water-limited ecosystems. Consequently, we suggest that terrestrial biosphere models could constrain leaf area predictions under climate change and rising $C_a$ in water-limited regions to realistic values by incorporating a climate-constrained trade-off between leaf area and canopy conductance into their foliage sub-model.

## Chapter 3. Incorporating non-stomatal limitation improves the performance of leaf and canopy models at high vapour pressure deficit

### 3.1 Abstract

Vapour pressure deficit (*D*) is projected to increase in the future as global temperatures rises. Higher *D* will reduce stomatal conductance ($g_s$) and potentially photosynthesis (*A*), both of which are key to the terrestrial carbon, water, and energy balance. It is thus important to test whether gas exchange models capture the responses of $g_s$ and *A* at high *D*.

I tested a series of coupled *A*-$g_s$ models against leaf gas exchange measurements from the Cumberland Plain Woodland (Australia), where *D* regularly exceeds 2 kPa, and can reach 7 kPa in summer. I first showed that the commonly used $g_s$ models (Leuning, 1995 and Medlyn et al., 2011) did not capture the observed decrease in *A* and $g_s$ with increasing *D* in leaf-scale measurements. I then tested two alternative hypotheses to explain this decrease: hydraulic limitation (i.e., plant downregulate $g_s$ and/or *A* due to insufficient water supply) and non-stomatal limitation (i.e., direct downregulation of photosynthesis). Here, the results show that the model incorporating non-stomatal limitation captured the observations with high fidelity and least number of parameters. The model incorporating plant hydraulics (Tuzet et al. 2003) could capture the observed *A* and $g_s$, but it did so via an incorrect mechanism, as evident in unrealistic leaf water potential predictions.

I incorporated a non-stomatal limitation and the Medlyn et al. (2011) $g_s$ model into the stand scale model MAESTRA. This modification reduced the over-prediction of transpiration, significantly improving predictions when compared sap flow measurements ($R^2$ = 0.87 vs. 0.64). With the projected increase of *D*, these findings suggest that future models need to incorporate non-stomatal limitation to accurately simulate *A* and $g_s$ in the future.

### 3.2 Introduction

Vapour pressure deficit ($D$) is the difference between the amount of water vapour that the air can hold at saturation ($e_s$) and the actual amount of water vapour in the air ($e_a$). As temperatures rise, $e_s$ increases exponentially and as result, $D$ is projected to increase strongly into the future. At the leaf-level, $D$ is the driving force of transpiration, but as $D$ increases and water supply becomes limiting, stomates adjust their aperture to regulate the flow of water vapour, which inevitable affects photosynthesis. This vegetation-climate feedback due to reduced stomatal conductance ($g_s$) has important implications for the global carbon-climate predictions (Reichstein et al., 2013; Will et al., 2013). Thus, it is important to understand the response of the vegetation to the projected increase in $D$ (Novick et al., 2016).

The challenges involved in modelling $g_s$ at high $D$ have been discussed since the late 1970's (Cowan, 1978; Farquhar, 1978). As described by Monteith (1995), there is a three-phase response of $g_s$ to $D$: (i) Regime A, where $g_s$ declines with $D$, resulting in a nearly linear increase of transpiration ($E$) with $D$; (ii) Regime B, where $g_s$ declines non-linearly with $D$, resulting in a turnover of $E$ (i.e., with increasing $D$, $E$ increases initially but declines at high $D$); and (iii) Regime C, where $g_s$ does not respond to $D$ due to extremely humid air. Regime A is the most commonly observed pattern and happens at intermediate $D$. It also represents the range of leaf-level measurements most commonly used to parameterise models of $g_s$ (e.g., Ball et al., 1987; Leuning, 1995; Medlyn et al., 2011). Regime B takes place at higher $D$ ($D$ > 2 kPa), which is typically rare in humid ecosystems but common in hot and dry ones (e.g., Franks et al., 1997; Thomas and Eamus, 1999; MacFarlane et al., 2004; Whitley et al., 2013; Gimeno et al., 2018; Renchon et al., 2018).

Notably, Regime B is also where the largest differences among $g_s$ models occur. Current representations of $g_s$ in terrestrial biosphere models differ in their sensitivity to $D$, especially at $D$ > 2 kPa (De Kauwe et al., 2015; Knauer et al., 2015; Franks et al., 2017). The model of Leuning (1995) has a strong $D$-dependence ($g_s$ depends on the reciprocal of $D$), which can yield a reduction in $E$ at high $D$ depending on parameter values. However, it can be difficult to obtain parameter values that allow the model to fit data at both high and low $D$ (Duursma et al., 2014). Alternatively, Medlyn et al. (2011) proposed an optimality model, in which $g_s$ depends on the reciprocal of $D^{0.5}$. Due to this lower sensitivity of $g_s$ to $D$, the Medlyn model does not always predict a reduction in $E$ at high $D$ (i.e., Regime B).

It has been proposed that the cause of Regime B could be a hydraulic limitation (Buckley, 2005). When water supply from the soil is insufficient to meet demand, plants typically reduce $g_s$, with a consequent reduction in photosynthesis. I explored this hypothesis with a model coupling $g_s$ to leaf water potential ($\psi_L$; Tuzet et al. 2003). This model was proposed because experimental observations show that $g_s$ is strongly linked to guard cell and epidermal turgor (e.g., Franks et al., 1998; Franks, 2004) and not simply environmental conditions (i.e., *D*), which is the underlying hypothesis in the Medlyn and Leuning coupled models. Although the Medlyn and Leuning models are usually employed with a water stress modifier (e.g., those used in the Community Atmosphere Biosphere Land Exchange (CABLE) land surface model (Kowalczyk et al., 2015) or the Sheffield Dynamics Global Vegetation Model (Woodward et al., 1995)), this modifier is usually related to soil water status, which has little diurnal variation, while the Tuzet model considers $\psi_L$, which varies strongly over the course of a day. The $\psi_L$ should be determined by the balance of plant water use via stomata and the supply, which is usually calculated with Darcy's Law as the product of hydraulic conductance and the difference between leaf and soil water potentials. $\psi_L$ is then solved iteratively by balancing the use and supply. If the hydraulic conductance is held constant, the Tuzet model will not yield a decline in transpiration at high *D* because a reduction in $\psi_L$ cannot occur at the same time as a reduction in transpiration (Farquhar 1978). However, a reduction in transpiration can occur if there is a loss of hydraulic conductance with low $\psi_L$ due to cavitation (Tyree and Sperry, 1989). As the $\psi_L$ gets more negative, the pressure gradient between the soil and leaf is larger but the hydraulic conductance becomes lower because of cavitation. At a very negative $\psi_L$, the net effect can lead to a reduction in water supply and thus allows a decrease in transpiration, $g_s$ and photosynthesis. Although theoretically plausible, the hydraulic limitation hypothesis has not been extensively tested against observations.

An alternative hypothesis to explain the response at high *D* is that the reduction in transpiration is associated with non-stomatal limitation to photosynthesis. For example, Duursma et al. (2014) proposed that the turnover in *E* at high *D* is actually driven by a decrease in carboxylation capacity ($V_{cmax}$) at the high temperatures that normally accompany high *D*. This reduction in $V_{cmax}$ causes a reduction in photosynthesis, which drives a reduction in $g_s$ in both Leuning and Medlyn stomatal models and captured the observations from a whole tree chamber experiment. Low leaf water potential at high *D* could potentially reduce photosynthetic capacity further via a reduction in either carboxylation capacity or mesophyll

conductance (Tezara et al., 1999; Lawlor and Cornic, 2002; Lawlor and Tezara, 2009), which subsequently drives a coupled reduction in $g_s$. Such an effect is increasingly reported in soil drought studies (e.g., Zhou et al., 2013 and 2014; Verhoef and Egea, 2014; Drake et al., 2017). Incorporating this effect into terrestrial biosphere models (TBMs) has led to improved predictions of soil drought responses (Keenan et al., 2010, Verhoef and Egea, 2014; De Kauwe et al., 2015; Drake et al., 2017a). Although these studies have shown the importance of non-stomatal limitation under soil drought, it is unclear whether high *D* can cause the same non-stomatal limitation.

A test against measurements is necessary to show whether the current leaf-level models embedded within TBMs can capture the high *D* response of both $g_s$ and photosynthesis. The goal of this study was thus to improve the representations of *D* response in forests. I tested a series of plausible modelling approaches at a woodland site where *D* reaches high level every summer (mean daily maximum = 2.7 kPa; overall maximum = 8 kPa). Previous studies at, or close to, the site provided the opportunity to evaluate the models and hypotheses across a range of scales. At the leaf scale, gas exchange measurements at the site showed a reduction in $g_s$ and photosynthesis with increasing *D* (Gimeno et al., 2016). Whole-tree scale transpiration estimations showed that transpiration decreased with *D* at high *D* (Gimeno et al., 2018). Here I evaluated the current $g_s$ models, and models incorporating hydraulic and non-stomatal limitations. I then implemented the best model into a canopy scale model to explore the improvements at whole-tree scale. The results from this study should inform with TBMs with key factor(s) the controls the response of the coupled *A*- $g_s$ model to rising *D*.

### 3.3 Methods

I tested five coupled $g_s$-photosynthesis models in this study (Table 3.1): (i) the Medlyn model (Medlyn et al., 2011), which is derived from optimal stomatal theory and assumes that $g_s$ depends on the reciprocal of $D^{0.5}$; (ii) the Leuning model (Leuning, 1995), which has a similar functional form to the Medlyn model but assumes a different $g_s$ sensitivity to *D*; (iii) the Tuzet stomatal model (Tuzet et al., 2003), which assumes a sensitivity to leaf water potential $\psi_L$ , incorporating a reduction of hydraulic conductance with low $\psi_L$ (hereafter referred as Tuzet K-PSI); (iv) the Tuzet stomatal model, but incorporating a non-stomatal limitation that increases at low $\psi_L$ (hereafter referred as Tuzet V-PSI); and (v) the Medlyn model, incorporating a non-stomatal limitation that increases with *D* (hereafter referred as Medlyn V-*D*). These five model combinations were chosen to test the following alternative hypotheses. The comparison between the performance of Medlyn and Leuning model tests

whether increasing the sensitivity of $g_s$ to *D* improves model performance. The Tuzet K-PSI model was chosen to test whether considering a hydraulic limitation improved model performance. The comparison between the Tuzet V-PSI and Medlyn V-*D* models was designed to explore the best way to represent non-stomatal limitation and to test whether this assumption was necessary to improve predictions at high *D.*

I first evaluated these five leaf-scale models against leaf gas exchange data, which were measured *in situ* at a range of *D* values. The best model at the leaf scale was then implemented into a canopy-scale model MAESTRA (Duursma et al., 2012), and I evaluated whether it improved the model's ability to capture *D* responses at the canopy scale. The following sections describe: (i) the sites where data were collected; (ii) how data was collected and processed; (iii) the leaf scale models tested; (iv) the parameterization of the tested models; and (v) the canopy-scale model used for evaluation at the whole-tree scale.

### 3.3.1 Sites

Data were obtained from two sites in the Cumberland Plain Woodland. The first site is the Free Air $CO_2$ Enrichment site (EucFACE), western Sydney, Australia (33.62ºS, 150.73º*E*, species = *Eucalyptus tereticornis*), which consists of six circular plots (referred to as "rings" hereafter), each of which has a diameter of 25 m. The rings receive two $CO_2$ treatments (Gimeno et al., 2016): control (ambient $CO_2 \approx 400$ μmol $mol^{-1}$) and experimental (+150 μmol $mol^{-1}$ $CO_2$). I used data from both treatments for this study. The data under elevated $CO_2$ were included in this study because: (i) $CO_2$ should not affect the model performance; (ii) a larger sample size increased the statistical power of the conclusions. Meteorological data measured at EucFACE during the measurement period are shown in Figure 3.1. The second site is in the Castlereagh Natural reserve, Sydney, Australia (Zeppel et al., 2008). This site is 10 km south of EucFACE (species = *E. parramattensis*; a species closely related to *E. tereticornis*).

### 3.3.2 Data

This study used three types of data: leaf gas exchange (Zeppel et al., 2008; Gimeno et al., 2016), xylem vulnerability, and sap flow (Zeppel et al., 2008; Gimeno et al., 2018). Leaf gas exchange and xylem cavitation data were used in parameterization as well as evaluation of the $g_s$ models. Sap flow data were used in whole-tree scale evaluations.

Diurnal gas exchange measurements were made throughout the day under prevailing field conditions using a LiCOR 6400 at EucFACE (Gimeno et al., 2016) and a LCpro+ system

(ADC BioScientific, Hoddesdon, UK) at Castlereagh (Zeppel et al., 2008). Canopy access at EucFACE was provided by a crane (canopy height = 20m) whereas canopy access at Castlereagh was provided by portable rising work platform (canopy height = 2-8m). The EucFACE data were measured at saturating photosynthetically active radiation (~1800 μmol $m^{-2}$ $s^{-1}$). The Castlereagh data were measured at ambient light level, so I chose data with saturating light only (>1200 μmol $m^{-2}$ $s^{-1}$). At EucFACE, leaf water potential measurements at pre-dawn, morning (9:30-11:30), and midday (13:00-15:00) were also made by Gimeno et al. (2016). The EucFACE diurnal data set contains ambient measurements in ambient rings under both ambient $C_a$ (400 μmol $mol^{-1}$) and measurements in elevated rings under elevated $C_a$ (550 μmol $mol^{-1}$). All these measurements as well as all the data from elevated rings in EucFACE were included in this study.

At EucFACE, gas exchange measurements also included photosynthesis-$CO_2$ response (A-Ci). There were repeated A-Ci curves corresponding to the four diurnal gas exchange campaigns in EucFACE (Crous et al., in prep.). These measurements were made in the same month as the diurnal gas exchange measurements described above and were used to calculate the maximum electron transport rate ($J_{max}$; μ mol $m^{-2}$ $s^{-1}$) and carboxylation capacity ($V_{cmax}$; μ mol $m^{-2}$ $s^{-1}$). Values were averaged by ring and date. The $J_{max}$ and $V_{cmax}$ are estimated with "fitacis" function (*planecophys* R package; Duursma 2015). The temperature dependences of the $J_{max}$ and $V_{cmax}$ were obtained from another set of A-Ci curves, measured at a range of leaf temperatures (20-40 ºC) during February 2016. I fitted peaked Arrhenius functions (Medlyn et al., 2002) to values of $J_{max}$ and $V_{cmax}$ to parameterise their temperature dependences; all other values of $J_{max}$ and $V_{cmax}$ were corrected to 25 ºC using these relationships and were averaged for each ring on each measurement date. I also estimated apparent $V_{cmax}$ from the diurnal measurements using the "one-point method" (De Kauwe et al. 2016). As a result, each diurnal measurement corresponded to a modelled $V_{cmax}$ based on A-Ci curve data and the temperature response, and an apparent $V_{cmax}$ based on the "one-point method".

A hydraulic vulnerability curve for *E. tereticornis* was constructed using benchtop dehydration (Peters, pers.comm.). Two-metre-long branches were excised from mature canopy trees at EucFACE. Collections were made in the early morning (between first light and sunrise). Branches were placed in large plastic rubbish bags with moist towels to prevent dehydration and cut ends were recut under water and allowed to rehydrate. Branches were transported in water and were stored in a cool room 24 hour before measurements. Stem percent loss of conductivity was measured using hydraulic flow measurements on

increasingly dehydrated branches using a flowmeter (Liqui-Flow L10, Bronkhorst High-Tech BV, Ruurlo, Gelderland, Netherlands) at low pressure (< 4kPa). Four to six stem segments were measured per large branch at progressively lower water potentials. To quantify the impact of cavitation for the Tuzet models, a Weibull function following Ogle et al. (2009) was fitted to produce a vulnerability curve using the 'fitplc' function (*fitplc* R package; Duursma and Choat, 2017).

At EucFACE, transpiration was estimated with sap flow measurements by Gimeno et al. (2018). The measurements (custom-built three-probe heat-pulse sensors) sampled two positions on each tree, from three trees per ring. Data from all six rings were used. The data were upscaled to estimate stand averages using sap wood area allometrically calculated with measured stem diameter. The volumetric soil water content ($\theta$) of the site was measured fortnightly using neutron probes and aggregated to the top 50 cm at 25 cm interval (Figure 3.2). Sapflow at Castlereagh site was obtained from (Zeppel et al., 2008). The measurements used two-probe heat pulse sensors and sampled six trees with two sensors per tree from June to December 2006. The corresponding soil moisture measurements of Castlereagh were recorded with an array of frequency domain reflectometry sensors (Theta Probe, ML2-X; Delta-T devices, Cambridge,UK) for the top 70cm.

### 3.3.3 Models tested

In this chapter, I tested four stomatal conductance models in combination with the leaf photosynthesis model of Farquhar et al. (1980). Here I will focus on the stomatal conductance models. The photosynthesis model is described in detail in Chapter 4.

I chose the Medlyn model as the baseline stomatal conductance model because it requires the fewest parameters (Medlyn et al., 2011):

$$g_s = 1.6 \cdot \left(1 + \frac{g_{1M}}{\sqrt{D}}\right) \cdot \frac{A}{C_a} \quad (1)$$

where $g_s$ is the stomatal conductance to water vapour (mol $m^{-2}$ $s^{-1}$); $g_{1M}$ is the optimal stomatal behaviour parameter ($kPa^{0.5}$; see detailed explanation in Medlyn et al., (2011)); $A$ is the $CO_2$ assimilation rate (μmol $m^{-2}$ $s^{-1}$); $C_a$ is the atmospheric $CO_2$ concentration (μmol $mol^{-1}$). I modelled $A$ with the "'plantecophys" R Package (Duursma, 2015), which uses the Farquhar-von Caemmerer-Berry model (Farquhar et al., 1980).

An earlier model was proposed by Leuning (1995), who assumed a different stomatal response to $D$ following Lohammar et al. (1980):

$$g_s = 1.6 \cdot g_{1L} \cdot \frac{A}{C_a} \cdot \frac{1}{1+D/D_0} \quad (2)$$

which has two parameters: $g_{1L}$ is an empirical slope determining the sensitivity of $g_s$ to $A$ and other environment variables (dimensionless); and $D_0$ reflects the sensitivity of $g_s$ to $D$ (kPa).

I also tested a modified version of the model proposed by Tuzet et al. (2003), following Duursma and Medlyn (2012):

$$g_s = 1.6 \cdot g_{1T} \frac{A}{C_a} \cdot f_s(\psi_L) \quad (3)$$

where $g_{1T}$ is an empirical slope parameter and $f_s$ is the sigmoidal function defined as:

$$f_s(\psi_L) = \frac{1+\exp(s_f \cdot \psi_f)}{1+\exp(s_f \cdot (\psi_f - \psi_L))} \quad (4)$$

Where $\psi_L$ is leaf water potential (MPa); $\psi_f$ is an empirical reference water potential (MPa), and $s_f$ is a sensitivity parameter describing the steepness of the response of $\psi_L$ to $\psi_f$ (MPa$^{-1}$). The Tuzet model resembles the Medlyn and Leuning models but replaces the dependence on $D$ with a function of $\psi_L$, which is obtained as follows.

Assuming that the transpiration is a balance of demand and supply, I have:

$$E = K \cdot (\psi_s - \psi_L) = g_s * D/P_{atm} \quad (5)$$

where $K$ is the hydraulic conductance (mol m$^{-2}$ s$^{-1}$ MPa$^{-1}$); $\psi_s$ is the soil water potential (MPa) and $P_{atm}$ is the atmospheric air pressure (kPa). To solve for $\psi_L$ requires a value for $K$, which is assumed to decrease as plant water potential becomes more negative (Tyree and Sperry 1989):

$$K = K_{max} \cdot R_{PLC} \quad (6)$$

where $K_{max}$ is the maximum hydraulic conductance (mol m$^{-2}$ s$^{-1}$); $R_{PLC}$ is the percentage loss of hydraulic conductance and takes the form of a Weibull function as fitted by Neufeld et al. (1992):

$$R_{PLC} = \frac{1}{1+\exp(a \cdot (\psi_L - \psi_{50}))} \quad (7)$$

where $a$ and $\psi_{50}$ are fitted parameters (32.4 and -4.1 MPa, respectively); $a$ represents the rate of decline of the curve and $\psi_{50}$ is the leaf water potential at which plant hydraulic conductance is reduced to 50%. These parameters were obtained from the vulnerability curves described above (Peters, pers. comm.) Combining Equations 3 – 7 allows both $\psi_L$ and $g_s$ to be predicted.

I tested two alternative ways to represent non-stomatal limitation. In the first, the maximum carboxylation capacity ($V_{cmax}$; μmol $m^{-2}$ $s^{-1}$) was assumed to decline with leaf water potential (the *V*-PSI hypothesis):

$$V = V_{cmax} \frac{1+\exp(s_{f.v} \cdot \psi_{f.v})}{1+\exp(s_{f.v} \cdot (\psi_{f.v} - \psi_L))} \quad (8)$$

where $V$ is the $V_{cmax}$ modified by non-stomatal limitation; $s_{f.v}$ and $\psi_{f.v}$ are fitted parameters; $\psi_{f.v}$ is an empirical reference water potential (MPa), and $s_{f.v}$ is a sensitivity parameter describing the "steepness" of the response of $\psi_L$ to $\psi_{f.v}$ ($MPa^{-1}$). Note that this is the same form of sigmoidal function as used in the Tuzet model (Eqn. 3).

In the second, I derived a direct empirical relationship between $V_{cmax}$ and $D$ (the *V*-*D* hypothesis):

$$V = V_{cmax} \cdot (1 - c_D \cdot D) \quad (9)$$

where $c_D$ is a fitted parameter ($kPa^{-1}$). This relationship is different from that in Eqn. 8 because it assumes the plant carboxylation capacity directly responds to *D*. I set a minimum $V_{cmax}$ of 10 (μmol $m^{-2}$ $s^{-1}$) to avoid negative values produced by the linear decline of $V_{cmax}$ with *D*.

I assumed that the impact of soil drought could be represented in the Tuzet model by the reduction of soil moisture potential ($\psi_s$), which was estimated from the pre-dawn leaf water potential ($\psi_{pd}$; MPa). For the Medlyn and Leuning models, I assumed an exponential dependence of the $g_1$ parameter on $\psi_{pd}$ following Zhou et al. (2013):

$$g_1 = g_{1.max} \cdot \exp(\beta \cdot \psi_{pd}) \quad (10)$$

where $g_1$ represents $g_{1M}$ and $g_{1L}$; $g_{1.max}$ is $g_1$ when $\psi_{pd} = 0$; $\beta$ represents the sensitivity of $g_1$ to $\psi_{pd}$. The impact of dry soil was implemented to account for the variation in the soil water availability among the campaigns.

### 3.3.4 Model fitting

I used R (version 3.4.1 R Core Team) as the modelling and statistical tool. I assumed measured values of incident photosynthetically active radiation, leaf temperature, atmospheric $CO_2$ concentration, *D*, $\psi_{pd}$, and $J_{max}$ and $V_{cmax}$ for the diurnal gas exchange data (at EucFACE only). I then parameterized the Medlyn and Leuning models at leaf scale using the differential evolution algorithm (DEoptim package) to fit all the parameters ($g_{1.max}$, $\beta$, $D_0$, and $c_D$) in the coupled *A*-$g_s$ model against the measured *A* and $g_s$ data. I used a similar

approach to determine the unknown parameter values in the Tuzet models. As a result, all the models tested at the leaf-scale were fitted to measured $A$ and $g_s$.

To determine the potential impact of dry soil on $g_s$, I used the fitBB function ('plantecophys' package; Duursma, 2015) to estimate the $g_{1M}$ in the Medlyn model. I fitted one $g_{1M}$ for each campaign and illustrated that $g_{1M}$ declined with decreasing $\psi_{pd}$ (Figure 3.3). However, these $g_{1M}$ values were not taken directly by the models but used to parameterise the stomatal response to soil moisture.

*Table 3.1. Summary of model parameter values and performance considered in this study. Note the differences in meanings and units in $g_{1.max}$ among models. Table shows both the coefficient of determination ($R^2$; higher is better) and inverse of Bayesian information criterion (BIC; lower is better) of both A and $g_s$. Each criterion is ranked for the best three model combinations (best to worst marked as dark to light shade).*

| $g_s$ model | $V_{cmax}$/$K_{max}$ model | Fitted parameters | $R^2$ of $A$ | $R^2$ of $g_s$ | -BIC |
|---|---|---|---|---|---|
| Medlyn (Eqn. 1) | $V$ constant | $g_{1.max}$ =5.5; $\beta$ = 0.69 | 0.45 | 0.61 | 2442 |
| Leuning (Eqn. 2) | $V$ constant | $g_{1.max}$ = 19.80; $\beta$ = 0.31; $D_0$ = 0.76 | 0.62 | 0.75 | 2420 |
| Tuzet (Eqn. 3) | $V$ constant $K$ = f($\psi_L$) (Eqn. 6) | $g_{1T}$ =11.55; $\psi_f$ = -3.78; $s_f$ = 2.23; $K_{max}$ = 1.49 | 0.77 | 0.69 | 2378 |
| Tuzet (Eqn. 3) | $V$ = f($\psi_L$) (Eqn. 8) $K$ = f($\psi_L$) (Eqn. 6) | $g_{1T}$ = 14.00; $\psi_f$ = -1.54; $s_f$ = 11.80; $K_{max}$ = 4.00; $c_2$ = -0.17; $c_1$ = 0.50 | 0.65 | 0.75 | 2397 |
| Medlyn (Eqn. 1) | $V$ = f($D$) (Eqn. 9) | $g_{1.max}$ =5.7; $\beta$ = 0.52; $c_D$ = 0.16 | 0.77 | 0.74 | 2380 |

Although exploring the mechanisms causing non-stomatal limitation is beyond the scope of this study, I used an extreme-case assumption to estimate the possible contribution of mesophyll conductance ($g_m$). I assumed that all of the discrepancy between the Medlyn model prediction and diurnal gas exchange data could be attributed to $g_m$, when $D$ is >2 kPa. For each diurnal measurement with $D$ >2 kPa, a $g_m$ value was estimated as that which minimized

the difference between the model predictions and the diurnal observations. This analysis indicates how much $g_m$ would have to change if it were solely responsible for non-stomatal limitation. However, the role of $g_m$ was not further explored in this study because it is not possible to determine how much of the apparent non-stomatal limitation can be attributed to reductions in gm.

The fidelity of the leaf-scale models was evaluated via: (i) the Bayesian Information Criteria (BIC), which considered the relative residuals of predictions (both *A* and $g_s$) as well as the number of parameters in the models; (ii) the coefficient of determination ($R^2$) of both A and gs. I thus ranked the models with these measures and selected the one with the highest overall ranking.

### 3.3.5 Stand scale modelling

I implemented the Medlyn model (Eqn 1) with *V-D* relationship (Eqn. 9) into a process-based stand-scale model, MAESTRA (Duursma and Medlyn, 2012). The stand simulation included all six rings in EucFACE and covered the period between 1 January 2013 to 31 December 2013 on a half hourly basis. MAESTRA considers the radiative transfer to an array of grid points within each tree crown and calculates gas exchange at each grid point based on light interception at each timestep. Understory plants were not included here because they do not contribute to tree transpiration. The model was parameterised with data on size, location, and position of each tree as well as total leaf area index (Duursma et al., 2016; Figure 3.1).

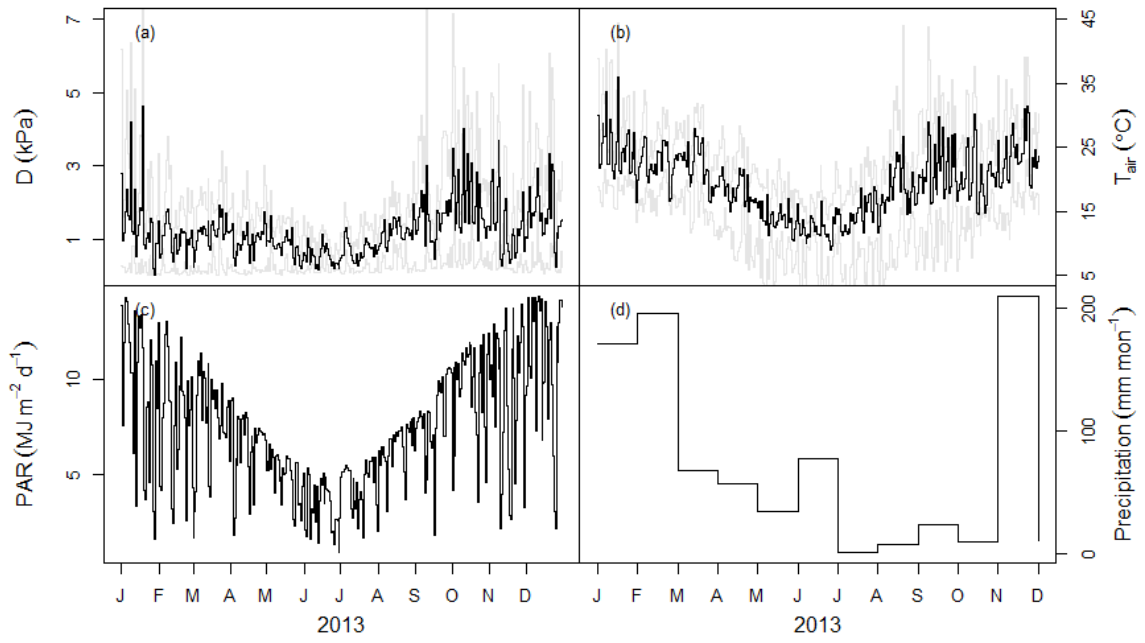


*Figure 3.1. The vapour pressure deficit, temperature, radiation, and precipitation of the site during the simulation period. Panels show (a) daily mean vapour pressure deficit (D) with shaded area marking the maximum and minimum of the day, (b) daily mean air temperature ($T_{air}$) with shaded area marking the maximum and minimum of the day, (c) daily total photosynthetically active radiation (PAR), and (d) monthly total precipitation.*

Meteorological data (Figure 3.1) and soil water content data (Figure 3.2) observed in each ring were input to the model. The original met data were aggregated to half-hourly averages and gap-filled (less than 1% of the total) with nearest available values. Canopy physiology was parameterized with measurements of the light response of photosynthesis, dark respiration rates, and the temperature response of photosynthesis and respiration, all made at EucFACE and assumed not to vary across rings (Crous et al. pers. comm). I assumed a minimum $g_s$ (Duursma et al., 2018) of 0.01 (mol $H_2O$ m$^{-2}$ leaf s$^{-1}$) during daytime to avoid zero transpiration at extreme environmental conditions (e.g., high *D*). The transpiration of the canopy in the model is given by the Penman-Monteith equation which considered net radiation, windspeed, relative humidity, and stomatal conductance.

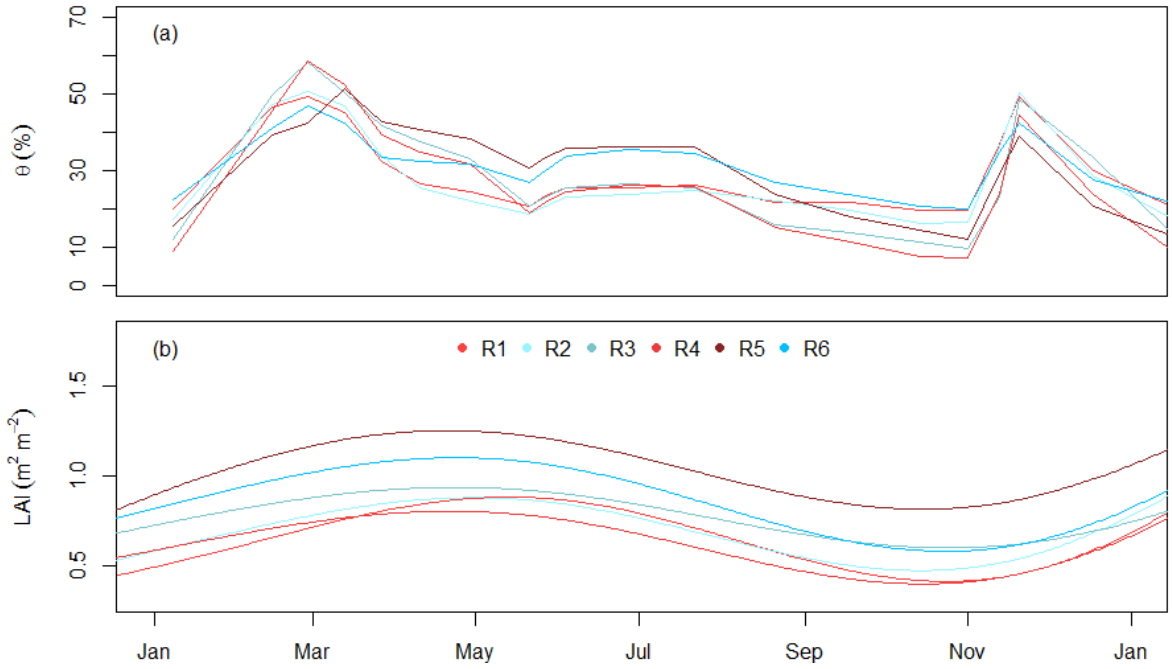


*Figure 3.2. (a) Soil water content (θ; dimensionless) and (b) Leaf area index from the top 50 cm of each ring over the simulated period. The LAI data were estimated by Duursma et al. (2016) from absorbed PAR measurements and smoothed with a generalized additive model fitting.*

The impact of soil drought on stomatal conductance was modelled as a function of $g_{1M}$ and volumetric soil water ($\theta$) content following Drake et al. (2017):

$$g_1 = g_{1.max} \cdot \left(\frac{\theta - \theta_{min}}{\theta_{max} - \theta_{min}}\right)^q \quad (11)$$

where $g_{1.max}$ is the maximum value of $g_1$ (kPa$^{0.5}$); $\theta_{max}$ and $\theta_{min}$ are empirically fitted parameters defining the upper and lower boundaries beyond which $g_1$ is not affected by $\theta$; $\theta_{min}$ was assumed to be 0 in the fitting; and $q$ is the parameter describing the non-linearity of the function. I fitted Eqn. 11 (Figure 3.3) to the data from Gimeno et al. (2016) and Drake et al., (2017a) to obtain the values of $\theta_{max}$ and $q$ (0.42 and 0.18 respectively) with the non-linear least squares method (nls, R function). The relationship between $g_{1M}$ and $\theta$ used in the model is in Figure 3.1. The stand-scale model did not use the same relationship as on leaf-scale (Eqn. 10) because: (i) the limitation of temporal coverage of leaf water potential measurements prohibited the simulation on annual scale; (ii) on leaf scale, the Tuzet models depends on $\psi_s$ instead of $\theta$; (iii) although $\psi_s$ could be estimated with $\theta$, doing so over the rooting depth (4 m) with different soil types would not give an accurate estimation of $\psi_s$. The

different requirements of leaf and whole-tree scale models thus led to distinct soil water stress functions.

The model used a phenology of $V_{cmax}$ and $J_{max}$ derived from canopy greenness (Green Chromatic Coefficient; GCC):

$$V_{cmax.25} = (V_{80} - V_{20}) \cdot f(GCC) + V_{20} \quad (12)$$

where $V_{cmax.25}$ is $V_{cmax}$ value at 25 ºC; $f$(GCC) is the phenology derived from the canopy greenness; $V_{80}$ and $V_{20}$ are fitted parameters describing the upper and lower range of $V_{cmax}$. This relationship is the same for $J_{max}$ with $J_{80}$ and $J_{20}$ (i.e., the upper and lower range of observed $J_{max.25}$, respectively) replacing $V_{80}$ and $V_{20}$. The GCC phenology was fitted to observed data:

$$GCC = f_a \cdot t^{f_b} + f_c{}^t \quad (13)$$

where $f_a$ and $f_b$ are fitted parameter values; $t$ is the arbitrary date of leaf flushing (number of days from October 1st in the previous year); $f_c$ was fixed to 0.0005 to reduce the degrees of freedom of the model and to improve fitting.

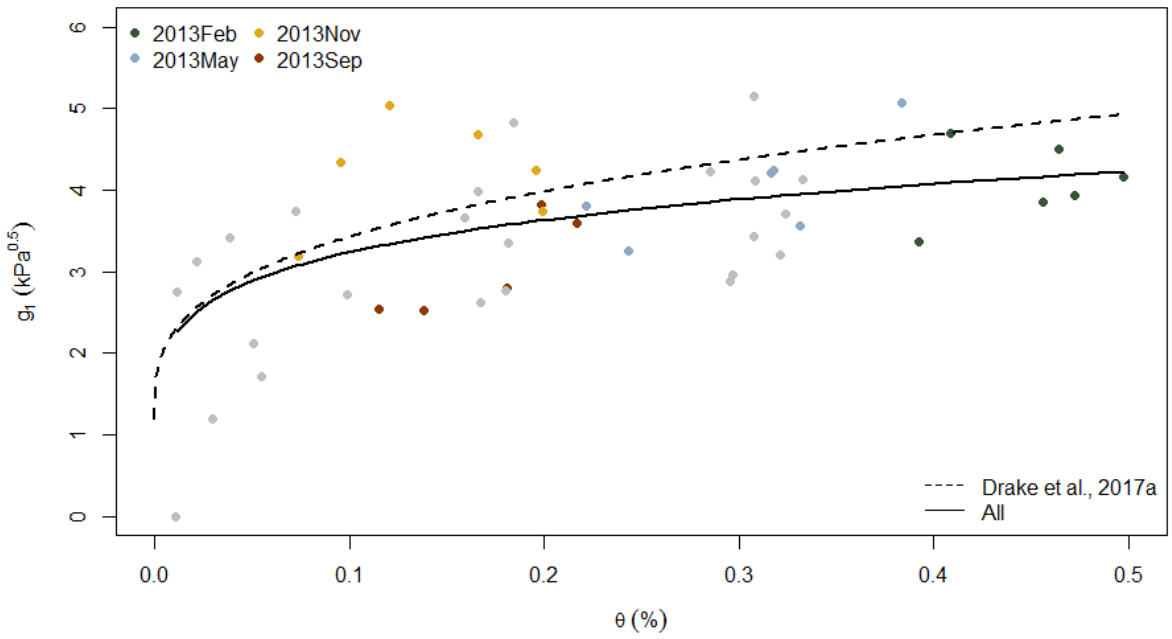


*Figure 3.3. The impact of soil moisture content (θ) at top 50 cm on stomatal regulation. Coloured points mark the $g_{1M}$ estimated from the data in Gimeno et al. (2016) with different colour for each campaign. The grey dots are data from Drake et al. (2017).*

*Table 3.2. List of parameters and variables. Note that abbreviations are not included in the list.*

| Parameter/variable | Definition | Unit | Value |
|---|---|---|---|
| $A$ | Net assimilation rate of $CO_2$ | μmol $m^{-2}$ $s^{-1}$ | - |
| $a$ | Rate of decline of PLC curve | $MPa^{-1}$ | 42.8 |
| $\beta$ | Stomatal sensitivity to drought | - | 0.69 for the Medlyn model; 0.97 for the Leuning model |
| $C_a$ | Atmospheric $CO_2$ concentration | μmol mol | ~400 for ambient and 550 for elevated |
| $c_D$ | Decline of carboxylation capacity with vapour pressure deficit | $kPa^{-1}$ | 0.174 |
| $g_{1.max}$ | $g_{1L}$ and $g_{1M}$ at zero predawn leaf water potential | $kPa^{0.5}$ | 5.5 for the Medlyn Model; 24.0 for the Leuning Model |
| $g_{1L}$ | Stomatal factor in the Leuning model | unitless | - |
| $g_{1M}$ | Stomatal factor in the Medlyn model | $kPa^{0.5}$ | - |
| $g_{1T}$ | Stomatal factor in the Tuzet model | unitless | - |
| $g_s$ | Stomatal conductance | mol $m^{-2}$ $s^{-1}$ | - |
| $D$ | Vapour pressure deficit | kPa | - |
| $D_0$ | Sensitivity of $g_s$ to $D$ | kPa | 0.82 |
| $E$ | Transpiration | kg $m^{-2}$ $hr^{-1}$ | - |
| $ET$ | Evapotranspiration | kg $m^{-2}$ $hr^{-1}$ | - |
| $J_{max}$ | Maximum electron transport rate | μmol $m^{-2}$ $s^{-1}$ | - |
| $K$ | Hydraulic conductance | mol $m^{-2}$ $s^{-1}$ $MPa^{-1}$ | - |
| $K_{max}$ | Maximum hydraulic conductance | mol $m^{-2}$ $s^{-1}$ | Depends on model |
| $\psi_{50}$ | Leaf water potential at which plant hydraulic conductance is reduced to 50% | MPa | -4.3 |
| $\psi_L$ | Leaf water potential | MPa | - |
| $\psi_f$ | Empirical reference water potential | MPa | - |
| $\psi_{f.v}$ | Leaf water potential at which plant $V_{cmax}$ is reduced to 50% | MPa | - |
| $s_f$ | Sensitivity of the response of $\psi_L$ to $\psi_f$ | - | - |
| $s_{f.v}$ | Sensitivity of the response of $\psi_L$ to $\psi_{f.v}$ | $MPa^{-1}$ | - |

| | | | |
|---|---|---|---|
| $P_{atm}$ | Atmospheric air pressure | kPa | - |
| $R_{PLC}$ | Percentage loss of hydraulic conductance | % | - |
| $V$ | $V_{cmax}$ modified by environmental conditions | μmol $m^{-2}$ $s^{-1}$ | - |
| $V_{cmax}$ | Maximum carboxylation capacity at given temperature | μmol $m^{-2}$ $s^{-1}$ | - |

## 3.4. Results

### 3.4.1 Baseline leaf gas exchange models

The leaf gas exchange data from EucFACE showed a clear decline in both $A$ and $g_s$ with increasing $D$ (Figure 3.4). The baseline model (Medlyn with constant V) was unable to capture the $D$ response of $A$ (Figure 3.5a) or $g_s$ (Figure 3.5b). As a result, this model ranked lowest among the models tested (Table 3.1). It over-predicted $A$ at high $D$ but under-predicted $g_s$ at low $D$. The Leuning model, despite its stronger sensitivity to $D$, shared the same problems as the Medlyn model (Table 3.1; Figure 3.5 c and d). The under-prediction of $g_s$ resulted from the adjustment of parameter values to capture $A$ at high $D$. When fitting the parameter values, there is a trade-off in the ability of the model to capture $A$ vs $g_s$, such that adjusting parameters to improve the prediction of one ($g_s$ in this case) decreases the ability of the model to predict the other ($A$ in this case). In addition, I obtained unrealistic parameter values for the Leuning model. The fitted $g_{1.max}$, $\beta$, and $D_0$ were beyond the common range of estimations. Utilising the default parameter values for the Leuning model used in the CABLE land-surface model, for example, led to severe under-prediction of $g_s$ (Figure 3.6). In other words, with standard parameter values, the Leuning model would have performed worse than all other models tested here (Figure 3.4). This comparison suggests that improvements in the model performance are unlikely to be achieved by varying stomatal sensitivity to $D$.

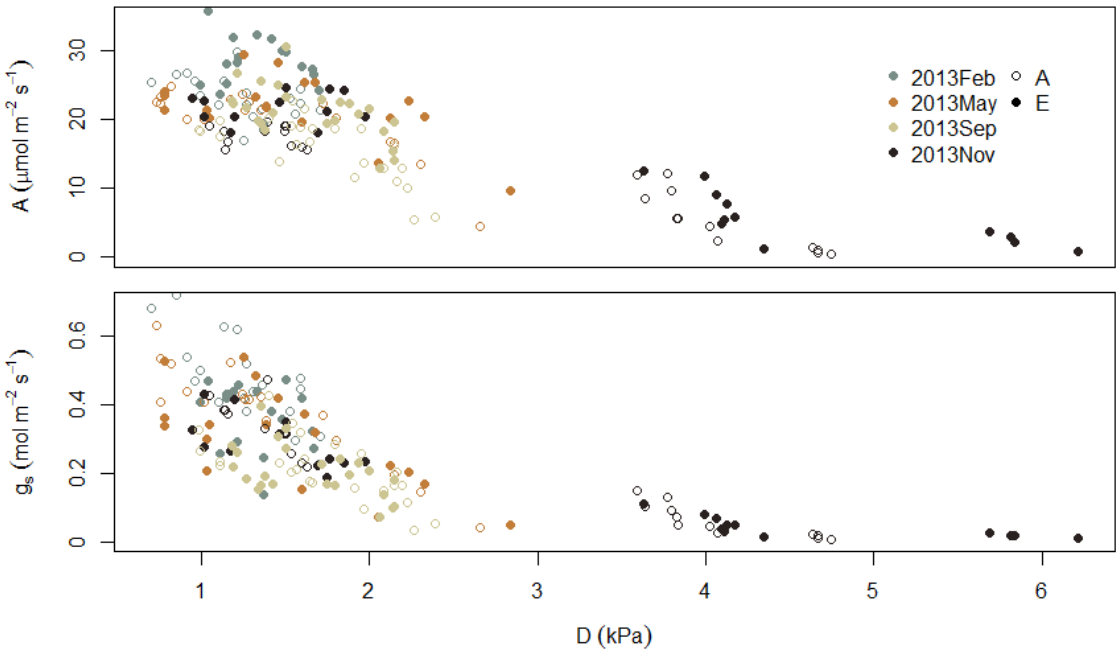


*Figure 3.4. The observed response of light-saturated photosynthesis (A) and stomatal conductance ($g_s$) to vapour pressure deficit (D) at EucFACE. Data are leaf gas exchange from four campaigns in 2013 in all six rings (obtained from Gimeno et al. 2016). Open circles: Ambient rings; Closed circles: Elevated rings.*

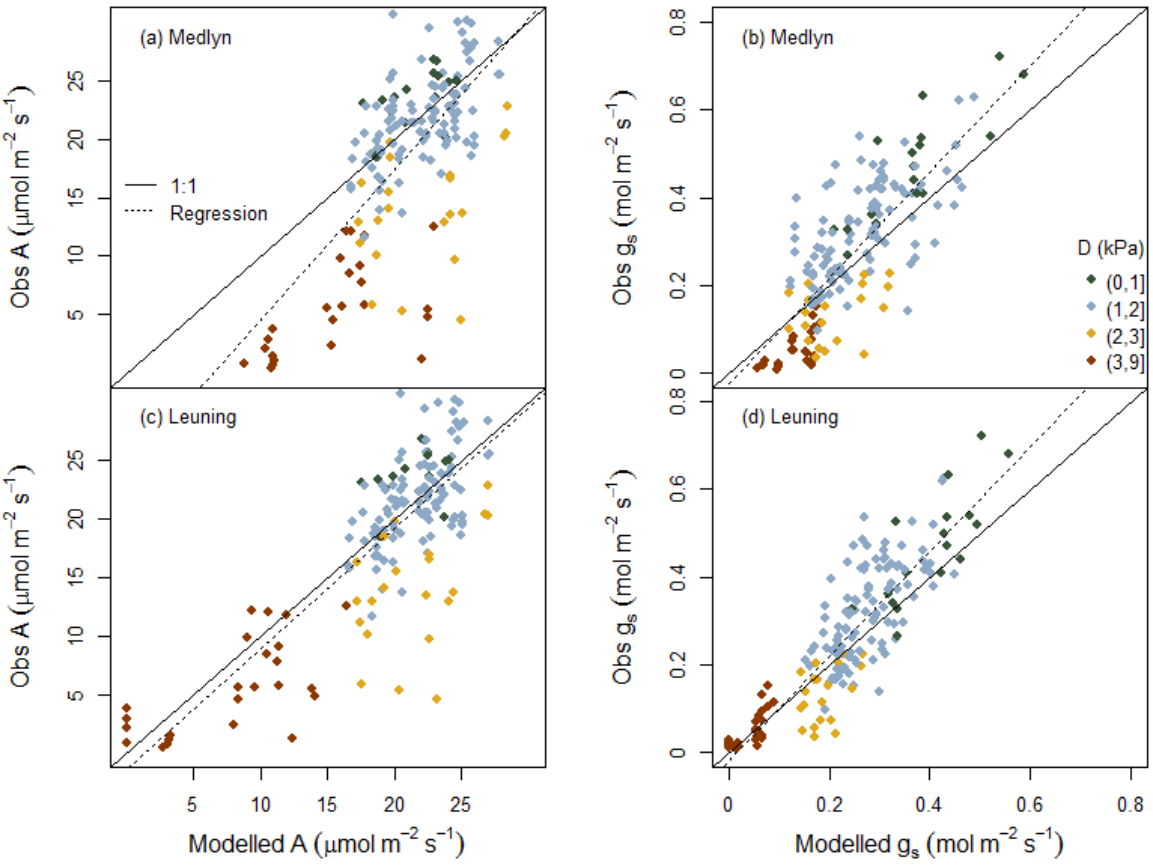


*Figure 3.5. Modelled photosynthesis (A) and stomatal conductance ($g_s$) compared with observations. (a) and (b) Medlyn model (Eqn. 1). (c) and (d) Leuning model (Eqn. 2). Models were fit to both A and $g_s$ data.*

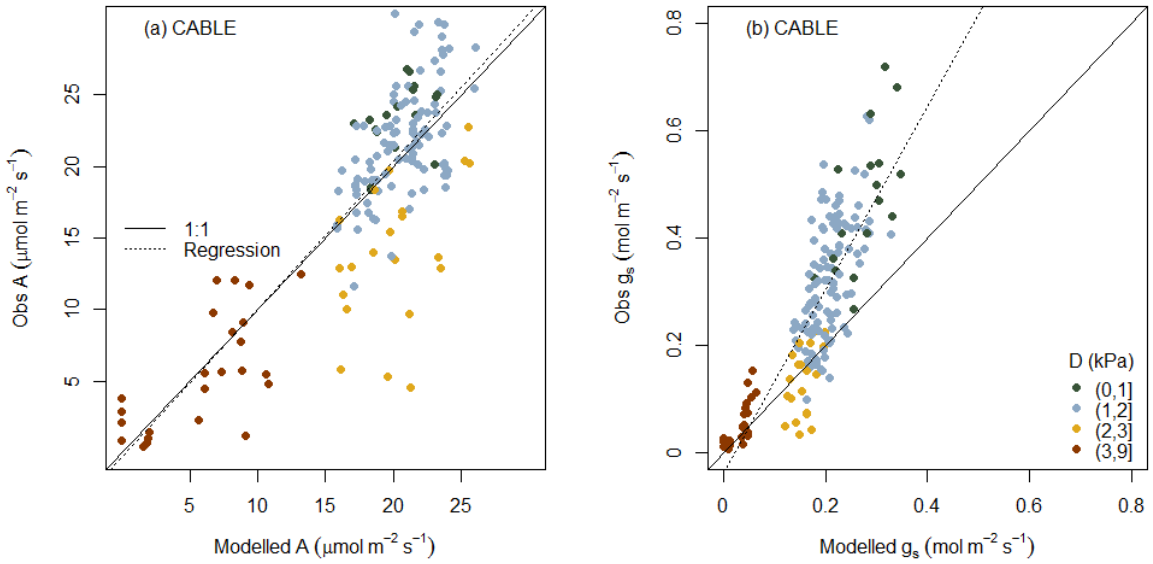


*Figure 3.6. The performance of the Leuning model (Eqn. 2) using default parameter values*

*from CABLE ($g_1$=9; $D_0$=1.5). The panels show scatter plots of the predictions against observations.*

### 3.4.2 Hydraulic limitation

The model incorporating hydraulic limitation (Tuzet K-PSI) showed good agreement with observations at both low and high *D* (Figure 3.7 and Table 3.1). It achieved the best BIC value and highest $R^2$ to *A* (Table 3.1). However, a comparison with leaf water potential values shows that the Tuzet model, although it performs well in predicting *A* and $g_s$, does so for the wrong reasons. Tuzet K-PSI predicted: (i) a decline of $\psi_L$ with increasing *D* (Figure 3.8a), (ii) a large gradient between $\psi_s$ and $\psi_L$ (~ 4 MPa), and (iii) $\psi_L$ values below $\psi_{50}$ (< -5 MPa), none of which was supported by observations (Figure 3.8 b and c). The observed $\psi_L$ did not change with *D* (Figure 3.8b). The estimated vulnerability curve (Figure 3.8b) also indicated that the plant maintained a $\psi_L$ higher than the point where cavitation starts (~ -3.5 MPa).

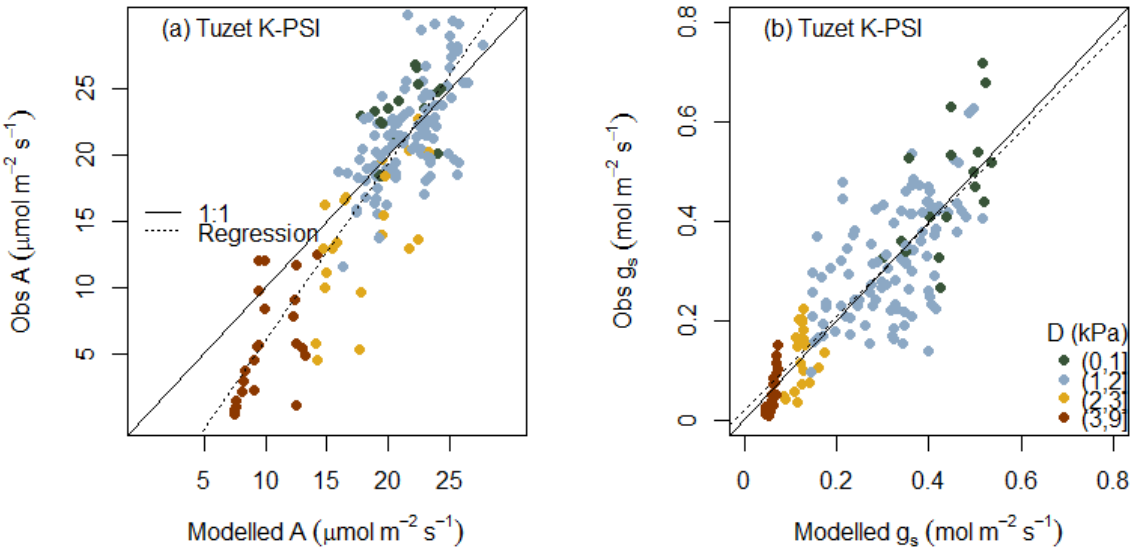


*Figure 3.7. Modelled photosynthesis (A) and stomatal conductance ($g_s$) incorporating hydraulic limitation (Tuzet K-PSI, Eqns. 3-7) compared with observations.*

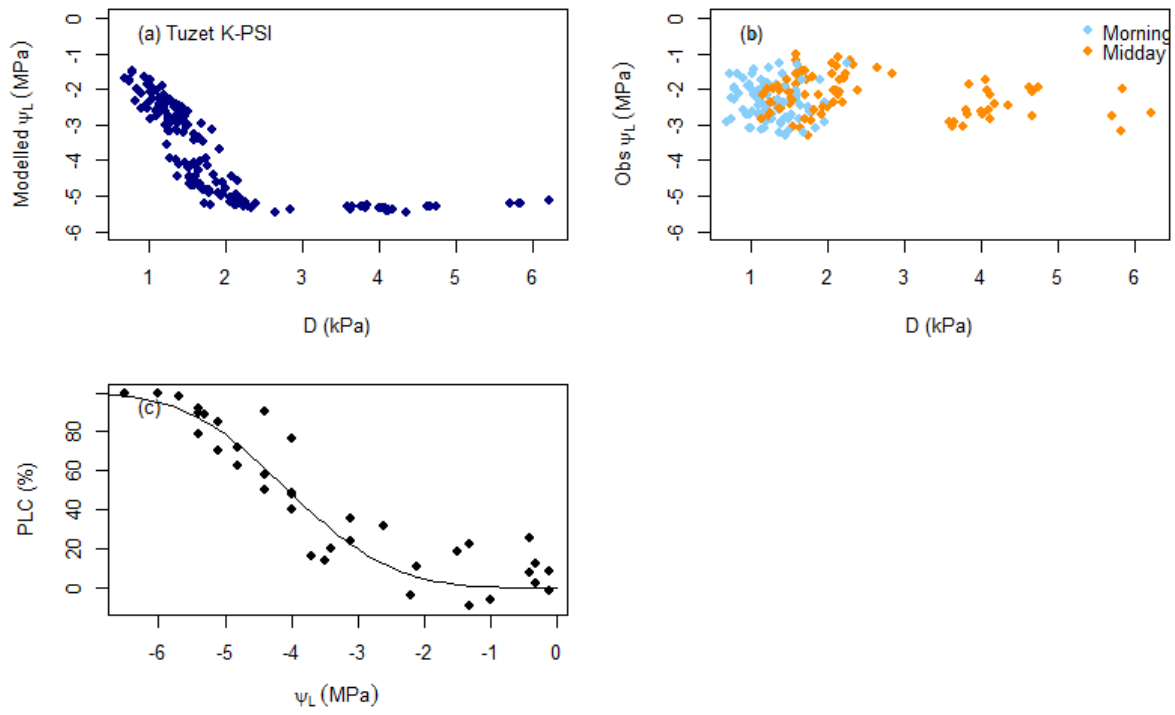


*Figure 3.8. The Tuzet K-PSI model did not capture the observed leaf water potential ($\psi_L$). (a) Predicted $\psi_L$ from the Tuzet model. (b) Observed $\psi_L$ of each tree in the morning (lower D) and at midday (higher D). (c) Estimated PLC curve based on dehydration measurements. Note that observed $\psi_L$ (b) stays above the point where cavitation occurs (c), but the model predicts this value to fall below this point (a).*

### 3.4.3 Non-stomatal limitation

I first examined whether there is evidence in the gas exchange data for non-stomatal limitation. Figure 3.9 shows that the ratio of apparent $V_{cmax}$ (estimated from gas exchange data using the "one-point" method) to the predicted $V_{cmax}$ at the same temperature (estimated from A-Ci curves performed at a range of temperatures) declined with increasing *D*. A similar pattern was also observed in gas exchange data from the nearby Castlereagh site (blue dots in Figure 3.9). This decline in the apparent $V_{cmax}$ indicates a reduction in $V_{cmax}$ or a decrease in $g_m$, neither of which can be linked to stomatal regulation. I also estimated mesophyll conductance and showed a reduction of mesophyll conductance with *D* in this study (Figure 3.10). Consequently, this finding supports the hypothesis that non-stomatal limitation is a factor in the decline of *A* at high *D*.

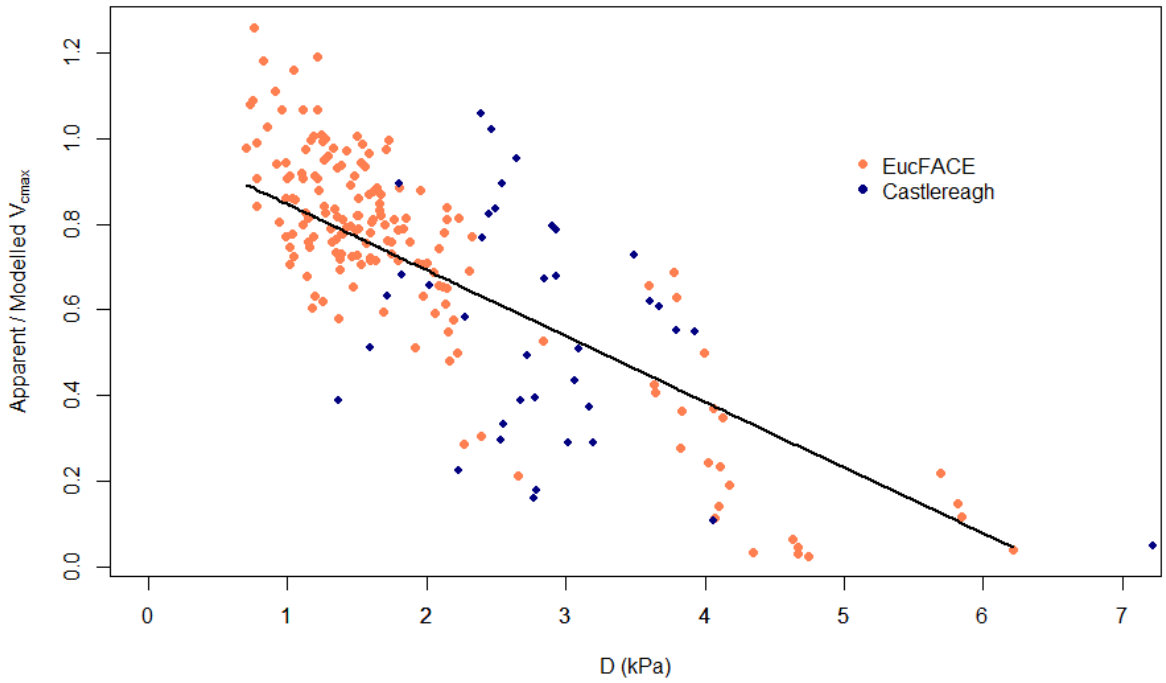


*Figure 3.9. Ratio of apparent $V_{cmax}$ (estimated from gas exchange data using the "one-point" method) to the predicted $V_{cmax}$ at the same temperature (estimated from A-Ci curves performed at a range of temperatures), as a function of D. EucFACE data (orange) are from Gimeno et al. (2016); Castlereagh data (blue) are from Zeppel et al. (2008). Only the EucFACE data are used in parameterization; the Castlereagh data are used to show that the pattern is consistent across sites. Black line shows a linear regression with a fixed intercept of 1.*

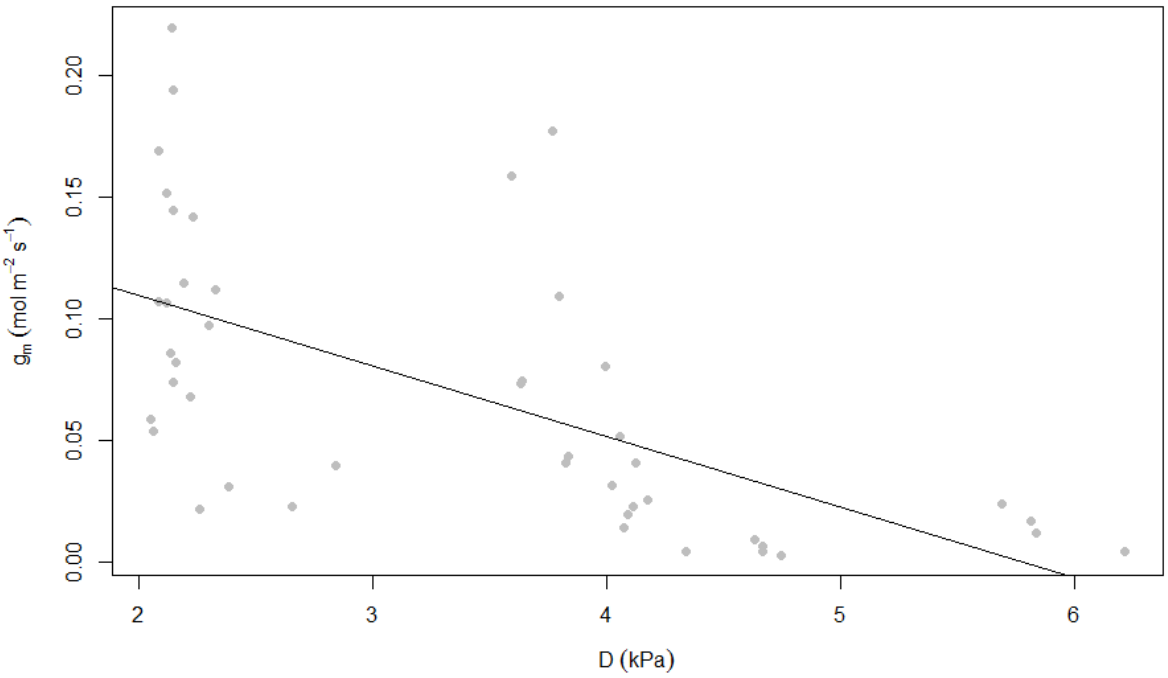


*Figure 3.10. Fitted mesophyll conductance ($g_m$; mol $m^{-2}$ $s^{-1}$) shows a decline with increasing vapour pressure deficit (D; kPa). The $g_m$ is estimated with diurnal leaf gas exchange measurements in EucFACE during 2013. The line marks the linear regression fit: $g_m$ = 0.17-0.03·D with a $R^2$ of 0.38. The fitting estimated a $g_m$ of 0.11 mol $m^{-2}$ $s^{-1}$at D =2 kPa; 0.05 mol $m^{-2}$ $s^{-1}$at D = 4 kPa.*

I then tested whether the non-stomatal limitation could be predicted as a function of leaf water potential (Tuzet V-PSI). Adding non-stomatal limitation to the Tuzet model comes at a cost of increased complexity, requiring six parameters to be fitted at the same time. This added complexity was not justified by the marginal improvements in $R^2$ resulting in the worst BIC value of all models tested (Table 3.1; Figure 3.11 a and b). Including the non-stomatal limitation in the Tuzet model did not lead to model improvement, which can be explained as follows. Firstly, I know that the plants do not reduce $\psi_L$ sufficiently to cause cavitation and a reduction in hydraulic conductance (see above). Given that the plants do not reduce $\psi_L$ beyond the critical value, it is not possible for non-stomatal limitation as a function of $\psi_L$ to predict a reduction in transpiration at high *D*. The observed decreased in $g_s$ at high *D* leads to a less negative $\psi_L$ at high *D*; a less negative $\psi_L$ implies a higher $V_{cmax}$; however, this contradicts the assumption and existing evidence, which suggested that at high *D*, a lower $V_{cmax}$ should be expected.

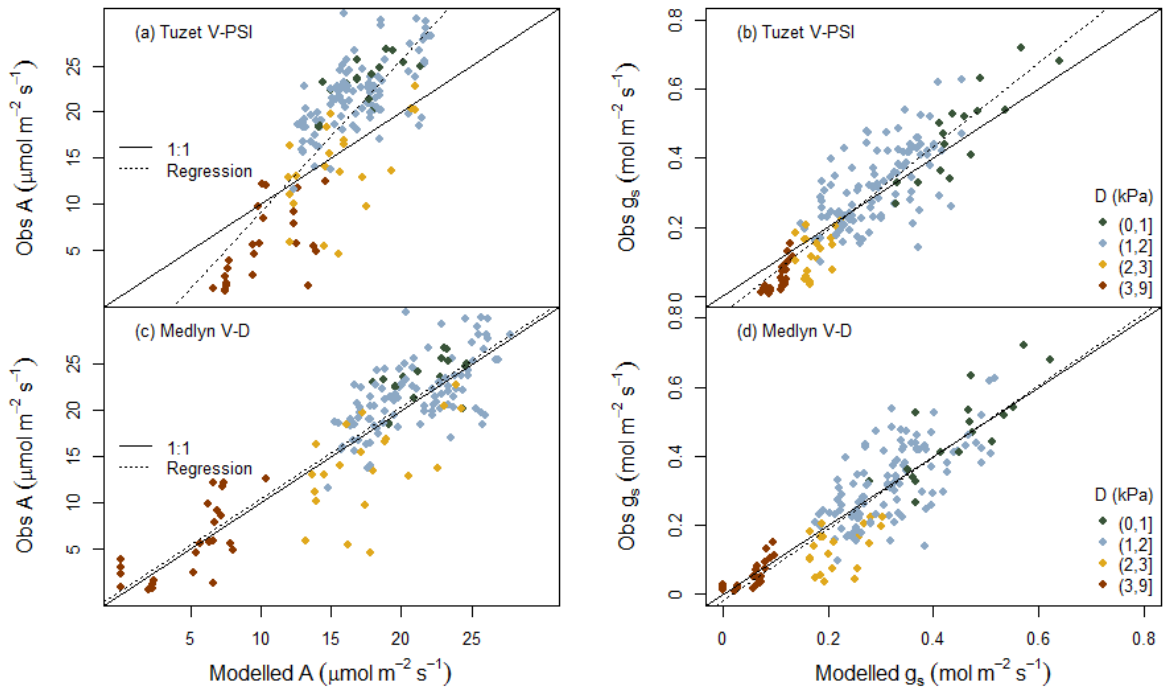


*Figure 3.11. Modelled photosynthesis (A) and stomatal conductance ($g_s$) incorporating non-stomatal limitation (Eqn. 9) into Tuzet (Tuzet V-PSI) and Medlyn models (Medlyn V-D) compared with observations.*

I also tested whether an empirical non-stomatal limitation incorporated into the Medlyn model would improve the prediction (Medlyn V-D; Figure 3.11 c and d). The Medlyn model, together with an empirical decline in $V_{cmax}$ with $D$, achieved better $R^2$ values for both $A$ and $g_s$ than the more complicated models, resulting in a low -BIC value (Table 3.1). This result suggests that the issues identified above with the Medlyn model are not with the model itself but rather a result of a lack of representation of non-stomatal limitation in the coupled $A$-$g_s$ scheme.

### 3.4.4 Stand scale evaluation

I then moved to evaluating the performance of the Medlyn *V-D* relationship at the whole-tree scale using the MAESTRA model. Since photosynthesis measurements at the whole-tree scale are not available, the evaluation focused on transpiration estimated from sap flow measurements. The standard MAESTRA using the Medlyn model over-predicted transpiration at EucFACE especially at high $D$ (Figure 3.12 a and b). There was a notable inconsistency in the errors at low and high $D$. The difference between the predicted and observed values increased strongly at high $D$ (compare green versus red dots in Figure

3.12b). However, after incorporating the Medlyn *V-D* model, MAESTRA closely followed the seasonal variation of the measurements (Figure 3.10c) and agreed with observations across the full range of *D*. Overall, the Medlyn *V-D* model increased the coefficient of determination from 0.64 to 0.87 and halved the root mean squared error (0.027 to 0.013; L $hr^{-1}$). The improvements were even larger at high *D* (>2.5 kPa) with a reduction of root mean squared error from 0.09 to 0.03. During the simulated four years (2013-2016), incorporating non-stomatal limitation into MAESTRA resulted in a ~10% reductions in predicted annual average transpiration (~46 kg $H_2O$ $m^{-2}$ $yr^{-1}$) and a ~7% reduction in gross primary production (~117 g C $m^{-2}$ $yr^{-1}$). These reductions happened mainly during summer months (December, January, and February) with transpiration reduced by ~21 kg $H_2O$ $m^{-2}$ $quarter^{-1}$ or 15%, and gross primary production reduced by ~48 g C $m^{-2}$ $quater^{-1}$ or 17%. These findings indicate a potentially large impact of non-stomatal limitation at high *D*.

I also explored whether the new model would improve predicted transpiration compared to observations at the Castlereagh site with similar species and climate conditions. Without canopy physiology or structure data to parameterize the Castlereagh site, I took the approach of standardizing the observed sap flow and modelled *E* by their respective maxima and comparing the relationships of *E* with *D* (Figure 3.13). Both sites show a peaked relationship of *E* with *D* with the turning point occurring between 2-3 kPa, which agrees with the prediction of MAESTRA incorporating non-stomatal limitation (black line in Figure 3.13). This finding suggests that the improvement obtained by incorporating non-stomatal limitation could also apply to sites with similar species and climate.

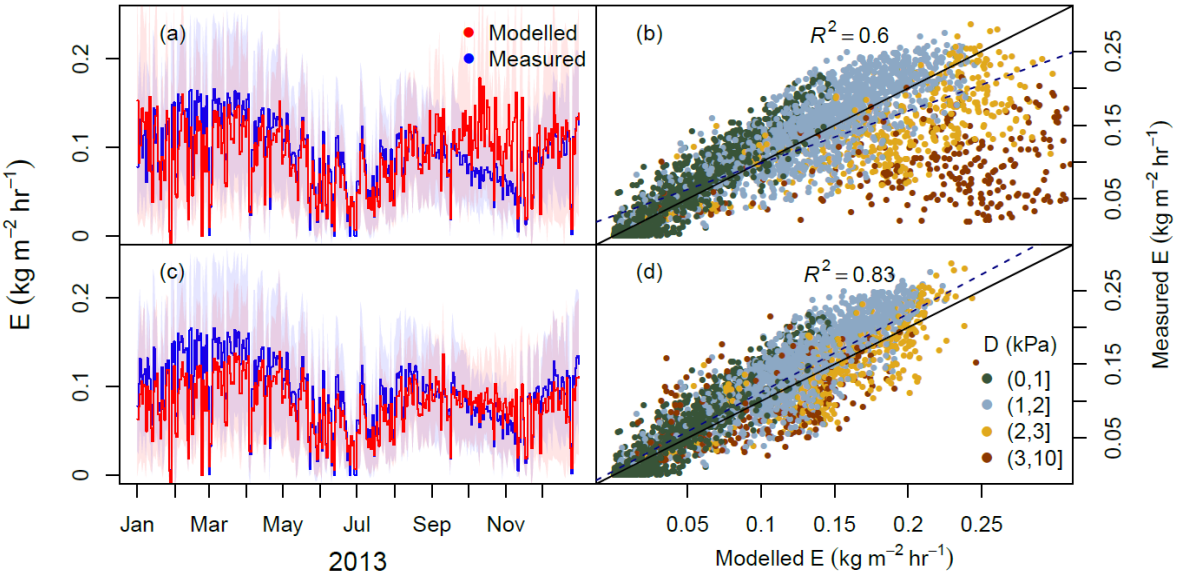


*Figure 3.12. Modelled transpiration (E) compared to sap flow estimated by heat pulse sensors (measured E). Data shown are daytime for one stand (Ring 3) in 2013. Other stands and time periods are similar (Supplementary Material for Chapter 3). Panels (a) and (b) show the result from original MAESTRA. Panels (c) and (d) show the result from MAESTRA with V-D hypothesis. The solid lines in Panels (a) and (c) show the daily average while the shading shows hourly variation (standard deviation).*

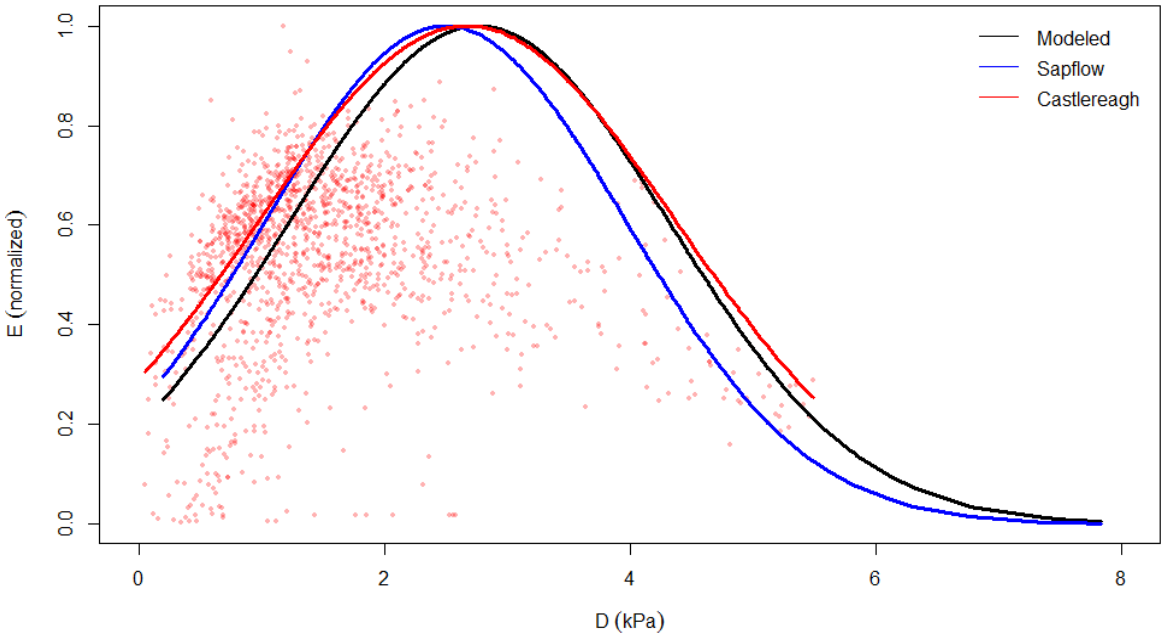


*Figure 3.13. Transpiration (E) across different sources/sites as a function of air vapour pressure deficit (D). The red dots are sapflow data from Castlereagh site (Zeppel et al., 2009). The red line indicates Eqn. 5 in Whitley et al. (2013) fitted to the 80% quantile of the data. The fitted line is slightly off in the peaked value compared to the observations because the measured transpiration concentrated at D = 1kPa and weighted more in the fitting. The black and blue lines represent the same equation fitted to the modelled and estimated (sapflow) half-hourly daytime E for Ring 3 at EucFACE in 2013. All the data were filtered with high PAR (> 1000 µmol $m^{-2}$ $s^{-1}$). There is a consistent turnover of E (peaked shape of the lines) among sites and sources.*

### 3.5 Discussion

The coupled response of *A* and $g_s$ to increasing *D* is a key component in the modelling of carbon and water fluxes of terrestrial vegetation. This is particularly true for dry ecosystems where high atmospheric demand frequently leads to stress for plants. In this paper, I evaluated a suite of commonly used $g_s$ models and assumptions (hydraulic and non-stomatal limitation) used to represent the physiological response to *D* at a native evergreen woodland. Overall, I concluded that the Medlyn *V-D* combination showed the best performance and improved simulations of canopy- and ecosystem-scale carbon and water fluxes. This finding highlights the importance of accounting for non-stomatal limitation in coupled *A*-$g_s$ models.

Previous studies on the non-stomatal limitation of photosynthesis in response to water stress focused on the response to soil moisture (Keenan et al., 2010, Verhoef and Egea, 2014; De Kauwe et al., 2015; Drake et al., 2017a). There is a surprising lack of information about whether apparent photosynthetic capacity responds to *D*. With the available literature, there are two plausible mechanisms for non-stomatal limitation, a reduction in carboxylation capacity or mesophyll conductance, both of which have some empirical and theoretical support. Lawlor and Cornic (2002) and Lawlor and Tezara (2009) illustrated that carboxylation capacity is down-regulated at high water deficit due to reduction in adenosine triphosphate (ATP) synthesis. Huang et al. (2006) explored the cause of "midday depression" of $g_s$ and *A*, and suggested that the regulation of photosynthetic capacity is the likely explanation as plants aim to protect chloroplasts. It is also possible that non-stomatal limitation is due to a reduction of mesophyll conductance with increasing *D*. Flexas et al. (2008) examined the current understanding of the response of mesophyll conductance to the environment (including *D*) and suggested that $g_s$ and mesophyll conductance could be co-regulated. Nevertheless, there have been few studies on the change of mesophyll conductance to *D*. Although Warren (2008) reported no mesophyll conductance response to *D* in *Eucalyptus* seedlings, the study only considered a small *D* range (1 kPa to 2 kPa) which is not sufficient to show the decline observed here. Bongi and Loreto (1989) showed that mesophyll conductance declined from 0.3 to 0.14 mol $m^{-2}$ $s^{-1}$ when *D* increased from 1 to 3 kPa in *Olea europea L*. These estimations are consistent with the values estimated in this study (0.11 mol $m^{-2}$ $s^{-1}$ at $D$ = 2 kPa and 0.05 mol $m^{-2}$ $s^{-1}$ at $D$ = 4 kPa) and the magnitude of decrease of mesophyll conductance with increasing *D*. von Cammerer and Evans (2015) showed increasing mesophyll conductance with temperature and *D*, but also found no decrease in $g_s$ with *D*, which is inconsistent with our data. The reason of their findings being different from this study may be because they were studying potted plants in growth chambers rather than large plants in the field. The mechanism(s) behind the observed ono-stomatal limitation thus remains to be clarified.

I chose not to include mesophyll conductance in the models because: (i) without the knowledge of the mechanism(s) and extensive data across species and over time, it is difficult to construct and parameterize a model to account for the decline of mesophyll conductance with increasing *D*; and (ii) the photosynthesis capacity and mesophyll conductance limitations are mathematically equivalent in the modelling of $g_s$ and *A*, but the former is much more parsimonious.

It is important to understand the underlying reasons that lead to the predicted responses even if the models do not work. The original Medlyn model does not have a mechanism that allows $g_s$ or $A$ to decrease at high $D$ except via the temperature dependence of photosynthesis (Duursma et al., 2015). Whilst the Leuning model does have a stronger regulation of $g_s$ at high $D$ than the Medlyn model, it performs poorly at low $D$, and requires an additional parameter compared to the Medlyn model. Furthermore, the findings in this study (Figure 3.9), and other studies focused on mesophyll conductance and photosynthetic capacity (e.g., Mediavilla et al., 2002; Nascimento and Marenco, 2013) all suggested that the non-stomatal limitation is a more plausible mechanism to regulate $g_s$, rather than a greater sensitivity to $D$. The Tuzet models all predicted a decline in $\psi_L$ with increasing $D$. However, this assumption leads to unrealistic $\psi_L$ predictions and prevented the use of a non-stomatal limitation as a function of $\psi_L$ (Figure 3.8). Models that incorporate the Tuzet model and consider predictions in response to future climate (i.e., at higher $D$) should evaluate the $\psi_L$ predictions together with photosynthesis and stomatal conductance.

There are limitations in this study that need further evaluations with more data. Firstly, the leaf-level evaluation used only data from one site and species. Focusing on this site allowed the use of detailed site-specific parameters, which helped to assess the impacts of each factor separately. The site- and species- specific measurements should also increase the credibility of the temperature dependence and stomatal parameters. However, whether the results apply to other species and ecosystems requires further testing. Secondly, there is a lack of photosynthesis measurements at the scale of the whole-tree model. However, a recent eddy covariance study (Renchon et al., 2018) reported declines of evapotranspiration and net ecosystem carbon uptake with increasing $D$, which are consistent with the finding in this study. I evaluated transpiration predictions against whole-tree scale sap flow measurements at two sites and showed that non-stomatal limitation improved the predicted transpiration of MAESTRA when compared to sap flow measurements particularly under high $D$. The improvements in predicting transpiration would likely translate into improvements in carbon uptake. Sap flow measurements in five other Eucalypt sites in Australia (Whitley et al., 2013) show a similar decline in transpiration with increasing $D$, indicating that the non-stomatal limitation might be widespread. This study does not aim to advance the understanding of the mechanism(s) by which photosynthetic capacity and/or mesophyll conductance decline with $D$. Instead, this study showed the potential improvement by incorporating a mechanistic or theoretical model of non-stomatal limitation into TBMs.

An alternative explanation for the decline of photosynthesis in the afternoon is sink limitation. It has been proposed that the accumulation of starch and sugar in the leaf over time causes an inhibition of photosynthesis (Paul and Foyer, 2001). The data, however, do not support this explanation for non-stomatal limitation at EucFACE. For instance, in February 2013, when daily maximum *D* was < 2 kPa, the mean photosynthesis of the control rings was measured at 25 ± 3 μmol $m^{-2}$ $s^{-1}$ in the morning and a similar 22 ± 2 μmol $m^{-2}$ $s^{-1}$ in the afternoon. However, in November 2013, when daily maximum *D* was > 2 kPa, the mean photosynthesis of the control rings changed from 18 ± 2 μmol $m^{-2}$ $s^{-1}$ in the morning to 5 ± 4 μmol $m^{-2}$ $s^{-1}$ in the afternoon. The magnitude of reduction in photosynthesis from morning to afternoon is thus smaller on days with higher morning photosynthesis rate, contradicting the assumption of sink limitation. Sink limitation thus is unlikely to explain the observed decline of photosynthesis in this study.

This study assumes that stomatal behaviour is uniform, and leaf water loss only happens through the stomata. The first assumption could be countered by stomatal heterogeneity (i.e., stomatal regulation differs across the leaf; also referred as "patchy stomatal closure"; cf. Mott and Buckley, 1998). Although theoretically plausible (Buckley et al., 1999) and observed in the field (e.g., Kamakura et al., 2011), the mechanism(s) of the heterogeneity is(are) not quantitatively defined (Weyers and Lawson, 1997). However, Cheeseman (1991) provided a mathematical frame work to test stomatal patchiness. Future studies may benefit from testing this hypothesis to explore for the mechanism(s). The second assumption raises the debate about the impacts of cuticular conductance (i.e., water loss unregulated by stomata; Cowen, 1978; Farquhar, 1978; Maier-Maercker 1983). Although a mechanistical model for cuticular conductance has been developed (Eamus et al., 2008), this study ignored cuticular conductance for the reasons summarized by Buckley (2005): (i) cuticular transpiration is only a small fraction of transpiration; (ii) epidermal turgor is more sensitive than that of the guard cell resulting in a mechanistic dilemma if cuticular transpiration has significant impact on $g_s$; (iii) uncontrolled water loss reduces the effectiveness of plant active water conservation and thus fitness, indicating a lack of evolutionary benefit of such behaviour.

### 3.6 Conclusions

The key finding of this study was that non-stomatal limitation could be important not only for the diurnal patterns of *A* and $g_s$ under extreme dry conditions but also for transpiration and production at annual timescales. Further studies would be useful to quantify the impact of non-stomatal limitation more broadly. I showed that the Medlyn model could capture the $g_s$

and photosynthesis response to *D* after incorporating non-stomatal limitation. The empirical relationship describing non-stomatal limitation is supported by experimental studies from two sites and could be easily replaced with theoretical or mechanistic alternatives as they emerge. The predictions of the combined model were comparable to leaf- and whole-tree-measurements. The findings suggest models should consider non-stomatal limitation in leaf gas exchange modelling particularly under future, drier, conditions.

## Chapter 4. Scaling from leaf to canopy to understand the response of photosynthesis to elevated $CO_2$ in a mature Eucalypt woodland

### 4.1 Abstract

The response of mature ecosystems to rising atmospheric carbon dioxide concentration ($C_a$) is one of the major uncertainties in projecting the future trajectory of the Earth's climate. Free Air $CO_2$ Enrichment (FACE) experiments are a main source of information on ecosystem responses to elevated $C_a$ under field conditions. To maximise the understanding of these experiments, it is essential to understand how the carbon cycle is modified by elevated $C_a$. In this chapter, I used the MAESTRA model to upscale leaf-level measurements at the Eucalyptus FACE (EucFACE) experiment and estimate the ambient Gross Primary Production (GPP) and its response to elevated $C_a$. In response to a 38% increase in $C_a$, measurements indicate that light-saturated leaf photosynthesis increased by 19% on average. MAESTRA estimated the annual GPP of the trees at the site to be ~1500 g C $m^{-2}$ $yr^{-1}$ under ambient $C_a$. With a 38% increase in $C_a$, GPP was estimated to increase by 12%. The smaller response simulated by the model at the canopy-scale as compared to that at the leaf-scale, was due to the prevalence of photosynthesis being limited by electron transport within the canopy. The simulated GPP had large inter-ring variability: across rings this variability reduced the estimated mean GPP response to ~8%. These results demonstrate that high natural variability (across experimental replicates) and a relatively low effect size can lead to a non-statistically significant response to elevated $C_a$. These results provide valuable insights into the response of GPP to elevated $C_a$ in evergreen woodland ecosystems, both in Australia and elsewhere.

## 4.2. Introduction

Forests are a large long-term store of carbon (Bonan, 2008; Pan et al., 2011) and are responsible for offsetting 25-33% of anthropogenic $CO_2$ emissions (Le Quéré et al. 2017). Atmospheric carbon dioxide concentration ($C_a$) has increased significantly since the beginning of the industrial era (Joos and Spahni, 2008) and is projected to continue to increase by 1.5-8 μmol $mol^{-1}$ per year into the future (IPCC, 2014). At the leaf scale, the direct physiological responses to increased $C_a$ are well understood: elevated $C_a$ (e$C_a$) stimulates plant photosynthesis (Kimball et al. 1993) and reduces stomatal conductance (Morison, 1985), which together increase plant water-use efficiency. These physiological responses have the potential to increase the amount of carbon stored in the terrestrial biosphere and thus, significantly slow the rate of climate change. However, projecting the response of the terrestrial carbon sink to future increases in $C_a$ is a major uncertainty in models (Friedlingstein et al. 2014), highlighting an urgent need to make greater use of data from manipulation experiments.

In line with observed responses to $CO_2$ in manipulative open-top chamber experiments (Eamus and Jarvis, 1989; Curtis and Wang 1998; Saxe et al. 1998; Medlyn et al., 1999) and ecosystem-scale FACE experiments (Ainsworth and Long, 2005; Norby et al., 2005), recent studies have highlighted evidence of $CO_2$ fertilisation in response to the gradual increase in $CO_2$ over the last 100 years, based on eddy-covariance measurements (Keenan et al. 2013) and satellite data (Donohue et al., 2009; Donohue et al., 2013; Yang et al., 2016; Zhu et al. 2016). By contrast, other studies have noted an apparent paradoxical lack of stimulation of vegetation growth (Peñuelas et al. 2011; Silva and Anand, 2013; van der Sleen et al. 2014), which raises questions about how mature ecosystems will respond to rising $C_a$.

In field-based $C_a$ experiments conducted on older trees (>30 years old), the response of tree growth to e$C_a$ has also been relatively small. In the first Web-FACE experiment, which was operated for four years at the single tree scale, there was no observed response of tree growth to e$C_a$ from a 35-metre-tall temperate deciduous forest (consisting of *Quercus*, *Fagus*, *Acer*, *Carpinus*, and *Tilia*) in Switzerland (Körner et al., 2005). Klein et al. (2016) later applied the same technique to the 110-year old, 40m tall *Picea abies* for five years and found no significant stimulation in above-ground biomass growth despite a 37% increase of leaf-level photosynthesis. These results were consistent with an earlier three-year whole-tree chamber study conducted in a 40-year old forest in Sweden with the same species (Sigurdsson et al.,

2013). Dawes et al. (2011) exposed three tree line species (~30 years old): *Larix decidua* L., *Pinus cembra* L. and *Pinus mugo* ssp. *uncinata* Ramond to e$C_a$ for nine years and found that the tree ring width of *Larix* increased but there was no significant response of tree ring width in the two *Pinus* species. However, whilst these e$C_a$ experiments focused on mature trees in the field, these experiments were on individual-tree scale, which limits the understanding of the potential ecosystem-scale response to e$C_a$.

The Eucalyptus FACE (EucFACE) is the first ecosystem-scale experiment with e$C_a$ in a mature native forest and provides a valuable case study of mature evergreen forest response to e$C_a$ under field conditions. This ongoing experiment started in 2012 and showed no significant increase in above-ground growth, despite a significant increase in leaf-level photosynthesis (Ellsworth et al. 2017). Results from the first three years of gas exchange measurements showed consistent stimulation of photosynthesis ($A$) of 19% (Gimeno et al., 2016; Ellsworth et al., 2017). Nevertheless, the leaf-level response did not lead to detectable changes in above-ground growth (Ellsworth et al., 2017) or transpiration (Gimeno et al., 2018). The findings from EucFACE are consistent with those from the individual-tree experiments described above (Körner et al., 2005; Dawes et al., 2011; Klein et al., 2016). These experiments also showed that in mature trees, above-ground growth was not statistically increased under e$C_a$ despite a stimulation of leaf-level photosynthesis.

These field experiments showed the response of tree growth to e$C_a$ to be smaller than that of leaf photosynthesis. Gross Primary Production (GPP) is the total carbon input to the canopy and provides the substrate for tree growth. The lack of response of tree growth to e$C_a$ could potentially be explained by a small response of GPP to e$C_a$. A key step is thus to calculate how leaf-level photosynthesis scales to the canopy GPP. Since GPP cannot be measured directly, previous studies have estimated GPP using a detailed model of canopy light interception that allows to scale leaf photosynthesis to the level of the canopy (Wang et al., 1998; Luo et al., 2001).

Wang et al. (1998) applied an array model, MAESTRO, to an open-top chamber experiment which exposed four-year old *Betula pendula* to e$C_a$ (+350 μmol mol$^{-1}$). The model was driven by site meteorological data and parameterised with leaf-level measurements. The effect of e$C_a$ stimulated leaf photosynthesis 46% in the model but the increase of canopy GPP was 110%.

Luo et al. (2001) further developed MAESTRO into a new version, MAESTRA, by updating the leaf gas exchange submodel and the code efficiency. They then applied MAESTRA to the Duke FACE site, where 14-year-old *Pinus taeda* dominated forest was exposed to $C_a$ +200 μmol $mol^{-1}$ since 1996. Their simulation showed that GPP of the site increased by ~39% under e$C_a$. However, the canopy GPP response rate was considerably smaller than that measured on current-year needles (67%) in the same site (Ellsworth, et al., 2011).

Several factors can account for the differences between the responses of leaf photosynthesis and GPP to e$C_a$. Firstly, the leaf-level response of photosynthesis is usually measured on sunlit leaves under saturating light. As a result, the leaf-level response represents the response of the photosynthesis rate when limited by maximum Rubisco activity ($V_{cmax}$). However, depending on the canopy architecture, the canopy could have a large number of shaded leaves, which would mean that the rate of photosynthesis could actually be limited by electron transport (i.e., RuBP regeneration; $J$). Electron-transport limited photosynthesis has a smaller response to e$C_a$ than Rubisco-limited photosynthesis (Ainsworth and Rogers, 2007), resulting in a smaller response of canopy GPP than leaf photosynthesis under saturating light.

The downregulation of photosynthesis under e$C_a$, or photosynthetic acclimation, is another important factor that controls the responses of photosynthesis and GPP to e$C_a$ (Long et al., 2004; Ainsworth and Rogers, 2007; Rogers, et al., 2017). Under long-term exposure to e$C_a$, some plants have been observed to reduce nitrogen allocation to Rubisco, which results in a decrease in photosynthetic capacity (Gunderson and Wullschleger, 1993). The average decrease in $V_{cmax}$ among plants in FACE experiments was a moderate 13% for all species and 6% for trees (Ainsworth and Long, 2005). However, maximum electron transport rate ($J_{max}$) was unaffected in most tree studies (Ainsworth and Long, 2007). Photosynthetic acclimation thus can change the JV ratio ($J_{max.25}$ : $V_{cmax.25}$), which determines the transition from Rubisco-limited to electron-transport-limited photosynthesis, and thus further modify the canopy GPP response to e$C_a$. Both Wang et al. (1998) and Luo et al. (2001) tested the impact of photosynthetic acclimation and showed a moderate reduction of canopy GPP (5-6%) due to photosynthetic acclimation (10-20%). However, whether that conclusion applies to other forest sites remains to be tested.

Another important factor determining differences between leaf and canopy responses is the feedback between GPP and leaf area index (LAI). For studies conducted on young forests before canopy closure, the increase of gross primary production (GPP) in response to e$C_a$

usually results in an increase in LAI which in turn further enhances GPP (Norby et al., 2005). This positive feedback amplified the effect of $CO_2$ and contributed to 60-90% of the increase in net primary production under e$C_a$ in the four FACE studies in Norby et al. (2005). However, in forests where LAI did not increase with e$C_a$ (i.e., after the canopy closure of the young forest or in mature forest), the response of canopy GPP to e$C_a$ was much smaller (e.g., Körner et al., 2005; Norby et al., 2010; Dawes et al., 2011; Ellsworth et al., 2017). In Wang et al. (1998), leaf area increased by 43% under e$C_a$, which alone increased GPP by 60%. In Luo et al. (2001), the trees had no detectable change in LAI. Consequently, GPP in their study showed a much smaller response (39%) to e$C_a$ (+60%). On the other hand, the sensitivity analysis conducted by Luo et al. (2001) showed that the canopy GPP was very sensitive to LAI and responded linearly to the change of LAI (i.e., 10% change in LAI translates into 10% change in GPP). Both the experiments and the modelling studies highlighted the important role of GPP-LAI feedback in determining the canopy GPP response to e$C_a$.

Following Wang et al. (1998) and Luo et al. (2001), I used MAESTRA (Duursma and Medlyn, 2012) to estimate canopy GPP at EucFACE. I first parameterised the model with *in situ* physiological and environmental measurements taken during the course of the experiment. Then, I partitioned the response to e$C_a$ into direct stimulation of GPP and the indirect effects of down-regulation of photosynthesis and differences in LAI. The goal of this study was to understand how ecosystem GPP responds to e$C_a$ and to provide a baseline against which to compare changes in other components of the ecosystem carbon balance.

## 4.3. Methods

### 4.3.1 Site

The EucFACE experiment is located in western Sydney, Australia (33.62º S, 150.7 º E). It consists of six circular plots, each of which has a diameter of 25 m (referred to as 'rings' hereafter). The rings are divided into two groups: control (with ambient e$C_a$; ≈ 400 μmol $mol^{-1}$; rings 2, 3, and 6) and treatment (e$C_a$; +150 μmol $mol^{-1}$; rings 1, 4, and 5). The tree canopy is dominated by *Eucalyptus tereticornis* which are ~20 m in height and have a basal area of ~24 $m^2$ $ha^{-1}$. The site receives a mean annual precipitation of 800 mm $yr^{-1}$, a mean annual photosynthetically active radiation (PAR) of 2600 MJ $m^{-2}$ $yr^{-1}$, and a mean annual temperature of 17 ºC.

### 4.3.2 Model

The MAESTRA model is a process-based tree-array model (Wang and Jarvis, 1990; Medlyn, 2004) that calculates canopy carbon exchange. In each timestep (30 min in this study), the model simulates the radiative transfer, photosynthesis, and transpiration of individual trees mechanistically. The following section will explain each of the processes in detail.

#### 4.3.2.1 Leaf scale model

The gas exchange submodel combines the leaf photosynthesis model of Farquhar et al. (1980) with the stomatal optimisation model, following Medlyn et al. (2011). This model is the same as the Medlyn V-D model in Chapter 3 but is described comprehensively and in more detail in this Chapter. The key equations are as follows. Stomatal conductance is modelled as:

$$g_s = 1.6 \cdot (1 + \frac{g_1}{\sqrt{D}}) \cdot \frac{A_{net}}{C_a} \quad (1)$$

where $g_s$ is the stomatal conductance to water vapour (mol $m^{-2}$ $s^{-1}$); $g_1$ is the optimal stomatal behaviour parameter, which combines the $g_s$ sensitivity to $D$ and photosynthesis ($kPa^{0.5}$; see definition in Medlyn et al. 2011); $A_{net}$ is the net $CO_2$ assimilation rate (μmol $m^{-2}$ $s^{-1}$); $C_a$ is the atmospheric $CO_2$ concentration (μmol $mol^{-1}$).

The impact of soil moisture on stomata is represented through an empirical function that links soil water availability to $g_1$ following (Drake et al., 2017):

$$g_1 = g_{1.max} \, (\frac{\theta - \theta_{min}}{\theta_{max} - \theta_{min}})^q \quad (2)$$

where the $g_{1.max}$ is the maximum $g_1$ value; $\theta$ is volumetric soil water content (%); $\theta_{max}$ and $\theta_{min}$ are the upper and lower limit within which $\theta$ has impact on $g_1$; $q$ describes the non-linearity of the curve.

$A_{net}$ was modelled as:

$$A_{net} = min(A_c, A_J) - R_{day} \quad (3)$$

where $A_c$ is the gross photosynthetic rate limited by carboxylation rate, while $A_J$ is the photosynthetic rate limited by electron transport rate; $R_{day}$ is the light respiration rate (μmol $m^{-2}$ $s^{-1}$).

$A_c$ is calculated as a function of maximum carboxylation capacity ($V_{cmax}$; μmol $m^{-2}$ $s^{-1}$) and intercellular $CO_2$ concentration ($C_i$):

$$A_c = V_{cmax} \frac{C_i - \Gamma^*}{K_c(1+\frac{O_i}{K_0})+C_i} \quad (4)$$

where $K_c$ and $K_o$ are the Michaelis–Menten coefficients of Rubisco activity for $CO_2$ and $O_2$, respectively (μmol $mol^{-1}$ and mmol $mol^{-1}$, respectively), and $\Gamma^*$ is the $CO_2$ compensation point in the absence of mitochondrial respiration (μmol $mol^{-1}$); $O_i$ is intercellular $O_2$ concentration (mmol $mol^{-1}$). The $K_c$, $K_o$, and $\Gamma^*$ are temperature dependent following Bernacchi et al. (2001). Following Yang et al. (Chapter 3), MAESTRA considers a non-stomatal limitation on $V_{cmax}$ at high $D$:

$$V_{cmax} = V_{cmax.t}(1 - c_D \cdot D) \quad (5)$$

where $V_{cmax.t}$ is calculated at given leaf temperature with $V_{cmax.25}$ and temperature response curve, and $c_D$ is a fitted parameter.

$A_J$ is calculated according to:

$$A_J = J \frac{C_i - \Gamma^*}{C_i + \Gamma^*} \quad (6)$$

where $J$ is the electron transport rate calculated by solving:

$$\theta_J \cdot J^2 - (\alpha_J \cdot Q_L + J_{max}) \cdot J + \alpha_J \cdot Q_L \cdot J_{max} = 0 \quad (7)$$

where $\theta_J$ describes the curvature electron transport rate (unitless); $\alpha_J$ is the quantum yield (μmol μmol $^{-1}$); $Q_L$ is the PAR absorbed by the leaf (i.e., incident PAR minus leaf reflectance and transmittance; μmol $m^{-2}$ $s^{-1}$); $J_{max}$ is the maximum electron transport rate at the given temperature (μmol $m^{-2}$ $s^{-1}$). Both $J_{max}$ and $V_{cmax}$ depend on leaf temperature and are modelled using a peaked Arrhenius function:

$$k_t = k_{25} \cdot \exp(E_a \frac{T_k - 298.15}{298.15 \cdot R_{gas} \cdot T_k}) \cdot (1 + \frac{\exp(298.15 \cdot \Delta S - H_d)}{298.15 \cdot R_{gas}}) / (1 + \frac{\exp(T_k \cdot \Delta S - H_d)}{T_k \cdot R_{gas}}) \quad (8)$$

where $k_t$ is the value of $J_{max}$ or $V_{cmax}$ at a given temperature (μmol $m^{-2}$ $s^{-1}$); $k_{25}$ is the value of $J_{max}$ or $V_{cmax}$ at 25 ºC; μmol $m^{-2}$ $s^{-1}$); $T_k$ is the leaf temperature in Kelvin; $E_a$ is the activation energy which describes the rate of increase of $k_t$ to temperature (J $mol^{-1}$); $H_d$ is the deactivation energy which describe the rate of decrease of $k_t$ to temperature (J $mol^{-1}$); $\Delta S$ is known as the entropy factor (J $mol^{-1}$ $K^{-1}$); $R_{gas}$ is the gas constant (J $mol^{-1}$ $K^{-1}$). Although MAESTRA has the capacity to calculate the leaf energy balance, for these simulations it was assumed that the leaf temperature equalled the air temperature because the canopy is sufficiently open that the leaves are well coupled with the atmosphere.

The model also assumes $R_{day}$ to be a fixed fraction (0.7) of $R_{dark}$ (dark respiration rate; μmol $m^{-2}$ $s^{-1}$), and uses an Arrhenius temperature response function:

$$R_{dark} = R_{dark.25} \cdot \exp(k_T \cdot (T_{leaf} - 25)) \quad (9)$$

where $k_T$ is the sensitivity of $R_{dark}$ to temperature ($^oC^{-1}$); and $T_{leaf}$ is the leaf temperature ($^oC$).

#### 4.3.2.1 Scaling to the canopy

The model represents the tree canopy as an array of tree crowns. The location and dimensions of each crown are specified based on site measurements. Calculations of carbon and water fluxes are made for each tree crown in turn. Each tree crown is divided into six layers. Here it was assumed that crowns are represented by an ellipsoidal shape and that leaf area is uniformly distributed across layers within the tree crown. Within each layer, the model evaluates the radiation transfer and leaf gas exchange at 12 grid points such that each crown is represented by a total of 72 grid points. The radiation intercepted at each grid point is calculated for direct and diffuse components by considering shading from the upper crown and surrounding trees and solar angle (zenith and azimuth), and light source (diffuse or direct). Penetration by direct radiation to each grid point is used to estimate the sunlit and shaded leaf area at each grid point. The radiation intercepted by the fraction of sunlit and shade foliage is then used calculate the leaf gas exchange.

Combining Eqns. 1- 9 yields the $g_s$ and $A_{net}$ of each grid point, which is then multiplied by leaf area at each grid point and summed to give whole-tree photosynthesis. Photosynthesis of individual trees is then summed to give whole-canopy photosynthesis.

### 4.3.3 Model Parameterisation

*Environmental forcing*

The model is driven by *in situ* PAR, temperature, vapour pressure deficit (*D*), wind speed, and soil moisture measurements (Figure 4.1 and 4.2). The PAR, temperature and *D* were measured every five minutes in each ring and then were gap-filled (by linear interpolation) and aggregated to 30 minute-mean time slices across all six rings (Figure 4.1). Two levels of atmospheric $CO_2$ concentration ($C_a$) were used in the model. The ambient $C_a$ was gap-filled and aggregated to 30 minute-mean time slices from the five-minute measurements across the three control rings. The e$C_a$ was processed in the same way but using data from the treatment rings.

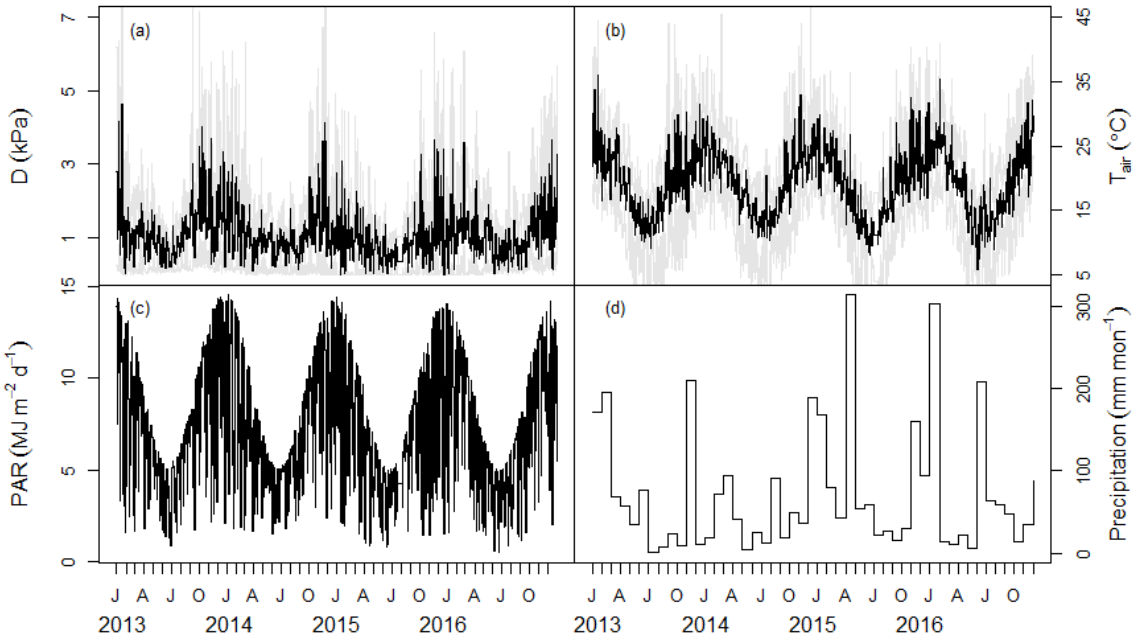


*Figure 4.1. Meteorological data measured at the site during the period 2013-2016. Panels show (a) daily mean vapour pressure deficit (D) with shaded area marking the maximum and minimum of the day, (b) daily mean air temperature ($T_{air}$) with shaded area marking the maximum and minimum of the day, (c) daily total photosynthetically active radiation (PAR), and (d) monthly total precipitation, respectively. Note that precipitation has no direct impact in the model but modifies stomatal conductance via the change in soil moisture, which is an input to the model.*

The volumetric soil water content ($\theta$) of the site was measured fortnightly using neutron probes. Measurements went to 4.5 m depth, but I found the strongest correlation of stomatal conductance with soil moisture averaged over the top two layers (25 and 50 cm) and hence used the average of these two depths as an input (Figure 4.2a). There were two probes in each ring and the average of these probes was used to represent the ring average for each measurement date.

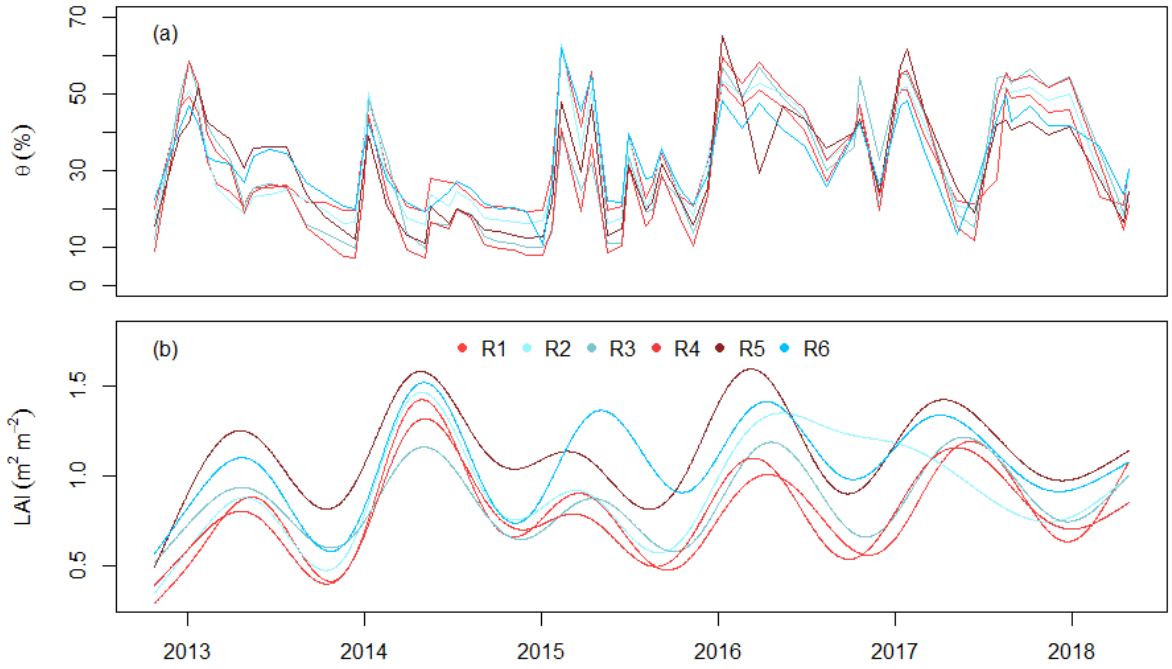


*Figure 4.2. (a) volumetric water content (θ) and (b) Leaf area index used to drive the model. Leaf area index was measured in each ring using the measured absorbed PAR and smoothed using generalized additive model following Duursma et al. (2016). θ was measured using neutron probes at top 50 cm biweekly and gap-filled using a linear interpolation between two nearest available data. Ambient rings (2, 3, 6) shown in blue colours; elevated rings (1,4,5) shown in red colours.*

*Canopy structure*

Trees in MAESTRA were represented by their actual location, height, and crown size to mimic the realistic effects of shading. Tree location, crown height, crown base and stem diameter were measured in January 2013 at the start of the experiment. For each ring, a time-series of LAI was obtained based on measurements of above- and below-canopy PAR (Duursma et al. 2016). This LAI represents plant area index, which includes the woody component as well as leaves. In order to retrieve the actual LAI, I assumed a constant branch and stem cover (0.8 $m^2$ $m^{-2}$) based on the lowest LAI during 2014 when the canopy shed almost all leaves. The LAI used in this study was thus the LAI from Duursma et al. (2016) subtracting 0.8 $m^2$ $m^{-2}$ (Figure 4.2a). Since LAI is the only parameters beside soil moisture that differed by ring, the canopy structure (i.e., the LAI and its distribution) was thus the major driver of inter-ring variability.

The total leaf area ($m^2$) of each ring was calculated as the product of LAI and ground area (491 $m^2$). This total leaf area (LA) was then assigned to each tree based on an allometric relationship between the total leaf area ($m^2$) and diameter at breast height (DBH; m). The allometric relationship was derived from data in the BAAD database (Falster et al., 2015) for *Eucalyptus* trees grown in natural conditions with DBH < 1 m to match the characteristics of EucFACE. In total, this database yielded a total of 66 observations with which to estimate the relationship between LA and DBH:

$$L_{allom} = a \cdot DBH^b \quad (10)$$

where $L_{allom}$ is the estimated leaf area based on the allometric relationship with DBH, The values obtained for $a$ and $b$ were 492.6 and 1.8 respectively. This relationship was used to assign the total LA of each ring to each tree in the following steps: (i) the $L_{allom}$ for each tree was calculated based on DBH; (ii) the $L_{allom}$ was summed to obtain a total leaf area for each ring; and (iii) the fractional contribution of each tree to the ring total leaf area was calculated. The total leaf area was then assigned to each tree based on this fraction.

The leaf angles were assumed to follow a spherical distribution, which is the default setting in MAESTRA.

The crown radius was calculated with a linear function with DBH based on measurements in August 2016. The data contained DBH and crown radius (one on North-South axis and one on East-west axis) of four trees in each ring. The original crown radius data were averaged for each tree and fitted to a linear model with DBH. The estimated slope and intercept of the relationship are 9.5 (m $m^{-1}$) and 0.765 (m), respectively.

MAESTRA also considered the shading from surrounding trees outside the rings. However, no measurements of locations or diameters were available for the trees surrounding the rings. Therefore, a total of 80 surrounding trees were arbitrarily assumed to form two circular layers around each ring. They were assigned with the mean height, mean radius, and mean leaf area estimated from all trees in EucFACE. Except for shading, the surrounding trees have no impact on the trees within the rings. Ring 1 is shown in Figure 4.3 as an example of the representation of canopy structure in MAESTRA.

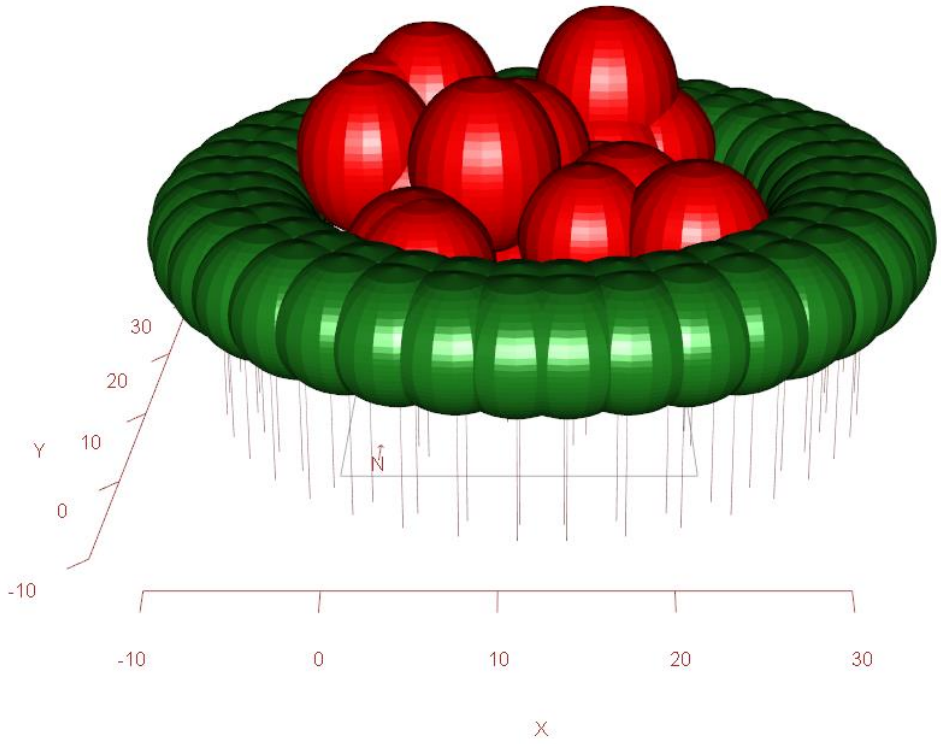


*Figure 4.3. Example of tree stand represented in MAESTRA. The figure shows the trees in ring 1 (red) and the surrounding trees outside the ring (green). Other rings look similar with realistic tree locations and sizes.*

*Physiology*

Field gas exchange measurements were used to parameterise the leaf gas exchange model. After examining the measurements from the ambient and elevated rings, the only significant effect of $CO_2$ was on $V_{cmax.25}$ (Figure 4.4 and 4.5). Hence, all other parameters (e.g., the temperature responses of photosynthesis and respiration) were estimated by combining all data. Fitted parameter values are given in Table 4.1.

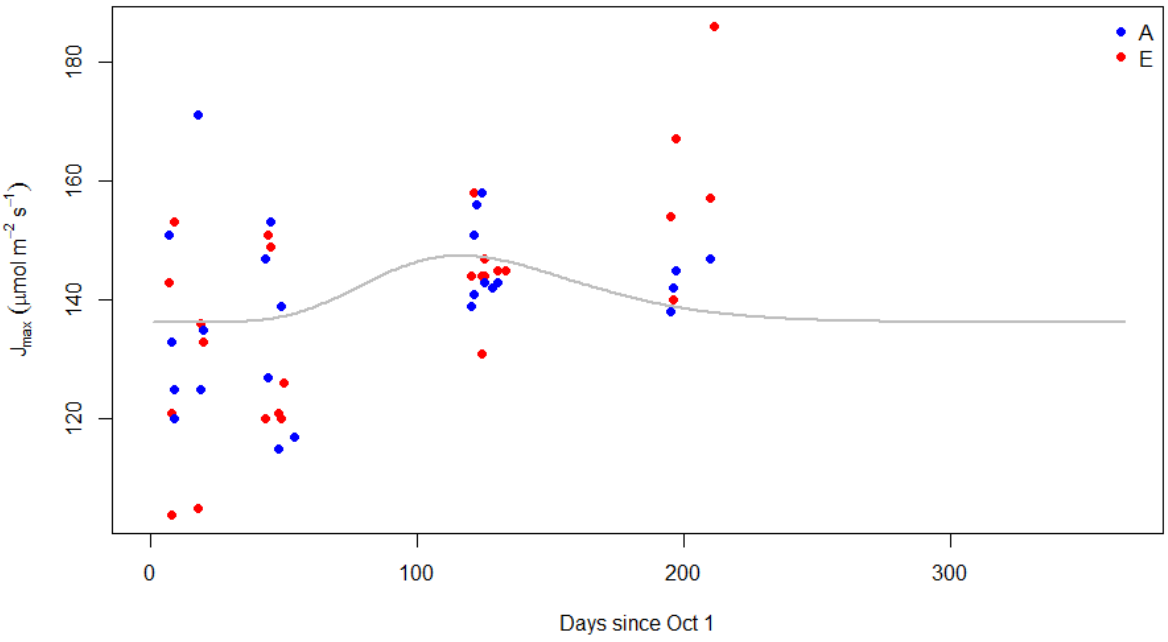


*Figure 4.4. $J_{max.25}$ seasonality. The dots indicate the estimated $J_{max}$ at 25 ºC from ACi curves, averaged by ring and date. The grey line shows the fitted phenology. Red colour indicates data treatment rings while blue colour indicates control rings.*

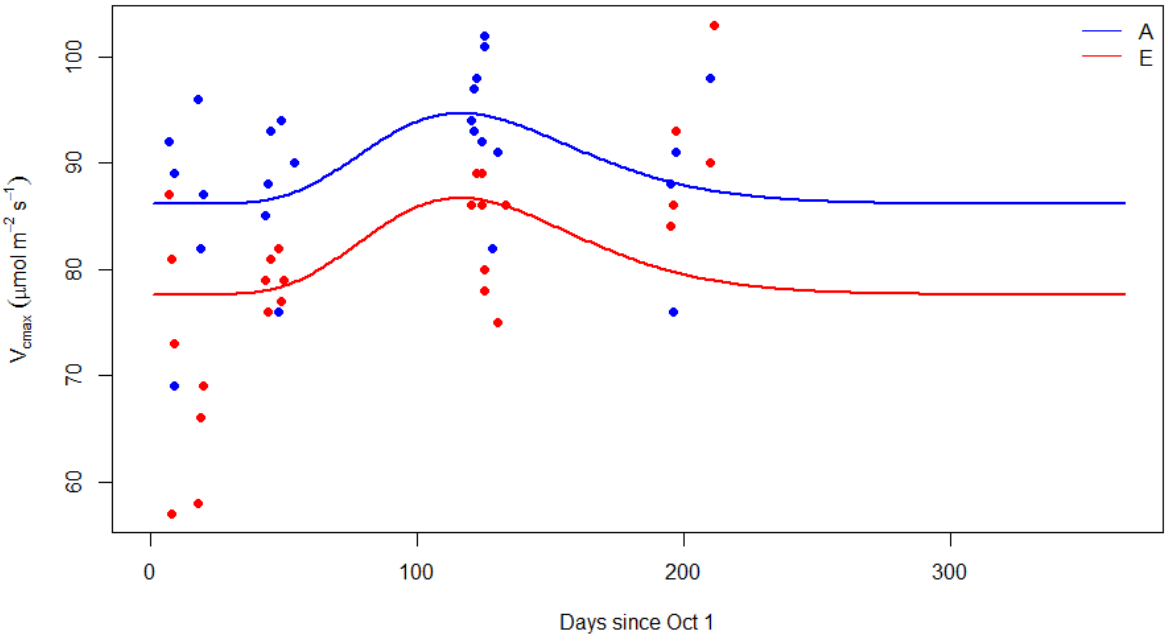


*Figure 4.5. $V_{cmax.25}$ seasonality. The dots showed the estimated $V_{cmax}$ at 25 ºC from ACi curves (averaged by ring and date). The lines were the fitted phenology. Red colour indicates data treatment rings while blue colour indicates control rings.*

Repeated gas exchange measurements were made on the same leaves in the morning and afternoon under prevailing field conditions and saturating light (1800 umol $m^{-2}$ $s^{-1}$) on four occasions in 2013 ("diurnal"; Gimeno et al., 2016). These data were used to estimate the $g_1$ parameter in the stomatal conductance model (Eqn. 1) using the fitBB function in the *plantecophys* R package (Duursma, 2015). One $g_1$ value was fitted to the data of each ring and date. The $g_1$ values were then regressed against $\theta$ measured in each ring to estimate the impact of soil moisture availability on leaf gas exchange, following Eqn. 2. The $g_1$ values were related to the nearest measurements of $\theta$ (within a week without rain). I combined this data set with $g_1$ and $\theta$ measurements from a drought manipulation experiment with the same species (Drake et al., 2017). Eqn. 2 was fitted to this combined data set using the non-linear least squares method (Figure 4.6).

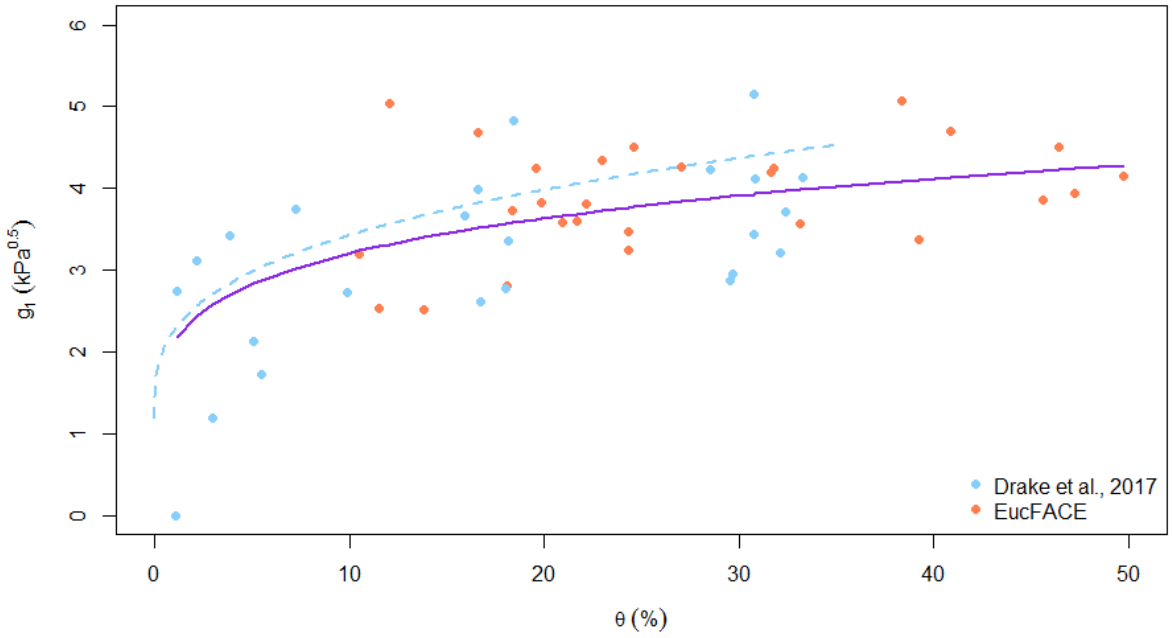


*Figure 4.6. The impact of soil moisture content on stomatal regulation. x axis shows the volumetric soil water content (θ; %) measured from top to 50cm below ground in each ring around the time of gas exchange measurements. Orange coloured points mark the $g_1$ estimated from the EucFACE data. The blue dots are data from Drake et al. (2017). The purple line is the fit to both of the data sets compared to the fit (blue dashed line) from Drake et al. (2017).*

A set of photosynthesis-$CO_2$ response (ACi) curves was measured at different leaf temperatures (20-40 ºC) under saturating light in February 2016 (Crous, et al., in prep.). The dataset was used to quantify the temperature dependences of $J_{max}$ and $V_{cmax}$ by fitting a

peaked Arrhenius function (Eqn. 8) to the measurements. The same temperature response functions were used for all the trees throughout this research.

Morning ACi curves were also measured at prevailing leaf temperatures for ten field campaigns during 2013 to 2016 (Crous, et al., in prep.). All ACi curves were started at ambient $C_a$ of 395 μmol $mol^{-1}$ with a saturating light of 1800 μmol $m^{-2}$ $s^{-1}$ and a flow rate of 500 μmol $s^{-1}$. These data were used to estimate $J_{max}$ and $V_{cmax}$ at 25 ºC using the fitaci function in the *plantecophys* R package (Duursma, 2015). The fitting used the measured temperature responses of $J_{max}$ and $V_{cmax}$ as described in the previous paragraph. Mean values of $J_{max.25}$ and $V_{cmax.25}$ were calculated for each ring and campaign. There were clear seasonal patterns in these values as leaves aged. This effect was captured using a phenology of $V_{cmax.25}$ and $J_{max.25}$ derived from canopy greenness (Green Chromatic Coefficient, GCC):

$$V_{cmax.25} = (V_{80} - V_{20}) \cdot f(GCC) + V_{20} \quad (11)$$

Where $V_{cmax.25}$ is $V_{cmax}$ value at 25 ºC; $f$(GCC) is the phenology derived from the canopy greenness; $V_{80}$ and $V_{20}$ are the 80 and 20% quantiles of observed $V_{cmax.25}$, respectively. This relationship is the same for $J_{max}$ with $J_{80}$ and $J_{20}$ (i.e., the 80 and 20% quantiles of observed $J_{max.25}$, respectively) replacing $V_{80}$ and $V_{20}$. The estimated $J_{max}$ and $V_{cmax}$ values along with the fitted lines are shown in Figure 4.4 and 4.5.

GCC values were derived from phenology cameras mounted above the canopy. Starting in November 2014, on each overcast day the cameras took four photos of each ring at noon. The GCC was taken to be the green channel of each RGB photo. These values were then aggregated to each ring and date, standardised to 80% and 20% quantiles, and used to calculate an annual phenology:

$$GCC = f_a \cdot t^{f_b} + {f_c}^t \quad (12)$$

where $f_a$ and $f_b$ are fitted parameter values; $t$ is number of days from the arbitrary date of leaf flushing (October 1st in the previous year); $f_c$ was fixed to 0.0005 to reduce the degree of freedom of the model and to improve fitting.

$R_{dark}$ was measured at least three hours after sun set at a range of leaf temperatures in February 2016 (Crous, et al., in prep.). The temperature dependence of $R_{dark}$ was fitted using non-linear least squared method to all of the measured data using Eqn. 9.

Light responses of photosynthesis were measured on two trees from each ring in October 2014 (Crous, et al., in prep.). These data sets were used to constrain the parameters in Eqn. 7.

The $\alpha_J$ and $\theta_J$ of $J$ were fitted to *in situ* light response curves. I assumed that $\alpha_J$ is related to quantum yield of photosynthesis ($\alpha$):

$$\alpha_J = 4 \cdot \alpha \cdot \frac{C_i + 2 \cdot \Gamma^*}{C_i - \Gamma^*} \quad (13)$$

A linear model was fitted to the measured photosynthesis fluxes and absorbed PAR from the initial part of the light response curves (< 100 μmol $m^{-2}$ $s^{-1}$) and the fitted slope was assumed to be $\alpha$. This slope was converted to $\alpha_J$ using Eqn. 13. The curvature of $J$ ($\theta_J$) was assumed to be the same as photosynthesis and thus could be estimated by fitting the following quadratic relationship:

$$A = \alpha \cdot Q_L + A_{max} - \frac{\sqrt{(\alpha \cdot Q_L + A_{max})^2 - 4 \cdot \alpha \cdot Q_L \cdot A_{max} \cdot \theta_J}}{2 \cdot \theta_J} \quad (14)$$

where $A$ is the photosynthetic rate (i.e., $CO_2$ assimilation rate; μmol $m^{-2}$ $s^{-1}$), $A_{max}$ is the maximum of $A$, $Q_L$ is the absorbed PAR and was calculated as a fraction (0.825) of incident PAR, after subtracting reflectance (0.082) and transmittance (0.093). Eqn. 14 was fitted to the full light response curves using non-linear least squared method to obtain the values of $A_{max}$ and $\theta_J$, assuming $\alpha$ from above. The measured light response data along with the fitted curves are shown in Figure 4.7. Since the fitting appears to be very similar in the ambient and elevated data, this study used one $\theta_J$ value fitted to all the data.

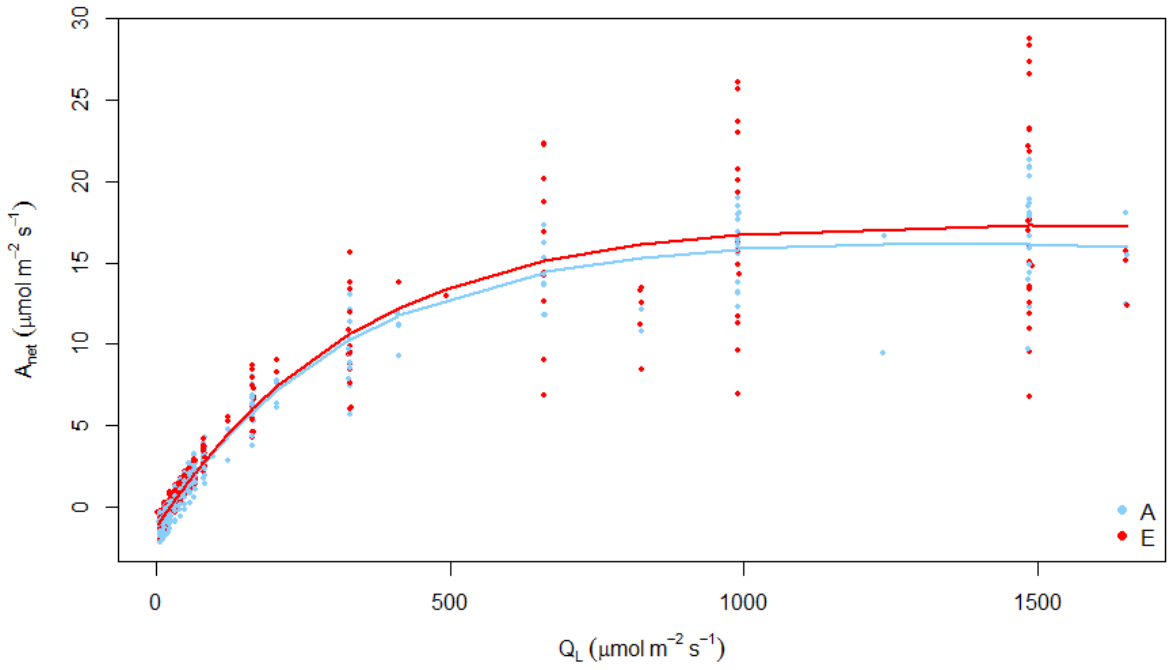


*Figure 4.7. The response of photosynthesis to light. The dots show the measured net assimilation rate ($A_{net}$) at different leaf absorbed PAR ($Q_L$). The curves are the fitted responses of photosynthesis to light using fitted parameter values (Eqn. 7, 12, and 13). The colours mark the $C_a$ at which the measurements were taken: red-elevated (550 µmol mol $^{-1}$); blue-ambient (400 µmol mol $^{-1}$). The variation of $A_{net}$ at each $Q_L$ level, shows the inter-tree and inter-ring variability.*

### 4.3.4 Model simulations and analysis

MAESTRA was used to simulate radiation interception and gas exchange of all six rings between the period of 1 January 2013 to 31 December 2016 on a half-hourly basis. The model simulated half-hourly gross primary production (GPP) of each tree, which was then summed for all trees in each ring to get the total annual GPP for each ring.

Four different sets of simulations were used to estimate the GPP under ambient and e$C_a$ and to identify the key limiting factor(s) on canopy GPP response to e$C_a$. Firstly, a simulation of leaf scale ("leaf scenario") photosynthesis with measured meteorological data but fixed physiological data ($g_1$ = 4.3 kPa$^{0.5}$, $V_{cmax.25}$ = 90 µmol m$^{-2}$ s$^{-1}$, and $J_{max.25}$ = 144 µmol m$^{-2}$ s$^{-1}$). This simulation aimed to quantify the $CO_2$ response size of Rubisco-limited and electron-transport limited photosynthesis at leaf scale. This calculation was made using the *photosyn*

function in *plantecophys* R package (Duursma, 2015). This function implements the leaf gas exchange routine used in MAESTRA.

Secondly, MAESTRA was run for all six rings with ambient $C_a$ and with $V_{cmax.25}$ from ambient measurements ("ambient scenario"). The results of this simulation were used to calculate the GPP of each ring under ambient conditions. The ambient GPP values were also used to evaluate the inherent variability among the rings.

Thirdly, all six rings were simulated with e$C_a$ and $V_{cmax.25}$ based on measurements from ambient rings ("elevated scenario"). The results of this simulation were compared to those from the ambient scenario to illustrate the direct response of canopy GPP to e$C_a$ in each ring and year. This simulation also quantitatively shows the variation of the GPP response to e$C_a$ across rings and years.

The last simulation consisted of simulating the three rings exposed to e$C_a$ (rings 1, 4, and 5) and using the $V_{cmax.25}$ measured from these elevated rings ("field scenario"). Results from the field scenario were used for two analyses: (i) to compare GPP from the field scenario to that of the three rings from the elevated scenario (i.e., e$C_a$ and ambient $V_{cmax}$), which quantified the impact of photosynthetic acclimation; (ii) to calculate the difference in GPP between the three ambient rings in ambient scenario and elevated rings in the field scenario to estimate the response of GPP to e$C_a$ in the field.

*Table 4.1. Summary table of parameter definitions, units, and sources used in this study.*

| Parameters | Definitions | Units | Values | Sources | Eqn. |
|---|---|---|---|---|---|
| $\alpha_J$ | Quantum yield of electron transport rate | μmol μmol $^{-1}$ | 0.30 | This study | 13 |
| $a$ | Fitted slope of LA and DBH | $m^2$ $m^{-1}$ | 492.6 | This study | 10 |
| $b$ | Fitted intercept of LA and DBH | - | 1.8 | This study | 10 |
| $c_D$ | Slope of $V_{cmax}$ to $D$ | $kPa^{-1}$ | 1.74 | Chapter 3 | 5 |
| $\Delta S$ | Entropy factor | - | 639.60 ($V_{cmax}$); 638.06 ($J_{max}$) | This study | 8 |
| $E_a$ | Activation energy | J $mol^{-1}$ | 66386 ($V_{cmax}$); 32292 ($J_{max}$) | This study | 8 |
| $f_a$ | Greenness parameter | - | 2738.2 | This study | 12 |
| $f_b$ | Greenness parameter | - | 8.8 | This study | 12 |
| $f_c$ | Greenness parameter | - | 0. 0005 | Assumed | 12 |
| $g_{1.max}$ | Maximum $g_1$ value | $kPa^{0.5}$ | 4.3 | This study | 2 |
| $H_d$ | Deactivation energy | J $mol^{-1}$ | 200000 | Medlyn et al. (2002) | 8 |
| $\theta_J$ | Curvature of electron transport rate to $Q_{APAR}$ | - | 0.48 | This study | 14 |
| $\theta_{max}$ | Upper limit which $\theta$ has impact on $g_1$ | % | 55 | This study | 2 |

| | | | | | |
|---|---|---|---|---|---|
| $\theta_{mim}$ | Lower limit which $\theta$ has impact on $g_1$ | % | 0 | This study | 2 |
| $J_{80}$ | 80% quantile of $J_{max.25}$ | µmol $m^{-2}$ $s^{-1}$ | 152 | This study | 11 |
| $J_{20}$ | 20% quantile of $J_{max.25}$ | µmol $m^{-2}$ $s^{-1}$ | 125 | This study | 11 |
| $k_T$ | Sensitivity of $R_{dark}$ to temperature | $^oC^{-1}$ | 0.078 | This study | 9 |
| $q$ | The non-linearity of the $g_1$ dependence of $\theta$ | - | 0.17 | This study | 2 |
| $R_{day.25}$ | Light respiration rate | µmol $m^{-2}$ $s^{-1}$ | 0.9 | This study | 9 |
| $R_{dark.25}$ | Dark respiration rate | µmol $m^{-2}$ $s^{-1}$ | 1.3 | This study | 9 |
| $R_{gas}$ | Gas constant | J $mol^{-1}$ $K^{-1}$ | 8.314 | - | 8 |
| $V_{80}$ | 80% quantiles of $V_{cmax.25}$ | µmol $m^{-2}$ $s^{-1}$ | 96 (ambient); 89 (elevated) | This study | 11 |
| $V_{20}$ | 20% quantiles of $V_{cmax.25}$ | µmol $m^{-2}$ $s^{-1}$ | 82 (ambient); 75 (elevated) | This study | 11 |

## 4.4. Results

Figure 4.8 summarises the results from measurements and the different simulations conducted in this study. It demonstrates that the impact of e$C_a$ diminishes after considering larger scales and more feedback effects. Each row of Figure 4.8 will be explained in detail in the following paragraphs.

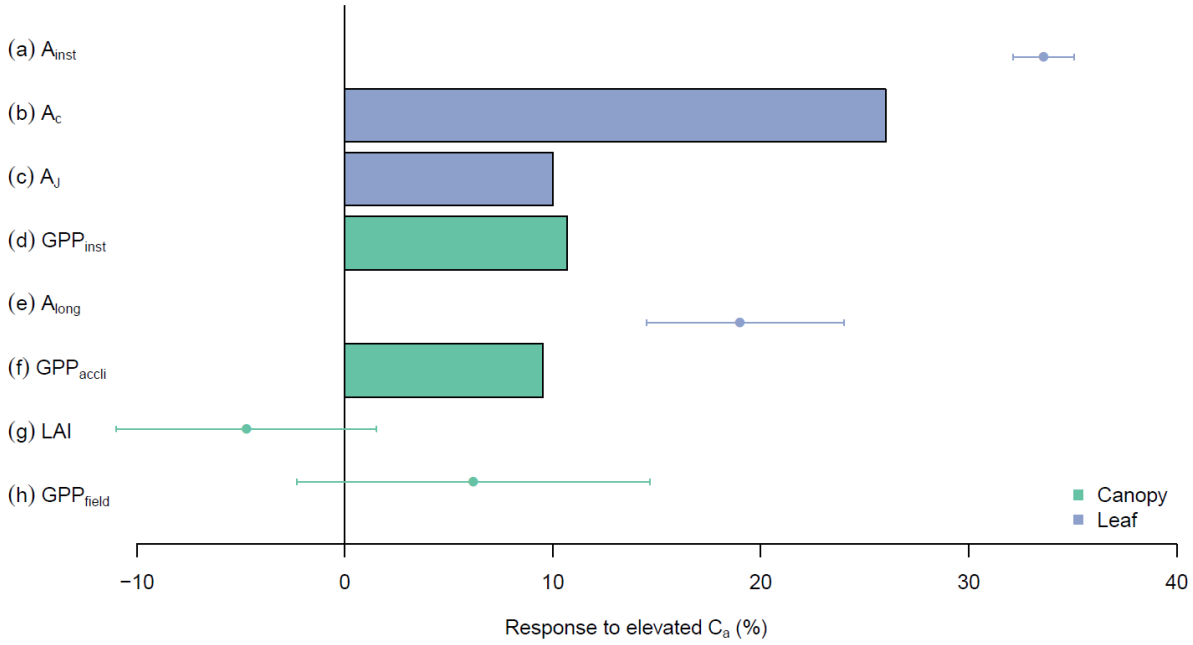


- *Figure 4.8. The response of photosynthesis to e$C_a$ on different scales and limited by different factors. In summary, from top to bottom, the figure demonstrates how a large increase in leaf photosynthesis can diminish into a non-statistically significant change in canopy GPP under e$C_a$. Entries from top to bottom are as follows. (a) $A_{inst}$, the short-term response of leaf photosynthesis to e$C_a$ obtained from A-$C_i$ measurements in ambient rings (error bars indicate 95% CI). (b) $A_c$, the modelled response of Rubisco-limited leaf photosynthesis, assuming no down-regulation, averaged over the range of diurnal air temperatures experienced during the*

*experimental period. (c) $A_J$, the modelled response of RuBP-regeneration limited leaf photosynthesis. (d) $GPP_{inst}$, the direct effect of $eC_a$ on canopy GPP, modelled with MAESPA, assuming no downregulation of photosynthesis and averaged across all six rings. (e) $A_{long}$, the long-term response of leaf photosynthesis to $eC_a$ obtained from leaf photosynthesis measured at treatment $CO_2$ concentrations (see Ellsworth et al. 2017). This value is different from $A_{short}$ because it incorporates photosynthetic acclimation. (f) $GPP_{long}$, the effect of $eC_a$ on canopy GPP once the measured down-regulation of $V_{cmax}$ is taken into account. (g) LAI, the measured difference in average LAI between $eC_a$ and ambient $C_a$ rings over the experiment period (data from Duursma et al. 2016). (h) $GPP_{field}$, the GPP response modelled with MAESPA comparing the three elevated rings with the three ambient rings. See text for further explanation.*

### 4.4.1 $C_a$ response of photosynthesis at leaf level

The mean instantaneous $C_a$ response of leaf-level photosynthesis ($A_{inst}$) was +33%, as shown in the top row of Figure 4.8. This response ratio is calculated from ACi curves measured in ambient rings. From those curves, I obtained the photosynthesis at 400 and 550 $C_a$ (μmol mol $^{-1}$) and calculated the $C_a$ effect as the ratio of those photosynthesis values. This approach allows an estimation of direct $CO_2$ response independent of the impact of photosynthetic acclimation.

In contrast, the mean direct canopy GPP response to e$C_a$ is considerably less, just +12%, as shown in row 4 of Figure 4.8. This canopy response rate is calculated by comparing the GPP of all six rings under ambient and elevated $C_a$ ("ambient" vs. "elevated" scenario). As a result, this direct canopy GPP response rate also excludes the impact of photosynthetic acclimation.

The transition from Rubisco to electron transport limited photosynthesis is a major explanation for the discrepancy between the responses of leaf photosynthesis and canopy GPP. Leaf gas exchange measurements were taken in saturating light and thus, are likely to be Rubisco limited, whereas some of the canopy may be electron-transport limited, and the response of photosynthesis to e$C_a$ is much smaller under electron transport limitation than under Rubisco limitation.

Figure 4.9 illustrates the response of Rubisco limited photosynthesis ($A_c$) to e$C_a$ under different temperature. The $A_c$ values are predicted with the same meteorological data as the stand-scale model, MAESTRA, but assumed constant $V_{cmax}$ and $g_1$. Figure 4.10 shows the

response of electron-transport limited photosynthesis ($A_J$) to e$C_a$ under different temperature. The $A_J$ values are predicted in the same way as $A_c$ but assuming constant $J_{max}$ and $g_1$. Although the response of $A_c$ and $A_J$ are temperature dependent, $A_c$ response to e$C_a$ on average (+26%; row 2 of Figure 4.8) is larger than when leaves are electron-transport limited (+10%; row 3 of Figure 4.8). The observed response rate of $A_{inst}$ is thus closer to that of $A_c$ due to the fact that measurements were taken under saturating light. Temperature is the reason for a higher response rate of $A_{inst}$ than the average of $A_c$. The response of photosynthesis increases with increasing temperature, and leaf gas exchange measurements are made at leaf temperatures in the higher range of leaf temperatures, from 24 to 32 ºC.

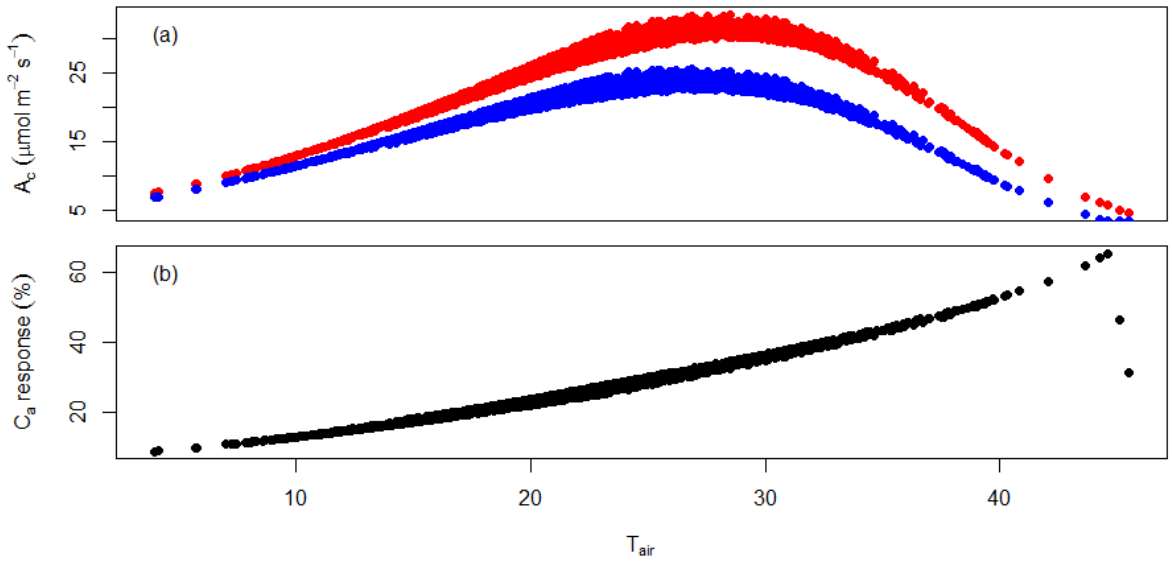


*Figure 4.9. The modelled $C_a$ response rate of Rubisco limited photosynthesis ($A_c$) against leaf temperature ($T_{air}$). These photosynthesis values were calculated with the same meteorology data as in the stand scale model for 2013-2016. However, $V_{cmax.25}$ and $g_1$ were assumed to be constant for the clarity of the figures ($g_1$ = 4.3 kPa$^{0.5}$ and $V_{cmax.25}$ = 90 µmol m$^{-2}$ s$^{-1}$). The leaf gas exchange model is from photosyn function (plantecophys package in R), which is the same as the leaf gas exchange submodel in MAESTRA.*

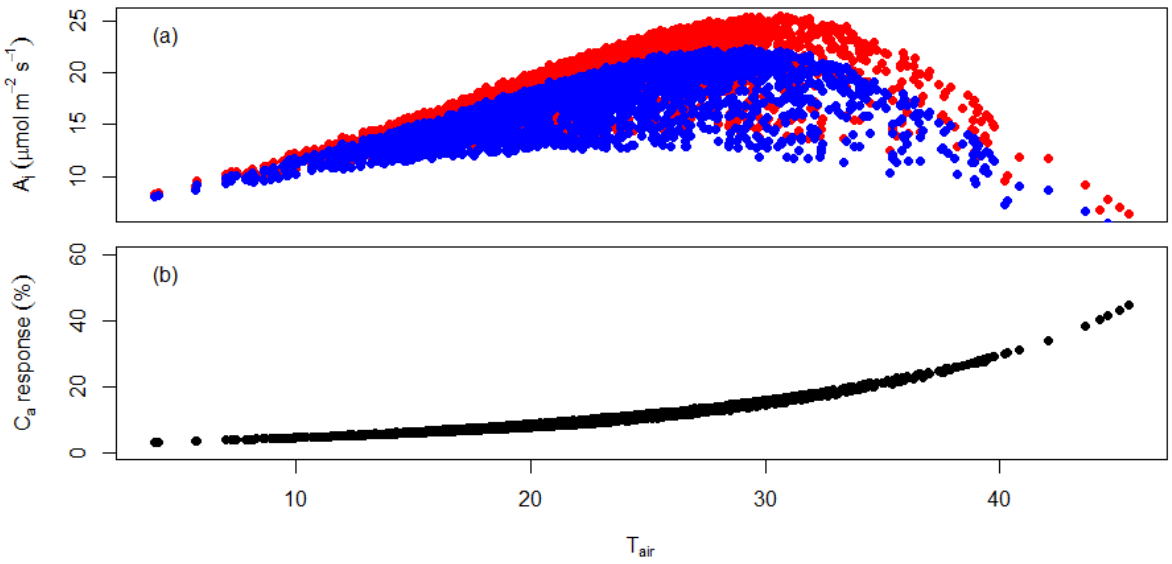


*Figure 4.10. The $C_a$ response rate of* electron transport *limited photosynthesis ($A_J$) against air temperature ($T_{air}$). These photosynthesis values were calculated with the same meteorology data as in the stand scale model for 2013-2016. Again, $g_1$, and $J_{max}$ were assumed to be constant for the clarity of the figures ($g_1$ = 4.3 $kPa^{0.5}$ and $J_{max.25}$ = 144 µmol $m^{-2}$ $s^{-1}$; i.e., assuming a* JV *ratio =1.6). The leaf gas exchange model is from photosyn function (plantecophys package in R), which is the same as the leaf gas exchange submodel in MAESTRA.*

### 4.4.2 $C_a$ response of GPP at canopy level

The response of canopy GPP to e$C_a$ is +12% according to MAESTRA (Row 4 of Figure 4.8). This response rate is calculated by directly comparing the GPP values under the "elevated" and "ambient" scenarios. The response of canopy GPP to e$C_a$ is smaller that of $A_c$ but closer to that of $A_J$, indicating the photosynthesis of most the canopy is electron-transport limited. Figure 4.14 shows a frequency histogram, output from MAESTRA, of absorbed PAR across all rings during 2013-2016. This histogram quantifies the leaf area falling into each PAR bin for every half-hour (during daytime). There are two peaks in Figure 4.14, which shows the absorbed PAR of sunlit (~1700 µmol m$^{-2}$ s$^{-1}$) and shaded leaves (~500 µmol m$^{-2}$ s$^{-1}$). Most (>80%) of the canopy has an absorbed PAR below 1700 µmol m$^{-2}$ s$^{-1}$, which translates into an incident PAR of 1800 µmol m$^{-2}$ s$^{-1}$ with the assumed reflectance and absorbance rate in the model.

In Figure 4.12, I estimate the PAR level at which Rubisco activity becomes limiting. The transition point from Rubisco to electron-transport limited photosynthesis is calculated with the leaf gas exchange submodel and assuming constant $C_a$ (400 μmol $mol^{-1}$), $D$ (1.5 kPa), $g_1$ (4.3 $kPa^{0.5}$), and $V_{cmax.25}$ (90 μmol $m^{-2}$ $s^{-1}$) but varying leaf temperature and $J_{max.25}$ : $V_{cmax.25}$ ratio (JV ratio). As shown, Rubisco activity is typically limiting above an incident PAR of 1800 μmol $m^{-2}$ $s^{-1}$. Comparing with Figure 4.11, this suggests that >80% of the leaf area is electron-transport limited rather than Rubisco-limited. This strong limitation by electron transport is due to the relatively low JV ratio of 1.6. As shown in Figure 4.12, using a higher JV ratio such as the more typical value of 2 would decrease the saturating PAR value at which photosynthesis becomes Rubisco limited. As a result, the smaller response of canopy GPP to e$C_a$ compared to that of leaf-level photosynthesis can be explained as an effect of electron-transport limitation through the canopy as well as lower leaf temperatures.

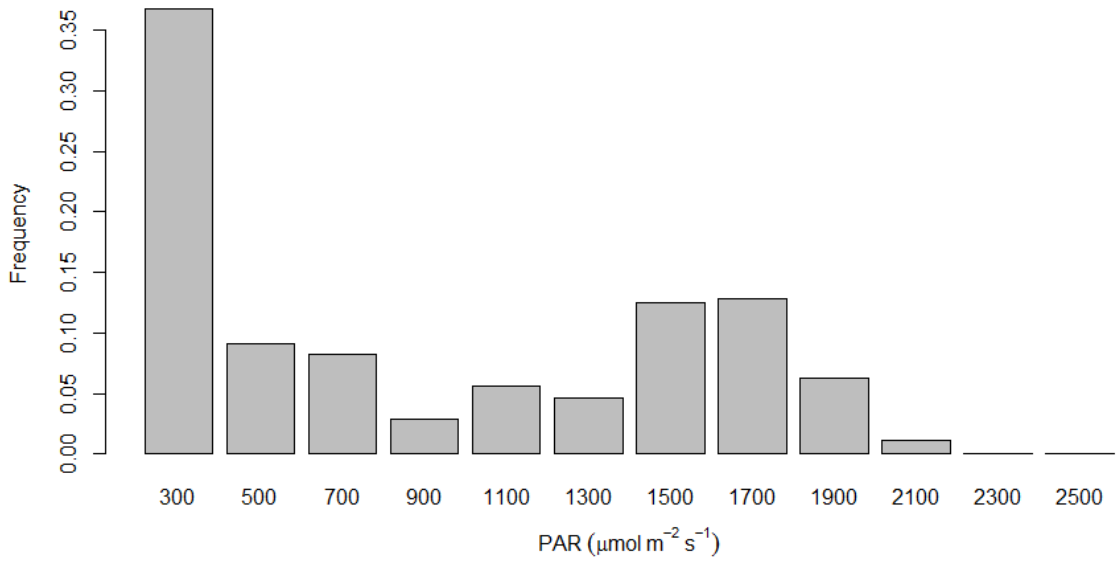


*Figure 4.11. Frequency histogram of absorbed PAR across all rings during 2013-2016. Histogram was constructed by calculating the leaf area falling into each PAR bin for every half-hour (during daytime). These values are summed and then normalised to give a frequency histogram. Each PAR bin is 200 μmol $m^{-2}$ $s^{-1}$ wide; the labels on the x-axis mark the maximum value of each bin. The bars thus show the relative leaf area falling into each PAR bin during the four years of simulation.*

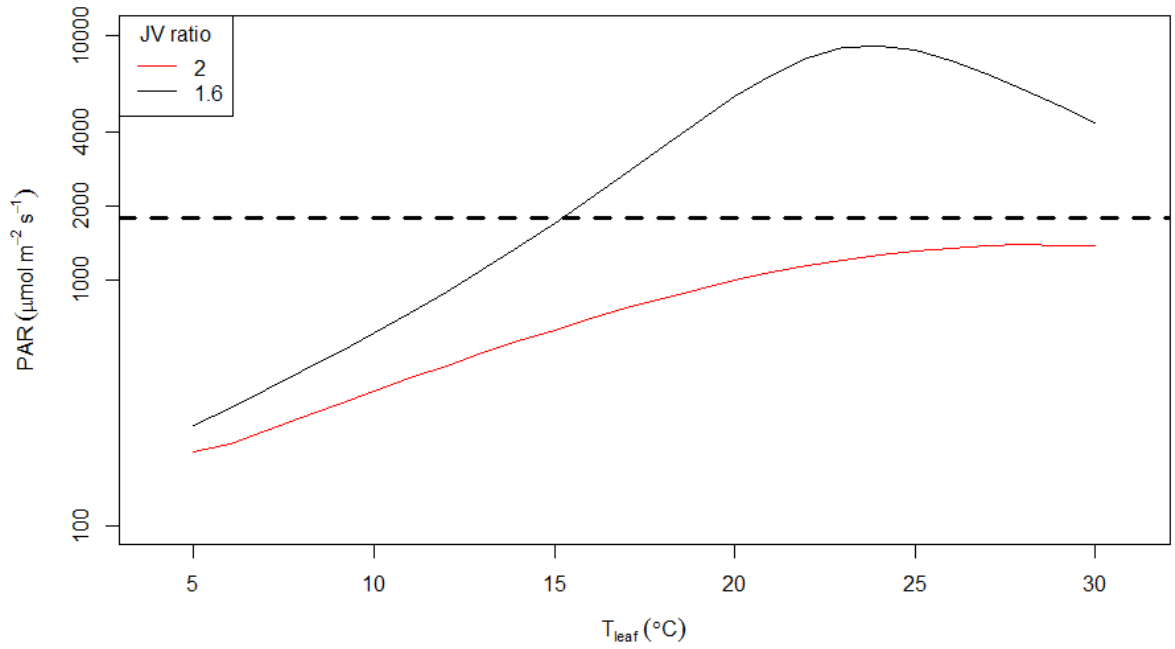


*Figure 4.12. Conceptual figure showing the transition PAR values for photosynthesis from electron transport limited to Rubisco limited under different leaf temperature. The curves were predicted using the Photosyn function in the plantecophys R package (Duursma, 2015). The parameters other than PAR and $T_{leaf}$ were assumed to be constant: $C_a$ = 400 µmol $mol^{-1}$; D =1.5 kPa; $g_1$ = 4.3 $kPa^{0.5}$; $V_{cmax.25}$ = 90 µmol $m^{-2}$ $s^{-1}$. The temperature and light dependences of photosynthesis were assumed to be the same as in MAESTRA. The black line was predicted by assuming $J_{max.25}$ = 144 µmol $m^{-2}$ $s^{-1}$ (i.e.,* JV ratio= *1.6). This JV ratio was observed consistently in EucFACE across campaigns and rings (Figure 4.13). The red line was predicted by assuming $J_{max.25}$ = 180 µmol $m^{-2}$ $s^{-1}$ (i.e.,* JV ratio= *2). This JV ratio has been commonly reported and used in other studies. The dashed line shows the PAR = 1800 µmol $m^{-2}$ $s^{-1}$ at which the measurements of EucFACE were made. Note the log scale of the y axis.*

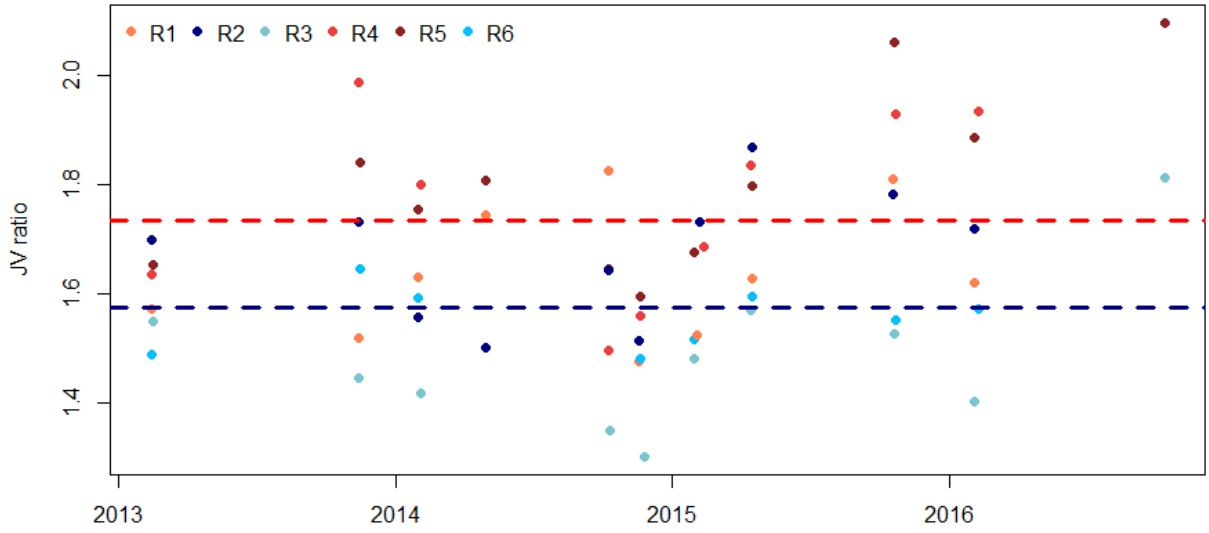

*Figure 4.13. The JV ratio estimated in EucFACE. The $J_{max.25}$ and $V_{cmax.25}$ values are ring averages based on ACi curves and corrected to 25ºC using in situ measurements of temperature dependence. The dots show the estimations of each campaigns with colour marking the ring number. The red dashed line is the mean of the three treatment rings (R1, R4, and R5). The blue dashed line is the mean of the three control rings (R2, R3, and R6).*

### 4.4.3 Acclimation

The above calculations are made considering only the direct response. However, photosynthetic acclimation was observed at leaf scale, and may also reduce the response of GPP to $C_a$ at the canopy scale. The mean value of $V_{cmax}$ estimated from the elevated rings was 10% smaller than in ambient rings (Figure 4.5). On leaf level, photosynthesis measured in the elevated rings ($A_{long}$) increased by 19% compared to those measured in ambient rings (Row 5 of Figure 4.8). $A_{long}$ thus accounts for the photosynthetic acclimation in the elevated rings after four years of exposure to e$C_a$. $A_{long}$ is considerably smaller than $A_{inst}$ (19% vs. 33%), indicating a large effect of photosynthetic acclimation on the response of light-saturated photosynthesis.

Accounting for the impact of photosynthetic acclimation in MAESTRA, by using the $V_{cmax}$ from ambient rings ("field" vs. "elevated" scenario) reduced the response of GPP to 9% ($GPP_{accli}$; Row 6 of Figure 4.8). Consequently, the photosynthetic acclimation had a relatively small impact on the annual GPP in the model. The smaller impact of photosynthetic acclimation can be explained by different conditions. The leaf scale photosynthesis data are measured under saturating light and thus are Rubisco limited. However, photosynthesis in the canopy is mostly limited by electron transport. Consequently, the change $V_{cmax}$ of has a larger impact at leaf level.

### 4.4.4 LAI

The actual GPP response to e$C_a$ also depends on the response of LAI to $C_a$. In other experiments, the response of LAI to e$C_a$ is an important indirect effect that amplifies the response of GPP. However, in this experiment, there was no significant increase in LAI with e$C_a$ (-4% ± 5%; Row 7 of Figure 4.8). The effect of e$C_a$ on LAI was calculated as the slope of a linear regression between the means of elevated and ambient LAI. The non-significant change in the observed LAI is not due to e$C_a$ but a result of the inherent variability across the rings, which was present pre-treatment (Figure 4.2a). As a consequence, this inherent inter-ring variability does not amplify the effect of e$C_a$ but adds noise to the results. The pre-

treatment difference in LAI across rings reduced the GPP response to e$C_a$ in the field to 8% (±10%; Row 8 in Figure 4.8).

This result is explored further in Figure 4.14, which combines the results from "ambient", "elevated", and "field" scenarios. The average GPP of across all six rings under ambient $C_a$ was 1557 g C $m^{-2}$ $yr^{-1}$ over the four-year simulation ("ambient scenario"; Figure 4.14). However, there is significant variability across rings, related to the initial difference in pre-treatment LAI ($LAI_i$). Rings 1 and 4 (both treatment rings) have the lowest $LAI_i$ (~0.1 $m^2$ $m^{-2}$) and thus the lowest average GPP under ambient conditions (~1200 g C $m^{-2}$ $yr^{-1}$). Ring 5 (the other treatment ring) has the second highest $LAI_i$ (~0.4 $m^2$ $m^{-2}$) and also the highest GPP under ambient condition (~1700 g C $m^{-2}$ $yr^{-1}$). The variability among rings in ambient GPP (SD = 17%) is thus larger than the modelled direct effect of $C_a$ on GPP, which is similar in all rings (+12%). Owing to the variability among rings, the estimated GPP response to e$C_a$ across the treatment rings is considerably less. The actual $C_a$ response was estimated as the slope of a linear regression between the ambient and elevated GPP values under field condition (i.e., with $C_a$ and $V_{cmax}$ as measured for each treatment). The average GPP of treatment rings under field conditions (e$C_a$) was 1723 g C $m^{-2}$ $yr^{-1}$ while the average GPP of control rings under field conditions (ambient $C_a$) was 1580 g C $m^{-2}$ $yr^{-1}$, an increase of 8% as shown in the bottom row of Figure 4.8.

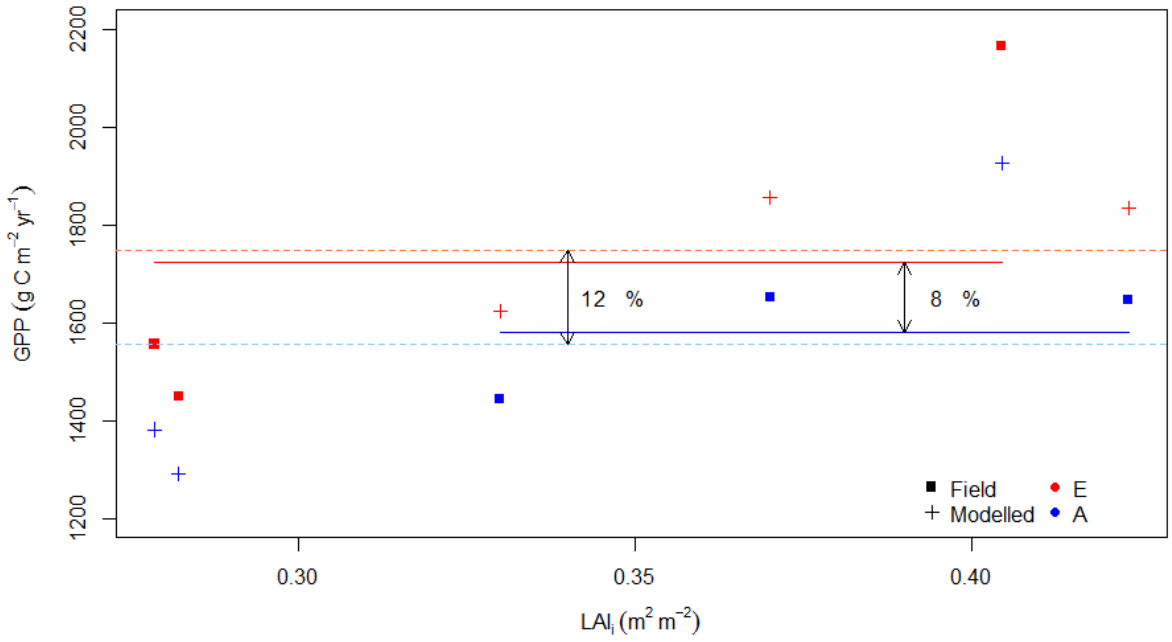


*Figure 4.14. The four-year average GPP of all six rings under ambient and e$C_a$ plotted against initial LAI ($LAI_i$). The initial LAI is the LAI measurement taken on the 26 October 2012 and thus is a proxy of the inherent variation among the rings. For all six rings,*

*estimated GPP is shown for ambient $C_a$ (blue) and e$C_a$ (red). Crosses indicate GPP from simulations by varying $C_a$ and squares indicate GPP as under field conditions. Dashed lines indicate average ambient $C_a$ and e$C_a$ GPP across all six rings (the means of blue and red symbols, respectively). Solid lines indicate the average ambient $C_a$ GPP for ambient rings only and average e$C_a$ GPP for elevated rings only (the average of squares). The dashed lines thus mark the theoretical response while the solid lines mark the realized response.*

### 4.5. Discussion

By synthesising four years of measurements with the stand-scale model, MAESTRA, this study showed how a large response of photosynthesis to e$C_a$ at leaf level could diminish at canopy level after considering more processes. I was able to quantify and attribute the response of GPP to e$C_a$ to various factors including: (i) Rubisco versus electron-transport limitations to photosynthesis; (ii) photosynthetic acclimation; (iii) inter-ring variability in LAI. Together these findings provide valuable insights into the relative importance of each factor and help close a key knowledge gap in the understanding of how a mature evergreen eucalyptus woodland would respond to e$C_a$.

This synthesis of model and observations showed that the ambient canopy GPP under ambient condition of a mature *Eucalyptus* woodland varied from 1400–1700 g C $m^{-2}$ $yr^{-1}$ by ring with a mean of 1500 g C $m^{-2}$ $yr^{-1}$. The model predicted that once scaled to the canopy, the response of GPP to e$C_a$ was only an increase of 8% (±10%) compared to 19% (±5%) from the leaf-scale measurements.

*Electron-transport limited photosynthesis*

The canopy GPP at EucFACE was predominantly limited by electron transport. The reason for the frequent electron transport limitation is that the JV ratio is relatively small in EucFACE (~1.6; Figure 4.13). A lower JV ratio increases the PAR value at which photosynthesis transitions from electron transport limitation to Rubisco limitation (Figure 4.13). Previous modelling studies (e.g. Wang et al., 1998; Luo et al., 2001) typically assume a higher JV ratio (~2) and thus estimate a higher GPP response to e$C_a$ presumably due to less frequent electron transport limitation. However, the relatively low JV ratio of EucFACE is not unique. In the Duke Forest FACE site in the US, Ellsworth et al. (2012) reported a JV ratio of ~1.6 which is close to that estimated in EucFACE. Kattge and Knorr (2007) analysed $V_{cmax}$ and $J_{max}$ values from 36 species across the world and discovered a low JV ratio (<1.8) in herbaceous, coniferous and broadleaved species. Kumarathunge et al. (2018) analysed an

even larger data set with 141 C3 species and showed that there is a consistent decreasing trend of JV ratio with growth temperature, such that the JV ratio decreases from >2 in high-latitude ecosystems to <1.5 in tropical ecosystems. Consequently, the low canopy GPP response to e$C_a$ in EucFACE highlights the impact of the more typical low JV ratio in ecosystems in warm environments. The reduction in JV ratio in warm environments will require explicit modelling to capture the correct response of GPP to e$C_a$.

The JV ratio depends on the values of maximum Rubisco activity and electron transport rate. Both of these two factors thus need to be considered in the models for a correct prediction of the transition from Rubisco to electron transport limited photosynthesis (Zaehle et al., 2014; Rogers et al., 2017). As shown by Zaehle et al. (2014) and Medlyn et al. (2015), the current models disagree on the relative importance of Rubisco to electron transport limitations. The analysis in Kumarathunge et al. (2018) thus provides a robust starting point to constrain the JV ratio based on growth temperature. Since the JV ratio was shown to decline with increasing growth temperature, electron transport limited photosynthesis could have a predominant impact in the most productive ecosystems. Future models thus could benefit by incorporating these findings to improve the prediction of GPP response to rising $C_a$.

*Photosynthetic acclimation*

Photosynthetic acclimation (i.e., reduction of $V_{cmax}$ under $eC_a$) has been widely reported in FACE studies and has been attributed to a reduction in leaf nitrogen concentration (Ainsworth and Long, 2005). The response of GPP to $eC_a$ would be very sensitive to acclimation of $V_{cmax}$ if photosynthesis is mostly limited by Rubisco activity. The treatment rings in EucFACE had a reduction of $V_{cmax}$ of ~ 10% (Figure 4.5) which is consistent with the mean reduction in a previous meta-analysis (13%; Ainsworth and Long, 2005). However, this reduction did not translate into an equal size reduction in GPP; GPP was reduced by ~3% after accounting for photosynthetic acclimation (Row 6 in Figure 4.8). Wang et al. (1998) also showed that the photosynthetic acclimation (-21% in $V_{cmax}$) reduced modelled canopy GPP by only 6%. These findings thus suggest that photosynthetic acclimation may have limited impact on the canopy GPP response to $C_a$ when photosynthesis is mostly limited by electron transport.

*Inherent ring-to-ring variability*

At the EucFACE experiment, after four years of e$C_a$ treatment, there has been no evidence of increased above-ground plant productivity (Ellsworth et al., 2017). The trees at EucFACE

showed no significant change in LAI after four years of exposure to e$C_a$ (Duursma et al., 2016). The small effect size of e$C_a$ in EucFACE could partially be due to the low $C_a$ increment: +150 μmol mol$^{-1}$ in EucFACE compared to +350 μmol mol$^{-1}$ in Wang et al. (1998) and +200 μmol mol$^{-1}$ in other FACE studies (Norby et al., 2005).

The inter-ring variability in GPP is larger than the estimated direct effect of $C_a$ (17% versus 13%). It is important to note that the EucFACE site is homogeneous for a mature woodland. The site is flat, trees are even-aged, and almost all belong to one species. In addition, rings were carefully sited to minimise variation in basal area. However, there are small-scale variations in soil type, depth, and nutrient availability that cause variation in LAI. This scale of variation is likely to be seen in other natural forests, and indeed, other studies on mature trees also note that background variability can contribute to the lack of statistically significant findings (Fatichi and Leuzinger, 2013; Sigurdsson et al. 2013). We highlight the need to focus on effect size and its uncertainty, rather than the dichotomous significant/non-significant approach when evaluating experimental results from native forests.

In advance of the EucFACE experiment, seven TBMs were applied to the site to make *a priori* predictions of the likely response to treatment (Medlyn et al. 2016). The ambient GPP diverged among the model predictions (1200-2600 g C m$^{-2}$ yr$^{-1}$; Medlyn et al., 2016). The main reason for the difference in GPP relates to the widespread discrepancy in LAI predicted by the models, which ranged from 1-4.5 m$^2$ m$^{-2}$. The predicted response of LAI under e$C_a$ also varied from 0 to 20% among the models. Combined with the fact that the lack of GPP-LAI feedback limited the canopy GPP response to e$C_a$, these findings pose challenge for models to constrain LAI and its response to e$C_a$. Indeed, current predictions of LAI under e$C_a$ were very different among models and larger than the observations in the field (De Kauwe et al. 2014; Mahowald et al. 2016; Medlyn, et al., 2016) due to the lack of constraints besides carbon allocation (De Kauwe et al. 2014). More factors thus need to be considered to predict LAI under rising $C_a$ (e.g., constrain LAI with water balance: Yang et al., 2018).

### 4.6. Conclusion

This study used a process-based stand-scale model and quantified the ambient (~1500 g m$^{-2}$ yr$^{-1}$) and response of GPP (12%) to e$C_a$. I also partitioned the $C_a$ response and discovered that photosynthesis of the canopy was frequently electron-transport limited which constrained the $C_a$ response. The model also illustrated how a 12% increase of GPP could be reduced to 8% in the field due to the inherent variability of the forest stands. This study makes a major

contribution to the understanding of EucFACE by quantifying the amount of extra carbon input into the system and thus providing a reference for the studies of growth and soil respiration.  The conclusions in this study suggest that terrestrial biosphere models to consider the impact of electron-transport limited photosynthesis.

## Chapter 5: Synthesis and future work

The work in this thesis aimed to improve terrestrial biosphere models (TBMs), particularly for Australian ecosystems under changing climate conditions. Rising $C_a$ may stimulate plant growth, but the benefit could be offset by an increase in dryness, driven by rising temperature and potential changes in precipitation. It is thus important for TBMs to be able to capture realistic plant responses to rising $C_a$ and dryness. The efforts here thus focused on three key components of TBMs which interact with water use and carbon uptake—LAI and gas exchange at leaf and canopy scales. For LAI, the optimality model in this study innovatively balanced long-term LAI and leaf water use strategy. For leaf-scale gas exchange, I introduced a non-stomatal limitation on photosynthesis and showed improved prediction with increasing atmospheric vapour pressure deficit. For canopy scale gas exchange, I successfully identified and attributed the relative contributions of key drivers, which explained discrepancies between leaf-scale measurements and canopy-scale estimates of GPP and the response to elevated $C_a$. This thesis thus identified several key gaps of current TBMs and employed newly available data and theory to provide solutions to fill these gaps.

The results in this thesis strongly suggest that the stimulation of long-term terrestrial carbon storage due to rising $C_a$ could be much smaller than that estimated at leaf scale in each site. Previous elevated $C_a$ studies reported a 31% increase of leaf photosynthesis on average with an increase of $C_a$ from 360 to 560 μmol $mol^{-1}$ (Norby et al., 1999; Ainsworth and Rogers, 2007; Norby and Zak, 2011). This number would be much smaller (roughly halved) at canopy and annual scales of each site if a large proportion of canopy carbon uptake is limited by RuBP-regeneration (Chapter 4). Moreover, if the future climate were to become hotter and drier, more frequent extreme conditions could future reduce the photosynthesis even further (Chapter 3), which is already widely observed globally across species and plant functional types (Tezara et al., 1999; Lawlor and Cornic, 2002; Lawlor and Tezara, 2009). Although there have been reports of an increase in LAI globally , which has been attributed to rising $C_a$ (Yang et al., 2016; Zhu et al., 2016), the increase in LAI has a diminishing marginal return with rising $C_a$, and may be accompanied by a reduction of $g_1$ in the long-term (Chapter 2). The combined effects thus could be that the future global terrestrial carbon storage shows limited response to the change of $C_a$.

### 5.1 Improving modelling of LAI

Plant leaf water use must be coordinated with LAI in the long-term. In order to scale our knowledge at the leaf scale, it is important to capture LAI and its response to rising $C_a$ accurately. Chapter 2 predicted optimal LAI with water balance taking leaf water use strategy into consideration. This approach illustrated the viability of adding water balance as a new constraint on LAI prediction in TBMs (previously based on carbon allocation).

I found that the parsimonious optimality model in Chapter 2 could successfully capture the long-term LAI across Australia. The optimality LAI agreed with both ground-based and satellite measurements. This finding suggests the ecohydrological equilibrium theory could be used to improve predictions of foliage carbon allocation and LAI in existing TBMs. An additional benefit of incorporating this optimality model into TBMs is to account for the impacts of increasing $C_a$ with the respect of changing climate. Despite the importance of LAI modeling and the improvements in Chapter 2, TBMs would also need to realistic representations of leaf gas exchange under increasing $C_a$ and changing climate to account for the carbon flux dynamics.

### 5.2 Improving leaf gas exchange modelling

In Chapter 2, I showed that an ecosystem optimal $g_1$ could be predicted by ecohydrological equilibrium theory. This conclusion was consistent with empirical studies on leaf (Kelly et al., 2015) and ecosystem scales (Lin et al., 2015; Prentice et al., 2014; Medlyn et al., 2017). Kelly et al. (2015) showed that plants exposed to short-term (~ weeks) water limitation reduce $g_1$ but when exposed to prolonged drought (~ 6 months) maintain a 'target' $g_1$ by reducing LAI. This finding was also supported by the meta-analyses by Prentice et al. (2014) and Lin et al. (2015) who showed that the $g_1$ increases with water availability. Improving the accuracy of the $g_1$ variable has been shown to improve the performance of the gas-exchange component of TBMs (De Kauwe et al., 2015) but it can be difficult to estimate without extensive data on different scales (Medlyn et al., 2017). Our optimal $g_1$ thus could be very useful and convenient for TBMs to use as a target value with variation modified by soil water availability (e.g., Keenan et al., 2010; Zhou et al., 2013; Smith et al., 2014; Drake et al., 2017).

This thesis also improved the performance of coupled leaf gas exchange models at high $D$, where models show large divergence (De Kauwe et al., 2015; Knauer et al., 2015; Franks et al., 2017). In Chapter 3, I incorporated a non-stomatal limitation to photosynthesis at high $D$ and demonstrate improvements in performance of model simulations of carbon and water

fluxes at leaf and canopy levels. This finding is particularly important for TBMs because *D* is predicted to increase in the future (Novick et al., 2016) and thus have a potentially larger impact.

### 5.3 Improving canopy gas exchange modelling

Even with accurate LAI and leaf gas exchange models, the GPP of the canopy and its response to rising $C_a$ might still be misrepresented. The reason is that the canopy is more complicated system than a simple product of LAI and the leaf-level gas exchange. As I showed in Chapter 5, the canopy carbon flux responded to e$C_a$ much less than that of the leaf because photosynthesis of the canopy was often electron transport regeneration limited. It is thus important for models to use realistic canopy structure representations (e.g., multi-layer models) to account for the impact of self-shading (Rogers et al., 2017).

In Chapter 5, I quantitatively assessed the response of GPP to elevated $C_a$ by isolating three important factors: the LAI, the ratio of electron transport limited to Rubisco limited photosynthesis, and photosynthetic acclimation. Although I demonstrated that GPP could increase by 13% with a $C_a$ increase from 400 to 550 μmol $mol^{-1}$, this prediction represents a relatively short-term (four years) response to $CO_2$. This prediction assumes that the plants do not alter their water-use strategy with rising $C_a$. This assumption is supported by the leaf gas exchange data, which did not show a detectable change in $g_1$ with e$C_a$ (Gimeno et al., 2016). Nevertheless, in Chapter 2, I showed that the optimal response to increasing $C_a$ includes changes in LAI and $g_1$ to maximise the carbon gain under high $C_a$. For EucFACE, according to the model in Chapter 2, plants should reduce $g_1$ in exchange for obtaining a higher LAI. The potential changes of LAI and $g_1$ indicate that the short- and long-term (decadal) response of plants to rising $C_a$ could be different and thus need to be modelled explicitly. In Chapter 3, I showed that the leaf gas exchange could be further reduced due to non-stomatal limitation under dry air. Since the air could be drier in the future due to rising temperature, the modelling of GPP response to rising $C_a$ needs to account for the feedback between climate and plants.

### 5.4 Future work

This thesis improved three aspects of modelling $C_a$-plant-climate interactions in the future, but the conclusions were not tested in a dynamic TBM. There are several barriers to overcome before undertaking such a test, including the representation of dynamics in LAI and the availability of data to parameterise the non-stomatal limitation effect. Future work may thus benefit from addressing these limitations and using the findings to inform TBMs.

*LAI variability*

The model presented in Chapter 2 predicts a long-term equilibrium LAI based on ecohydrological equilibrium but ignores the inter- and intra- annual variability of LAI. However, TBMs need to be able to predict a far more dynamic LAI: varying from some optimum value based on seasonal phenology and water availability. One way my research could be used to bridge the gap would be as a mechanism to identify the environmental target LAI, which would govern the long-term allocation to foliage. It would need to be accompanied by a dynamic sub-module to represent phenology at intra-annual timescales with the inter-annual variability represented by the annual water availability to the plants. This approach, combining optimisation with water availability, was taken by Neilson (1995) and Haxeltine et al. (1996). Neilson (1995) calculated the LAI that maximises GPP constrained by soil water content within each month. The inter- and intra- annual variability of LAI is thus represented by the change of optimal LAI of each month. Haxeltine et al. (1996) used the water deficit calculated as the difference between potential evapotranspiration and soil water supply to predict daily fraction of absorbed photosynthetically active radiation that maximised carbon uptake. Essentially, both Neilson (1995) and Haxeltine et al. (1996) applied the ecohydrological equilibrium theory to a sub-annual temporal resolution to account for the inter- and intra- annual variability of LAI. I envisage that a TBM incorporating my long-term equilibrium approach could first consider using the LAI from the equilibrium model as a target, with the LAI dynamics predicted by water and carbon balance (e.g., Battaglia et al. 2004). A synthesis of optimal LAI and process-based hydraulic models (Fatichi et al., 2016) thus could improve the modelling of both vegetation and soil moisture in the future.

Australia is dominated by evergreen angiosperm trees and grassland. The inter- and intra-annual variation of LAI is predominately driven by water availability (e.g., Ma et al., 2013; Broich et al., 2014). At EucFACE, for instance, the LAI varies temporally from 0.2 to >2 $m^2$ $m^{-2}$, correlating with soil moisture (Figure 4.2) and demonstrating the impact of water on the inter- and intra- annual variation of LAI in a mature evergreen woodland. The predicted LAI of EucFACE by current models showed distinct LAI variability among each other and did not agree with the observed LAI response to soil moisture (Medlyn et al., 2016). Similarly, in a prairie heating study in the US, the models failed to capture the observed intra-annual variation of LAI which was obviously driven by water availability (De Kauwe et al., 2017). The mismatch among the models and between the predictions and observations is due to the

lack of proper representation of carbon-water interaction in the models. The findings in this thesis improved the carbon flux predictions under future climate. This is a very important step to advance the predictions of the of the dynamics in the TBMs (e.g., root and leaf phenology). Future studies may consider using this information to predict optimal carbon allocation scheme which would allow the plants to adaptively adjust their strategies (e.g., timing of leaf flushing and abscission) according to the changing environment (e.g., Franklin et al., 2012; Manzoni et al., 2015).

*Non-stomatal limitation*

In Chapter 3, I showed the importance of non-stomatal limitation on leaf and canopy carbon and water fluxes. The empirical approach incorporated in this study successfully improved the performance of the model when compared with leaf gas exchange data and whole-tree sap flow measurements. However, the empirical relationship may not generalise to other sites/species. More efforts are needed to assess the effect of non-stomatal limitation globally and explore the mechanism(s) that cause non-stomatal limitation. Currently, two processes are most plausible explanations: the down regulation of carboxylation (Lawlor and Cornic, 2002; Lawlor and Tezara, 2009) and the reduction of mesophyll conductance (Flexas et al., 2008). The two plausible causes are mathematically equivalent (Dewar et al., 2017), but the down regulation of carboxylation is the more testable hypothesis due to its parsimony and data availability.

Future TBMs could adopt a mechanistic representation of non-stomatal limitation when new approaches emerge. In the interim, comparing the half-hourly predictions of TBMs to eddy covariance carbon and water fluxes particularly for the sites experiencing frequent high $D$ (i.e., 20% daytime $D$ >2kPa) could help assess the impact of nonstomatal limitation across sites and species. The findings of this global analysis could be directly used in TBMs to improve leaf gas exchange modelling, particularly under high $D$.

*Testing with global data*

I have focused on evaluating models against data from Australian woody ecosystems, demonstrating only the applicability of the conclusions to evergreen ecosystems in relatively dry environments. However, the conclusions may hold across ecosystems and plant functional types.

Firstly, observations around the world have shown a clear dependence of LAI on water availability (Iio et al., 2015). The observed greening trend over most parts of the world (Zhu

et al., 2016; Yang et al., 2016) also agreed with the predicted change of LAI in Chapter 2. These facts show that ecohydrological equilibrium theory could be used to improve the LAI prediction globally.

The reduction of photosynthesis under high *D* has long been reported world-wide (Tezara et al., 1999; Lawlor and Cornic, 2002; Lawlor and Tezara, 2009). Although the empirical relationship used in Chapter 3 might not hold universally, the indication that non-stomatal limitation is important for leaf gas exchange modelling is strong given the widely observed midday reduction of photosynthesis and decrease of mesophyll conductance at high water deficit.

The transition from Rubisco to electron-transport limited photosynthesis has also been noted as a key factor determining the ecosystems response to rising $CO_2$ (Rogers et al., 2017). EucFACE has high PAR (2600 MJ $m^{-2}$ $yr^{-1}$) and low LAI (~0.9 $m^2$ $m^{-2}$) so the canopy photosynthesis was expected to be mainly limited by Rubisco activity. However, as I have shown in Chapter 4, the canopy GPP of EucFACE was largely limited by electron transport. These findings suggest that electron transport limited photosynthesis could have a large impact in other ecosystems with lower PAR and higher LAI.

Consequently, existing evidence strongly suggests that the findings in this thesis will apply to other ecosystems and species. Future studies thus could benefit from testing the conclusions in this thesis with data from other sites and species. The results of those studies could directly address the key gaps in current TBMs.

*Incorporating the impact of nutrient availability*

The carbon cycle and nutrient cycle are inter-dependent (e.g., Meyerholt and Zaehle, 2018). EucFACE, for instance, has a relatively low LAI (0.9 $m^2m^{-2}$) for its precipitation (800 mm $yr^{-1}$), presumably due to the nutrient limitation of the site (Crous et al., 2015). The observed photosynthetic acclimation might also be a result of nutrient limitation (e.g., Luo et al., 2004) or optimal nutrient allocation (e.g., Franklin, 2007) under elevated $C_a$. Since nutrient limitation has been shown to be a major limiting factor in terrestrial ecosystems (Elser et al., 2007), the interaction of these processes thus needed to be clarified before theoretical and mechanistic models could be presented. McMurtrie et al. (2008) applied an optimality model to account for the influence of nitrogen on LAI and stomatal conductance. These studies demonstrated the practicability of simple approaches to account for nutrient. The findings in this thesis could be useful to provide information of the leaf dynamics, the leaf

photosynthesis, and the biomass production, all of which could lead to mechanistic methods to predict the impact of fire and nutrients.

*Conclusion*

This thesis addressed several key gaps in current TBMs by using a synthesis of data and modelling approaches. The body of work adds insight into the constraints on tree leaf area, how plants respond to high *D* and how the response of photosynthesis scales from the leaf to the canopy in response to elevated $C_a$. The major findings of this thesis could be readily and beneficially incorporated into TBMs. The ecohydrological equilibrium theory could benefit the current models by predicting the paired optima of LAI and $g_1$. The optima could improve the predictions of carbon, water, and energy fluxes, especially under future climate and increasing $C_a$. In addition, non-stomatal limitation could be a significant factor under high atmospheric water demand. Incorporating both optimal $g_1$ and non-stomatal limitation would thus be crucial under future conditions (i.e., change of water balance accompanied with increasing $C_a$). Although the increase of $C_a$ is expected to stimulate growth, the stand-scale model in this study showed the impact of $C_a$ on the canopy to be much smaller than that on leaf scale due to electron transport limited photosynthesis. These findings quantitatively showed the impacts of the factors (i.e., LAI, $g_1$, and electron transport limited photosynthesis) that caused most of the uncertainties in current TBMs (e.g., Zaehle et al., 2014; Medlyn et al., 2016) and the factors that were not extensively explored in TBMs (i.e., non-stomatal limitation). Consequently, current TBMs should benefit from updating the LAI and leaf gas exchange components under rising $C_a$ and changing climate.

## Supplementary Material for Chapter 2

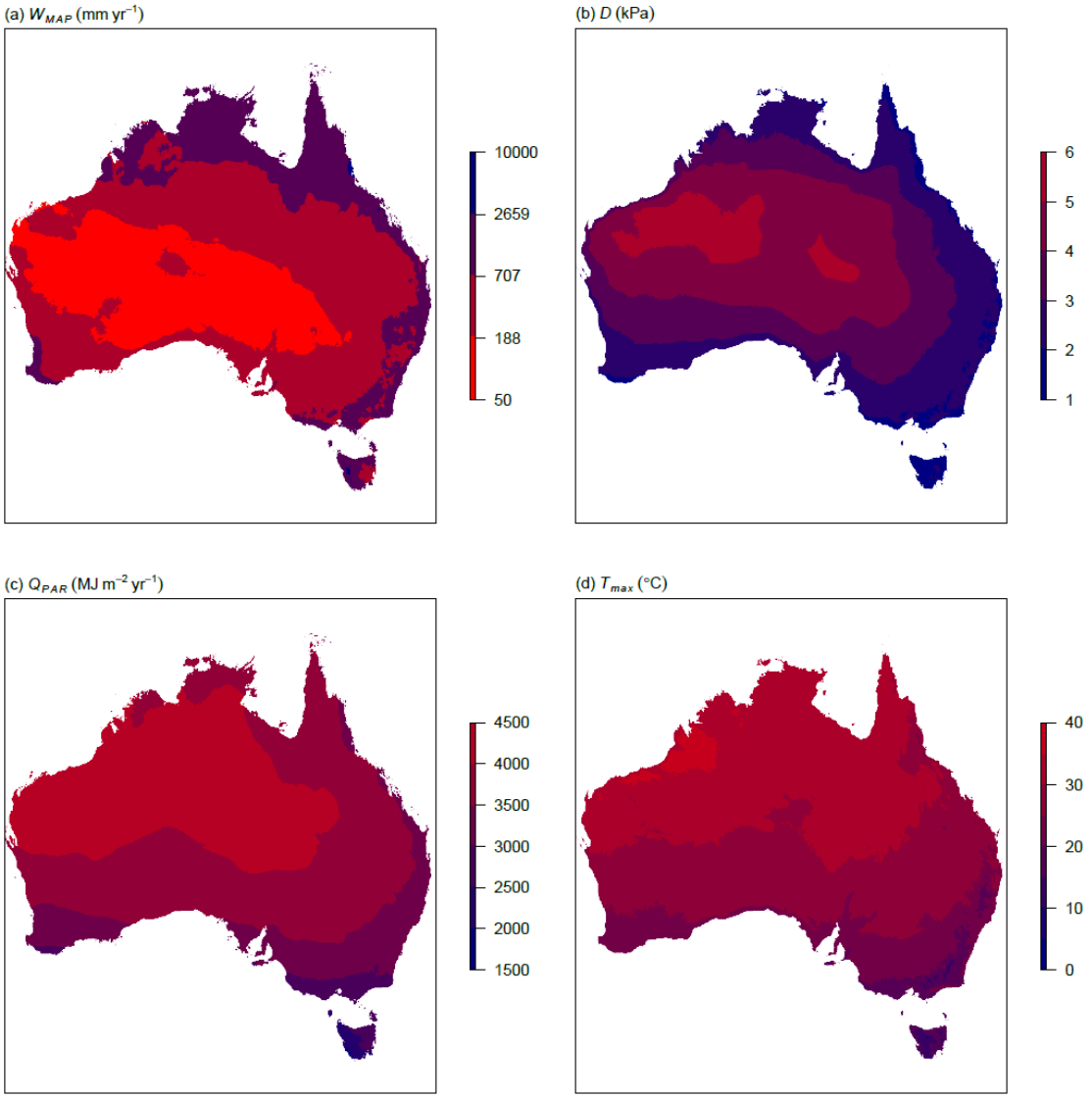


*Figure S.1. Climate inputs. Values shown are the mean over 21 years (1991-2011) aggregated from Whitley et al. (2014). Note the log scale of mean annual precipitation (a).*

## Alternative hypotheses test in Chapter 2

There are several potential options to calculate the key parameters (i.e., $M_{area}$, $t_f$, $W_T$, and $R_m$) in the model. It is therefore important to investigate how the underlying assumptions differ among equations and how those differences affect the predictions. In the following section, we compared the alternative functions to those implemented, illustrated the differences among the assumptions, and explained the reasoning behind our choice of assumptions for the final model.

**Text S.1.The transpiration fraction**

The final model included the assumptions that the transpiration fraction varies with LAI (Eqn. 1; Wang et al., 2014) and with precipitation (Eqn. 2; Zhang et al. 2001). An alternative potential assumption is to take transpiration as a constant fraction (0.8) of precipitation as in McMurtrie et al. (2008). A constant transpiration fraction resulted in higher prediction at low observed LAI (red dots and lines in Figure S.2 a and b). Including the Zhang et al. (2001) relationship with precipitation only slightly improved the result (orange dots and lines in Figure S.2 a and b). Assuming the transpiration fraction to be a function of LAI gave the lowest results of all three assumptions tested here (blue dots and lines in Figure S.2 a and b). Although calculating transpiration fraction as a function of LAI added complexity and required iteration, we included this assumption in the final model for its fitness to data (blue line in Figure S.2b). Alternatively, it may be viable to reduce prediction error at high AI by increasing respiration cost at high AI empirically (see following section).

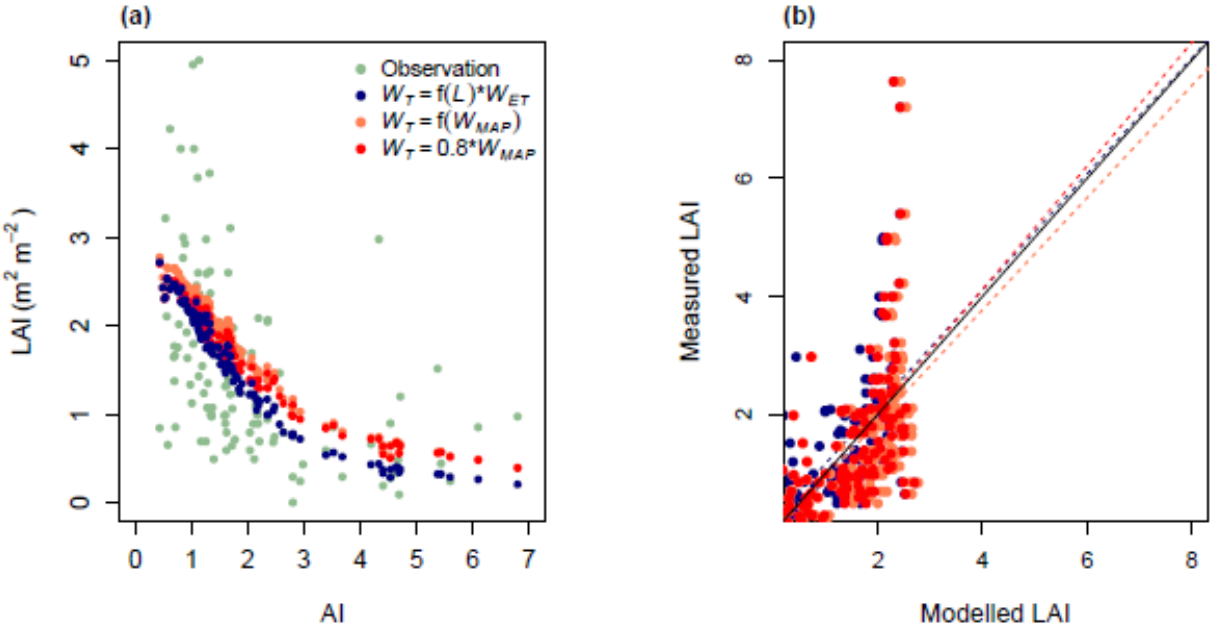


*Figure S.2. Impact of different transpiration fraction assumptions on $L_{opt}$. Panel (a) shows the impact of different assumptions along the Aridity Index (gradient) and how they compared to observations. The $L_{opt}$ from final model are the blue dots. "$W_T$=f($W_{MAP}$)" means substituting Eqn. 1 with a constant fraction of 1. "$W_T$ =0.8* $W_{MAP}$" means neither Eqn. 1 nor 2 is used but instead a constant fraction is implemented (0.8). Panel (b) shows scatter plot of measured and modelled LAI with the solid line being 1:1 ratio and dashed lines regression colored by assumptions.*

**Text S.2. Maintenance respiration**

$R_m$, maintenance respiration per unit leaf area (μmol $m^{-2}$ leaf $s^{-1}$), is a key factor in determining the cost of leaf growth. The final model assumed a constant value (1.59 μmol $m^{-2}$ $s^{-1}$). This section explained the alternative assumptions we considered for $R_m$ and showed how they affected the model predictions. We fitted an empirical relationship between $R_m$ and $W_{MAP}$ ($R^2$ = 0.36) to data from the Australian subset of the GLOBRESP dataset (Atkin et al., 2015):

$$ln(R_m) = a_r \cdot \ln(W_{MAP}) + b_r \quad \text{(S1)}$$

where $a_r$ and $b_r$ are fitted parameters, -0.589 and 4.235, respectively.

A constant $R_m$ was chosen over the empirical relationship for the final model because: (i) the $R_m$-$W_{MAP}$ relationship does not improve prediction at low in situ LAI (AI from 3 to 7 in Figure S.3a); (ii) the final model captured the observations better overall (blue dashed line was closer to 1:1 ratio than the orange dashed line in Figure S.3b); (iii) a climate-modified $R_m$ added unnecessary complexity to the model assumptions.

Eqn. S1 predicts an exponential decline of $R_m$ with $W_{MAP}$ (Figure S.3c). However, the impact of incorporating this relationship on model predictions did not follow the same pattern. The difference between the two assumptions was negligible at low LAI because when LAI is very low, $R_m$ has limited impact on the optimization compared to the exponential relationships of $f_{APAR}$ and transpiration fraction to LAI (Eqn. 1). However, at high LAI, both $f_{APAR}$ and transpiration fraction were nearly saturated and thus a small change in $R_m$ has a large impact on the prediction.

The impact of the $R_m$ assumption would be larger if the model did not include the transpiration fraction to LAI relationship. As mentioned in the previous section, the model prediction could be improved by either incorporating the transpiration fraction – LAI relationship or a climate-modified $R_m$. The transpiration fraction – LAI assumption is more empirically justifiable, but requires iteration to solve. It may thus be possible to improve the computational efficiency of the model by using an empirical $R_m$-$W_{MAP}$ relationship instead of the transpiration fraction-LAI relationship, but this risks the limited applicability of the empirical relationship.

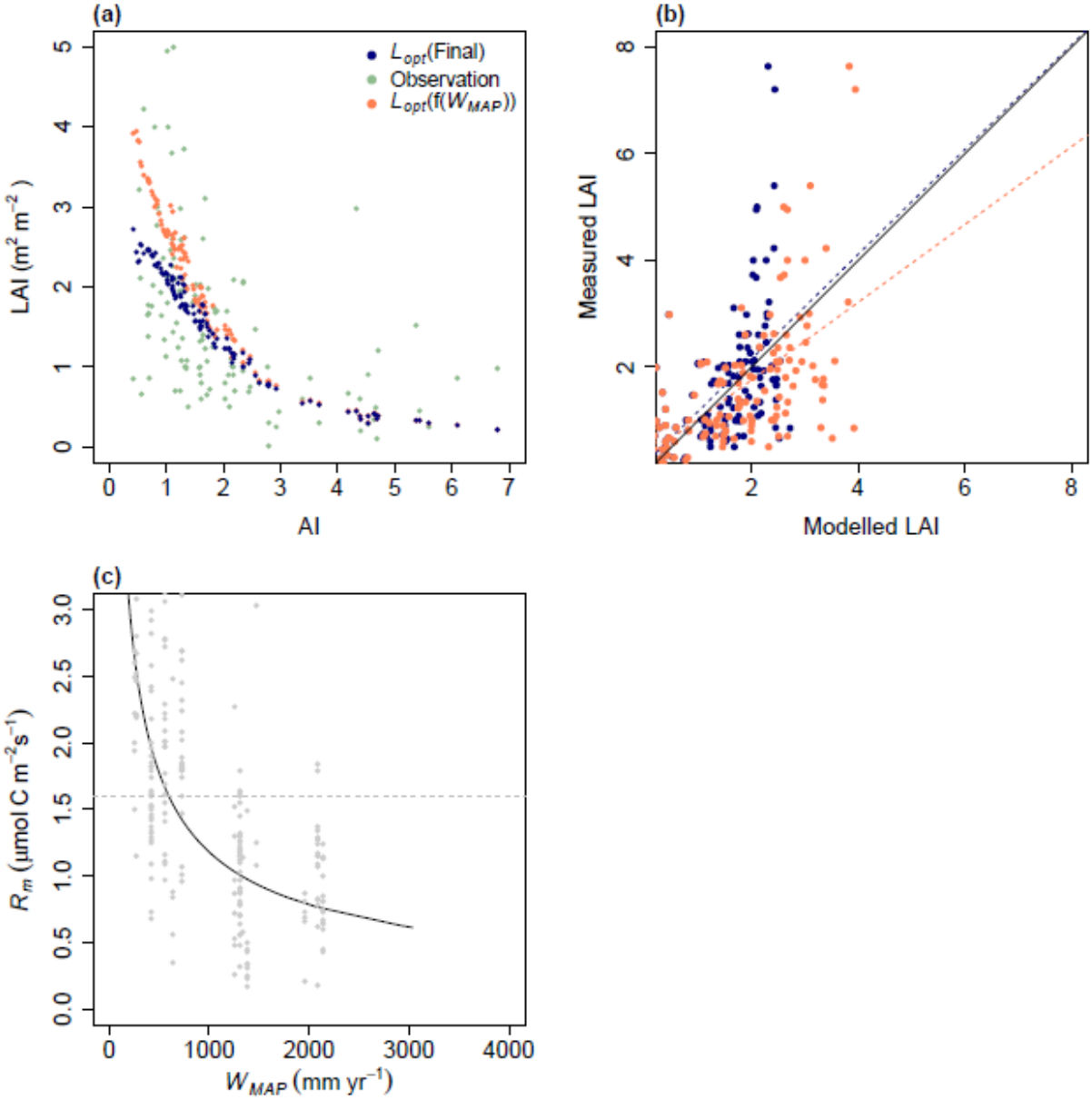


*Figure S.3. Comparison of the impacts of different $R_m$ assumptions. Panel (a) shows $L_{opt}$ under different $R_m$ assumptions compared to the in situ measurements along an AI gradient. Note that the final model uses constant $R_m$ (blue dots). Panel (b) shows the difference between constant $R_m$ and the final model. Panel (c) shows the tested $R_m$-$W_{MAP}$ relationship with the dashed line indicating the value used in the final model and grey dots being the measurements from the Australian subset of the GLOBRESP dataset (Atkin et al., 2015). Note that different assumptions are used here and in Figure S.4d.*

**Text S.3. Leaf economics**

The parameters describing leaf economics in the model are $R_m$, $M_{area}$ , and $t_f$, which are assumed constant in this study (Method and Table 2.1). Previous studies (e.g. Wright et al., 2004) have suggested correlations among $R_m$, $M_{area}$, and $t_f$. In this section, we test the alternatives of calculating $R_m$, $M_{area}$, and $t_f$ with empirical relationships and the impacts on predictions.

$t_f$ correlates best with $M_{area}$ according to GLOPNET data set ($R^2$ = 0.44; Wright et al., 2004):

$$ln(t_f) = a_l \cdot ln(M_{area}) - b_l \quad \text{(S2)}$$

where $a_l$ and $b_l$ are fitted parameters equal to 1.14 and -5.64, respectively. Similarly, $R_m$ can be expressed as a function of $M_{area}$:

$$ln(R_m) = a_{rm} \cdot \ln(M_{area}) - b_{rm} \quad \text{(S3)}$$

where $a_{rm}$ and $b_{rm}$ are fitted parameters and equal to 0.63 and -2.94, respectively. Here, Eqn. S3 was derived from the Australian subset of GLOBRESP (Atkin et al., 2015) with an $R^2$ of 0.25. $M_{area}$ correlates best with mean annual precipitation according to the same data set ($R^2$ = 0.22; Atkin et al., 2015):

$$ln(M_{area}) = a_m \cdot \ln(W_{MAP}) + b_m \quad \text{(S4)}$$

where $a_m$ and $b_m$ are fitted parameters with value of -0.36 and 7.52, respectively.

Although these relationships are statistically significant, we did not implement them in the final model because making $M_{area}$ and $t_f$ functions of climate had no effect on model predictions in dry regions (AI>2 in Figure S.4 a and b). The reason is that the carbon investment per unit time (proportional to $M_{area} / t_f$) and $R_m$ is relatively insensitive to climate (Figure S.4 c and d). (ii) The regression line between the final model and observations was closer to 1:1 ratio than the one based on leaf economics (blue versus orange dashed lines in Figure S.4b). For parsimony, the final model thus used the constant $M_{area}$ and $t_f$. The values $M_{area}$ and $t_f$ in the final model were based on GLOPNET, while the $M_{area}$ correlation with $W_{MAP}$ was derived from GLOBRESP. The reason we tested the correlation from GLOBRESP is that the same correlation is not significant in GLOPNET. We chose to use the constant values of $M_{area}$ and $t_f$ from GLOPNET because $t_f$ is not reported in GLOBRESP. We thus used values from one data set for consistency. Consequently, the grey line in Figure S.4c was not the mean of the dots.

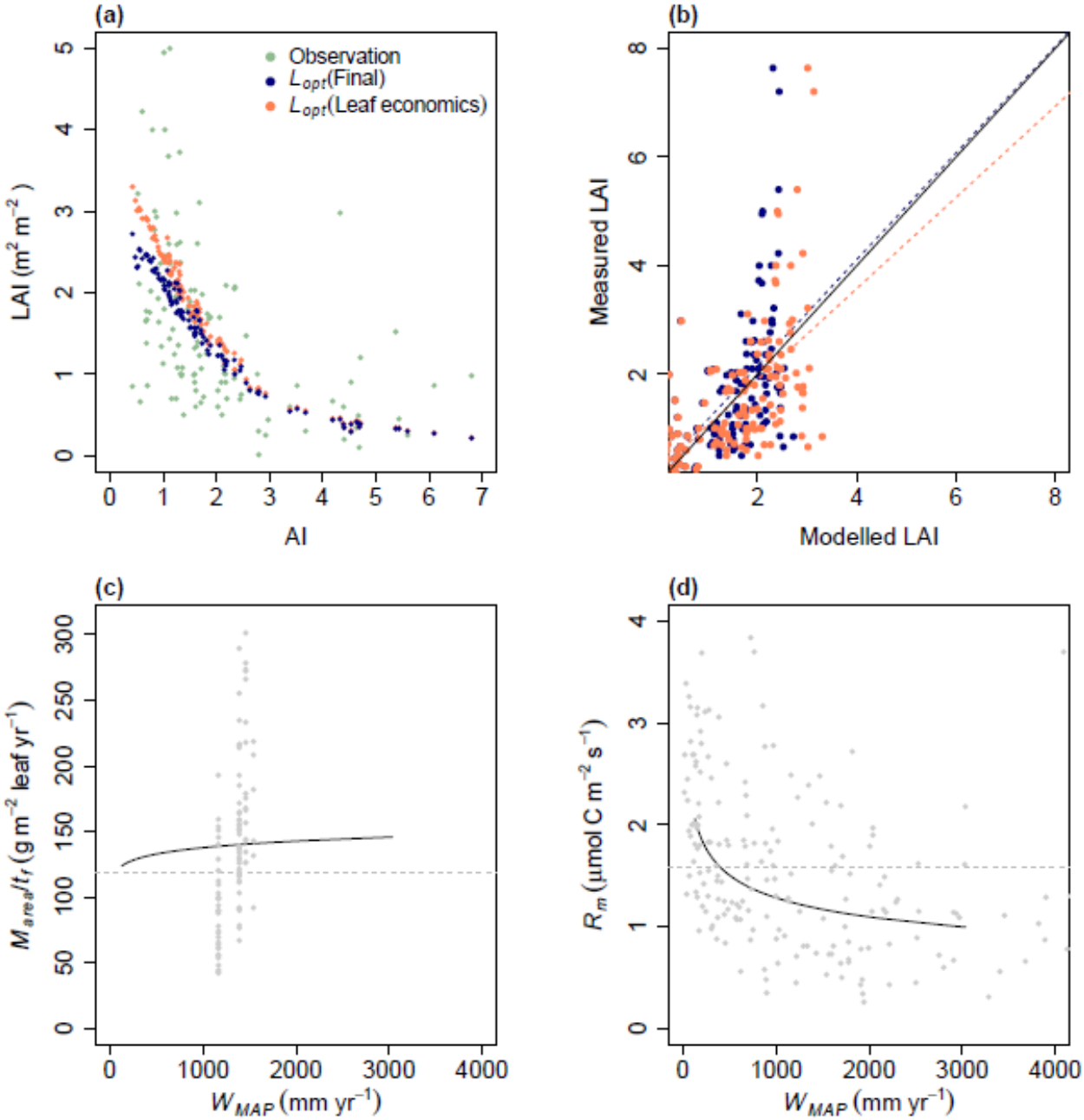


*Figure S.4. $L_{opt}$ based on leaf economics compared to that of the final model. Panel (a) shows $L_{opt}$ based on leaf economics and final model compared to the measurements along an AI gradient. Panel (b) shows the scatter plots of measurements against leaf economics and final model. Panel (c) shows the change of leaf carbon investment ($M_{area}$ / $t_f$) over a rainfall gradient. Panel (d) shows the change of $R_m$ based on $M_{area}$ over a rainfall gradient. The solid lines show the regression. The grey dashed lines in (c) and (d) mark the values used in the final model. The grey dots are measurements.*

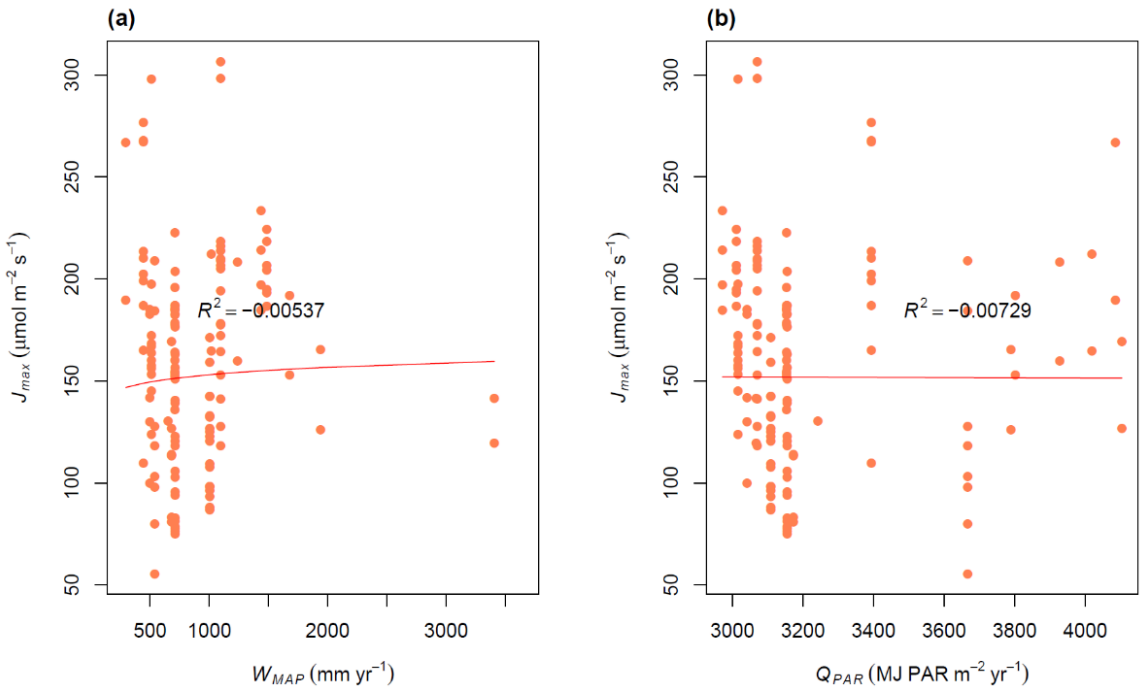


*Figure S.5. Relationships of $J_{max}$ measured at growth temperature with (q) $W_{MAP}$ and (b) $Q_{PAR}$. The inter-site variability of $J_{max}$ is larger than the change over climate gradient, resulting in little predicting power of climate over $J_{max}$.*

**Supplementary Material for Chapter 3**

*Figure S.6. Modelled transpiration (E) compared to sap flow estimated by heat pulse sensors (measured E) of ambient (R2, R6) and elevated rings (R1,R4, R5) in 2013. The data of ring 3 already shown in the main text. Panels (a) and (b) show the result from original MAESTRA. Panels (c) and (d) show the result from MAESTRA with V-D hypothesis. The solid lines in Panels (a) and (c) show the daily average while the shade shows hourly variation (standard deviation).*

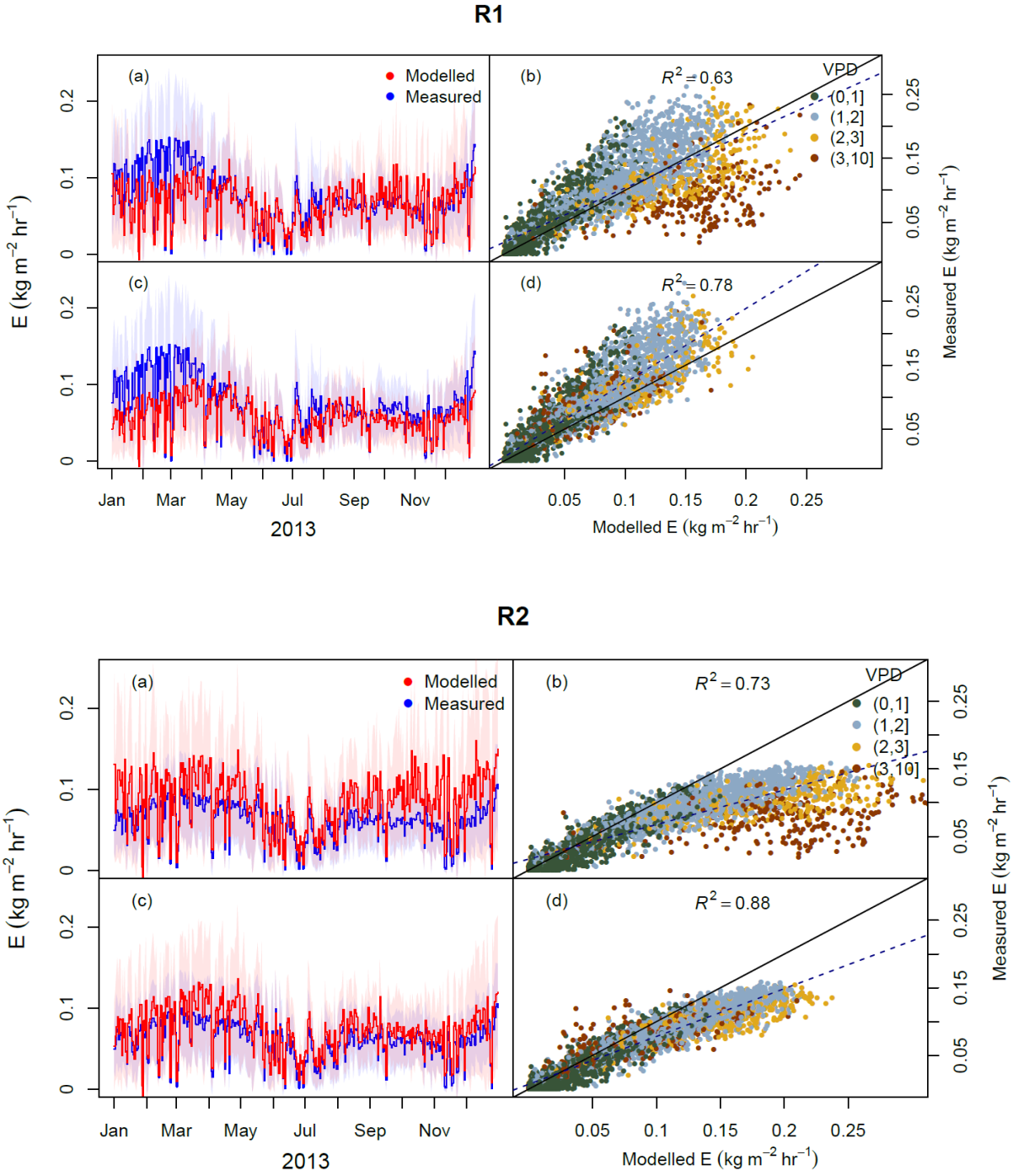

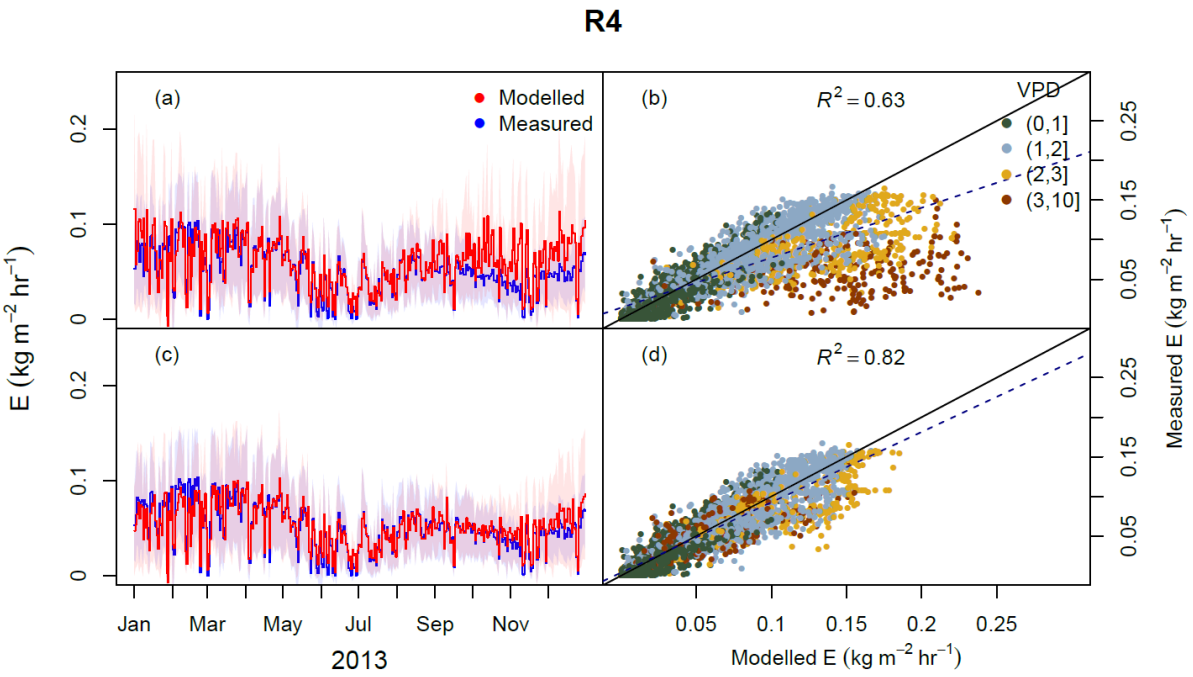
R4
(a)
Modelled
Measured
(b)
$R^2 = 0.63$
VPD
(0,1]
(1,2]
(2,3]
(3,10]
(c)
(d)
$R^2 = 0.82$
E (kg m$^{-2}$ hr$^{-1}$)
Measured E (kg m$^{-2}$ hr$^{-1}$)
Jan
Mar
May
Jul
Sep
Nov
2013
Modelled E (kg m$^{-2}$ hr$^{-1}$)

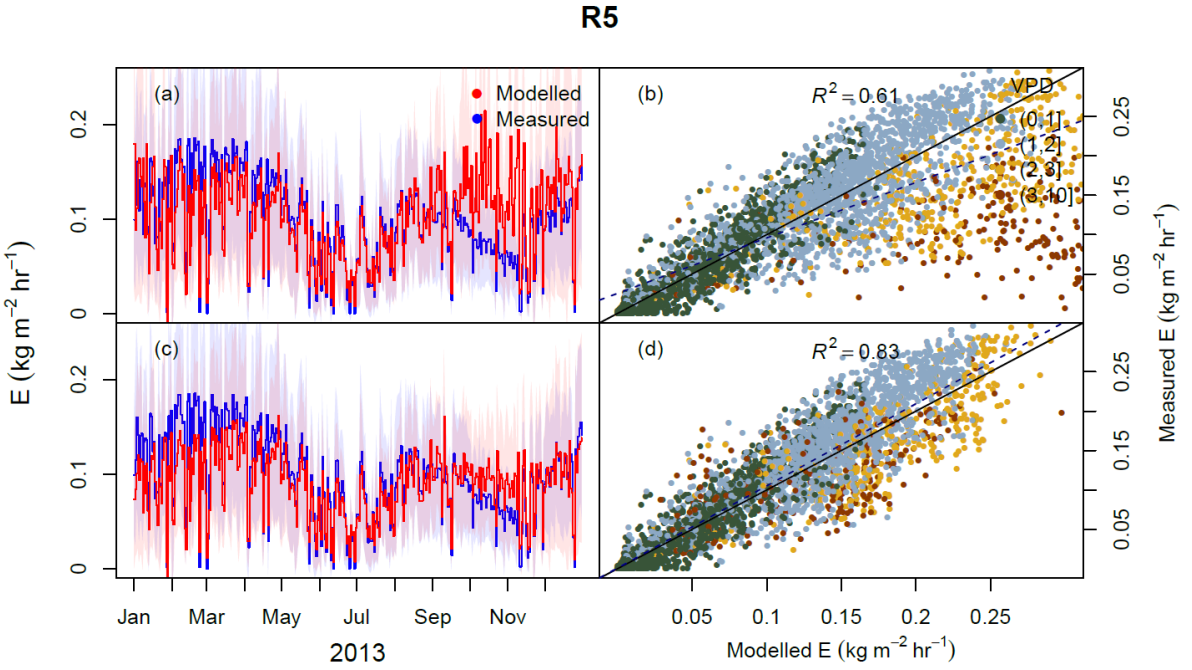
R5
(a)
Modelled
Measured
(b)
$R^2 = 0.61$
VPD
(0,1]
(1,2]
(2,3]
(3,10]
(c)
(d)
$R^2 = 0.83$
E (kg m$^{-2}$ hr$^{-1}$)
Measured E (kg m$^{-2}$ hr$^{-1}$)
Jan
Mar
May
Jul
Sep
Nov
2013
Modelled E (kg m$^{-2}$ hr$^{-1}$)

**R6**

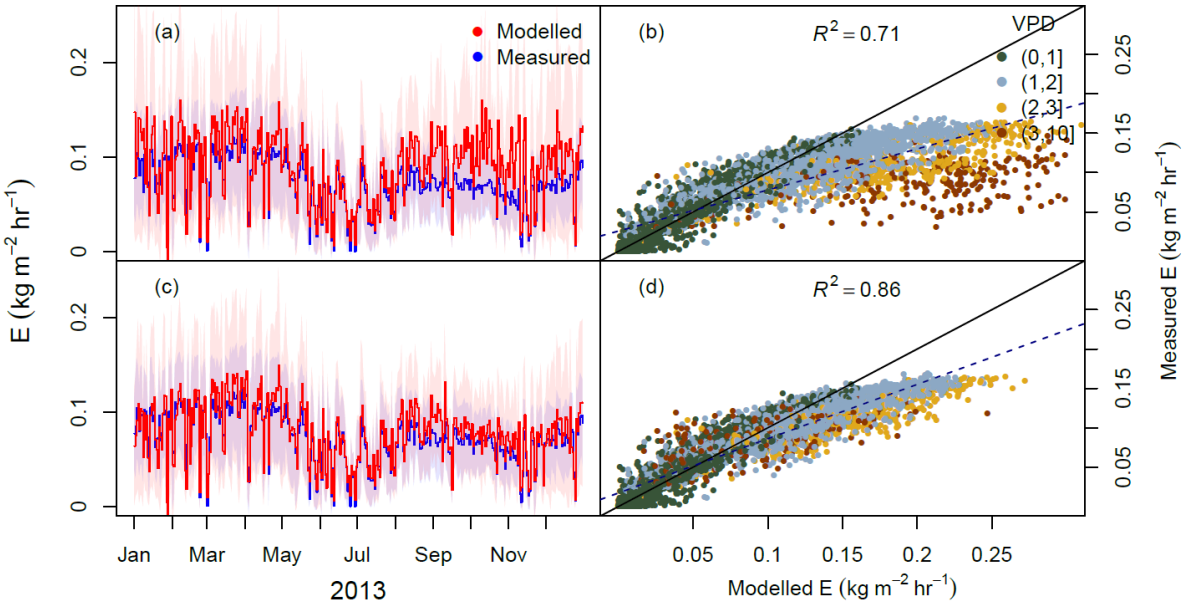
(a)
Modelled
Measured
(b)
$R^2 = 0.71$
VPD
(0,1]
(1,2]
(2,3]
(3,10]
(c)
(d)
$R^2 = 0.86$
E (kg m$^{-2}$ hr$^{-1}$)
Measured E (kg m$^{-2}$ hr$^{-1}$)
Modelled E (kg m$^{-2}$ hr$^{-1}$)
Jan
Mar
May
Jul
Sep
Nov
2013
0
0.1
0.2
0.05
0.15
0.25

## References


Ahlstrom, A. et al. (2015), The dominant role of semi-arid ecosystems in the trend and variability of the land CO2 sink, *Science (80).*, *348*(6237), 895–899, doi:10.1126/science.aaa1668.

Ahlström, A., G. Schurgers, and B. Smith (2017), The large influence of climate model bias on terrestrial carbon cycle simulations, *Environ. Res. Lett.*, *12*(1), 014004, doi:10.1088/1748-9326/12/1/014004.

Ainsworth, E. A., and S. P. Long (2005), What have we learned from 15 years of free-air $CO_2$ enrichment (FACE)? A meta-analytic review of the responses of photosynthesis, canopy properties and plant production to rising $CO_2$, *New Phytol.*, *165*(2), 351–372, doi:10.1111/j.1469-8137.2004.01224.x.

Ainsworth, E. A., and A. Rogers (2007), The response of photosynthesis and stomatal conductance to rising [$CO_2$]: Mechanisms and environmental interactions, *Plant, Cell Environ.*, *30*(3), 258–270, doi:10.1111/j.1365-3040.2007.01641.x.

Ali, A. A., Xu, C., Rogers, A., Fisher, R. A., Wullschleger, S. D., Massoud, E. C., Vrugt, J. a., Muss, J. D., McDowell, N. G., Fisher, J. B., Reich, P. B. and Wilson, C. J. (2016), A global scale mechanistic model of photosynthetic capacity (LUNA V1.0), *Geosci. Model Dev.*, *9*(2), 587–606, doi:10.5194/gmd-9-587-2016.

Ali, A. A., Xu, C., Rogers, A., McDowell, N. G., Medlyn, B. E., Fisher, R. A., Wullschleger, S. D., Reich, P. B., Vrugt, J. A., Bauerle, W. L., Santiago, L. S. and Wilson, C. J (2015), Global-scale environmental control of plant photosynthetic capacity, *Ecol. Appl.*, *25*(8), 2349–2365, doi:10.1890/14-2111.1.

Allen, C. D. et al. (2010), A global overview of drought and heat-induced tree mortality reveals emerging climate change risks for forests, *For. Ecol. Manage.*, *259*(4), 660–684, doi:10.1016/j.foreco.2009.09.001.

Anav, A., P. Friedlingstein, M. Kidston, L. Bopp, P. Ciais, P. Cox, C. Jones, M. Jung, R. Myneni, and Z. Zhu (2013), Evaluating the land and ocean components of the global carbon cycle in the CMIP5 earth system models, *J. Clim.*, *26*(18), 6801–6843, doi:10.1175/JCLI-D-12-00417.1.

Atkin, O. K., Bloomfield, K. J., Reich, P. B., Tjoelker, M. G., Asner, G. P., Bonal, D., Bönisch, G., Bradford, M. G., Cernusak, L. A., Cosio, E. G., Creek, D., Crous, K. Y., Domingues, T. F., Dukes, J. S., Egerton, J. J. G., Evans, J. R., Farquhar, G. D., Fyllas, N. M., Gauthier, P. P. G., Gloor, E., Gimeno, T. E., Griffin, K. L., Guerrieri, R., Heskel, M. A., Huntingford, C., Ishida, F. Y., Kattge, J., Lambers, H., Liddell, M. J., Lloyd, J., Lusk, C. H., Martin, R. E., Maksimov, A. P., Maximov, T. C., Malhi, Y., Medlyn, B. E., Meir, P., Mercado, L. M., Mirotchnick, N., Ng, D., Niinemets, Ü., O'Sullivan, O. S., Phillips, O. L., Poorter, L., Poot, P., Prentice, I. C., Salinas, N., Rowland, L. M., Ryan, M. G., Sitch, S., Slot, M., Smith, N. G., Turnbull, M. H., Vanderwel, M. C., Valladares, F., Veneklaas, E. J., Weerasinghe, L. K., Wirth, C., Wright, I. J., Wythers, K. R., Xiang, J., Xiang, S. and Zaragoza-Castells, J. (2015), Global variability in leaf respiration in

relation to climate, plant functional types and leaf traits, *New Phytol.*, *206*(2), 614–636, doi:10.1111/nph.13253.

Arora, V. K. ., Boer, G. J., Friedlingstein, P., Eby, M., Jones, C. D., Christian, J. R., Bonan, G., Bopp, L., Brovkin, V., Cadule, P., Hajima, T., Ilyina, T., Lindsay, K., Tjiputra, J. F. and Wu, T. (2013), Carbon-concentration and carbon-climate feedbacks in CMIP5 earth system models, *J. Clim.*, *26*(15), 5289–5314, doi:10.1175/JCLI-D-12-00494.1.

Ball, J. T., I. E. Woodrow, and J. A. Berry (1987), A Model Predicting Stomatal Conductance and its Contribution to the Control of Photosynthesis under Different Environmental Conditions, in *Progress in Photosynthesis Research*, pp. 221–224.

Battaglia, M., M. L. Cherry, C. L. Beadle, P. J. Sands, and A. Hingston (1998), Prediction of leaf area index in eucalypt plantations: effects of water stress and temperature, *Tree Physiol.*, *18*(8–9), 521–528, doi:10.1093/treephys/18.8-9.521.

Battaglia, M., and P. Sands (1997), Modelling Site Productivity of Eucalyptus globulus in Response to Climatic and Site Factors, *Aust. J. Plant Physiol.*, *24*(6), 831, doi:10.1071/PP97065.

Battle, M. (2000), Global Carbon Sinks and Their Variability Inferred from Atmospheric O2 and 13C, *Science (80).*, *287*(5462), 2467–2470, doi:10.1126/science.287.5462.2467.

Beerling, D., and F. Woodward (2001), *Vegetation and the terrestrial carbon cycle modelling the first 400 million years*, Cambridge University Press, Cambridge.

Bernacchi, C. J., E. L. Singsaas, C. Pimentel, A. R. Portis Jr, and S. P. Long (2001), Improved temperature response functions for models of Rubisco-limited photosynthesis, *Plant, Cell Environ.*, *24*(2), 253–259, doi:10.1046/j.1365-3040.2001.00668.x.

Bonan, G. B., and S. C. Doney (2018), Climate, ecosystems, and planetary futures: The challenge to predict life in Earth system models, *Science (80-. ).*, *359*(6375), doi:10.1126/science.aam8328.

Bongi, G. and Loreto, F.: Gas-Exchange Properties of Salt-Stressed Olive (*Olea europea L.*) Leaves, *Plant Physiol.*, 90(4), 1408–1416, doi:10.1104/pp.90.4.1408, 1989.

Broxton, P. D., X. Zeng, D. Sulla-Menashe, and P. A. Troch (2014), A global land cover climatology using MODIS data, *J. Appl. Meteorol. Climatol.*, *53*(6), 1593–1605, doi:10.1175/JAMC-D-13-0270.1.

Buckley, T. N. (2005), The control of stomata by water balance, *New Phytol.*, *168*(2), 275–292, doi:10.1111/j.1469-8137.2005.01543.x.

Buckley, T. N., G. D. Farquhar, and K. A. Mott (1999), Carbon-water balance and patchy stomatal conductance, *Oecologia*, *118*(2), 132–143, doi:10.1007/s004420050711.

Caldararu, S., D. W. Purves, and P. I. Palmer (2014), Phenology as a strategy for carbon optimality: A global model, *Biogeosciences*, *11*(3), 763–778, doi:10.5194/bg-11-763-2014.

Campany, C. E., M. G. Tjoelker, S. von Caemmerer, and R. A. Duursma (2016), Coupled response of stomatal and mesophyll conductance to light enhances photosynthesis of shade leaves under sunflecks, *Plant Cell Environ.*, *39*(12), 2762–2773, doi:10.1111/pce.12841.

Cernusak, L. A., L. B. Hutley, J. Beringer, J. A. M. Holtum, and B. L. Turner (2011), Photosynthetic physiology of eucalypts along a sub-continental rainfall gradient in northern Australia, *Agric. For. Meteorol.*, *151*(11), 1462–1470, doi:10.1016/j.agrformet.2011.01.006.

Cheeseman, J. M. (1991), Patchy - Simulating and Visualizing the Effects of Stomatal Patchiness on Photosynthetic $CO_2$ Exchange Studies, *Plant Cell Environ.*, *14*(6), 593–599, doi:10.1111/j.1365-3040.1991.tb01530.x.

Cheng, L., L. Zhang, Y.-P. Wang, J. G. Canadell, F. H. S. Chiew, J. Beringer, L. Li, D. G. Miralles, S. Piao, and Y. Zhang (2017), Recent increases in terrestrial carbon uptake at little cost to the water cycle, *Nat. Commun.*, *8*(1), 110, doi:10.1038/s41467-017-00114-5.

Choat, B., T. J. Brodribb, C. R. Brodersen, R. A. Duursma, R. López, and B. E. Medlyn (2018), Triggers of tree mortality under drought, *Nature*, *558*, 531–539, doi:10.1038/s41586-018-0240-x.

Ciais, P. et al. (2013), *Carbon and Other Biogeochemical Cycles*, Cambridge University Press, Cambridge, United Kingdom and New York, NY, USA.

Cowan, I. R., and G. D. Farquhar (1977), Stomatal function in relation to leaf metabolism and environment., *Symp. Soc. Exp. Biol.*, *31*(1973), 471–505, doi:0081-1386.

Cox, P. M., R. A. Betts, C. D. Jones, S. A. Spall, and I. J. Totterdell (2000), Acceleration of global warming due to carbon-cycle feedbacks in a coupled climate model (vol 408, pg 184, 2000), *Nature*, *408*(6813), 750, doi:10.1038/35041539.

Cramer, W., Bondeau, A., Woodward, F. I., Prentice, I. C., Betts, R. A., Brovkin, V., Cox, P. M., Fisher, V., Foley, J. A., Friend, A. D., Kucharik, C., Lomas, M. R., Ramankutty, N., Sitch, S., Smith, B., White, A. and Young-Molling, C. (2001), Global response of terrestrial ecosystem structure and function to $CO_2$ and climate change: Results from six dynamic global vegetation models, *Glob. Chang. Biol.*, *7*(4), 357–373, doi:10.1046/j.1365-2486.2001.00383.x.

CSIRO and Bureau of Meteorology (2015), *Projections: Atmosphere and the land*.

Curtis, P. S., and X. Wang (1998), A meta-analysis of elevated $CO_2$ effects on woody plant mass, form, and physiology, *Oecologia*, *113*(3), 299–313, doi:10.1007/s004420050381.

Dawes, M. A., S. Hättenschwiler, P. Bebi, F. Hagedorn, I. T. Handa, C. Körner, and C. Rixen (2011), Species-specific tree growth responses to 9 years of $CO_2$ enrichment at the alpine treeline, *J. Ecol.*, *99*(2), 383–394, doi:10.1111/j.1365-2745.2010.01764.x.

De Kauwe, M. G., J. Kala, Y. S. Lin, A. J. Pitman, B. E. Medlyn, R. A. Duursma, G. Abramowitz, Y. P. Wang, and D. G. Miralles (2015), A test of an optimal stomatal conductance scheme within the CABLE land surface model, *Geosci. Model Dev.*, *8*(2), 431–452, doi:10.5194/gmd-8-431-2015.

De Kauwe, M. G., Lin, Y., Wright, I. J., Medlyn, B. E., Crous, K. Y., Ellsworth, D. S., Maire, V., Prentice, I. C., Atkin, O. K., Rogers, A., Niinemets, Ü., Serbin, S. P., Meir, P., Uddling, J., Togashi, H. F., Tarvainen, L., Weerasinghe, L. K., Evans, B. J., Ishida, F. Y. and Domingues, T. F. (2016), A test of the 'one-point method' for estimating maximum carboxylation capacity from field-measured, light-saturated photosynthesis, *New Phytol.*, *210*(3), 1130–1144, doi:10.1111/nph.13815.

De Kauwe, M. G., B. E. Medlyn, J. Knauer, and C. A. Williams (2017), Ideas and perspectives: How coupled is the vegetation to the boundary layer?, *Biogeosciences*, *14*(19), 4435–4453, doi:10.5194/bg-14-4435-2017.

De Kauwe, M. G. et al. (2017), Challenging terrestrial biosphere models with data from the long-term multifactor Prairie Heating and $CO_2$ Enrichment experiment, *Glob. Chang. Biol.*, *23*(9), 3623–3645, doi:10.1111/gcb.13643.

De Kauwe, M. G. et al. (2014), Where does the carbon go? A model-data intercomparison of vegetation carbon allocation and turnover processes at two temperate forest free-air $CO_2$ enrichment sites, *New Phytol.*, *203*(3), 883–899, doi:10.1111/nph.12847.

Delworth, T. L., and F. Zeng (2014), Regional rainfall decline in Australia attributed to anthropogenic greenhouse gases and ozone levels, *Nat. Geosci.*, *7*(8), 583–587, doi:10.1038/ngeo2201.

Dey R., Lewis S.C., Arblaster J.M., Abram N.J. (2019), A review of past and projected changes in Australia's rainfall. *Wiley Interdiscip Rev Clim Chang*, 10(3), 1–23, doi: 10.1002/wcc.577.

Dong, N., I. C. Prentice, B. J. Evans, S. Caddy-Retalic, A. J. Lowe, and I. J. Wright (2017), Leaf nitrogen from first principles: field evidence for adaptive variation with climate, *Biogeosciences*, *14*(2), 481–495, doi:10.5194/bg-14-481-2017.

Donohue, R. J., T. R. Mcvicar, and M. L. Roderick (2009), Climate-related trends in Australian vegetation cover as inferred from satellite observations, 1981-2006, *Glob. Chang. Biol.*, *15*(4), 1025–1039, doi:10.1111/j.1365-2486.2008.01746.x.

Donohue, R. J., M. L. Roderick, T. R. McVicar, and G. D. Farquhar (2013), Impact of $CO_2$ fertilization on maximum foliage cover across the globe's warm, arid environments, *Geophys. Res. Lett.*, *40*(12), 3031–3035, doi:10.1002/grl.50563.

Donohue, R. J., M. L. Roderick, T. R. McVicar, and Y. Yang (2017), A simple hypothesis of how leaf and canopy-level transpiration and assimilation respond to elevated $CO_2$ reveals distinct response patterns between disturbed and undisturbed vegetation, *J. Geophys. Res. Biogeosciences*, doi:10.1002/2016JG003505.

Drake, J. E., Power, S. A., Duursma, R. A., Medlyn, B. E., Aspinwall, M. J., Choat, B., Creek, D., Eamus, D., Maier, C., Pfautsch, S., Smith, R. A., Tjoelker, M. G. and Tissue, D. T. (2017), Stomatal and non-stomatal limitations of photosynthesis for four tree species under drought: A comparison of model formulations, *Agric. For. Meteorol.*, *247*(September), 454–466, doi:10.1016/j.agrformet.2017.08.026.

Duan, H., R. A. Duursma, G. Huang, R. A. Smith, B. Choat, A. P. O'grady, and D. T. Tissue (2014), Elevated [$CO_2$] does not ameliorate the negative effects of elevated temperature on drought-induced mortality in Eucalyptus radiata seedlings, *Plant. Cell Environ.*, *37*(7), 1598–1613, doi:10.1111/pce.12260.

Duursma, R. A., and B. E. Medlyn (2012), MAESPA: a model to study interactions between water limitation, environmental drivers and vegetation function at tree and stand levels, with an example application to [$CO_2$] × drought interactions, *Geosci. Model Dev.*, *5*(4), 919–940, doi:10.5194/gmd-5-919-2012.

Duursma, R. A. (2015), Plantecophys - An R package for analysing and modelling leaf gas exchange data, *PLoS One*, *10*(11), 1–13, doi:10.1371/journal.pone.0143346.

Duursma, R. A., C. V. M. Barton, Y. S. Lin, B. E. Medlyn, D. Eamus, D. T. Tissue, D. S. Ellsworth, and R. E. McMurtrie (2014), The peaked response of transpiration rate to vapour pressure deficit in field conditions can be explained by the temperature optimum of photosynthesis, *Agric. For. Meteorol.*, *189–190*, 2–10, doi:10.1016/j.agrformet.2013.12.007.

Duursma, R. A., C. J. Blackman, R. Lopéz, N. K. Martin-StPaul, H. Cochard, and B. E. Medlyn (2018), On the minimum leaf conductance: its role in models of plant water use, and ecological and environmental controls, *New Phytol.*, doi:10.1111/nph.15395.

Duursma, R. A., T. E. Gimeno, M. M. Boer, K. Y. Crous, M. G. Tjoelker, and D. S. Ellsworth (2016), Canopy leaf area of a mature evergreen Eucalyptus woodland does not respond to elevated atmospheric [$CO_2$] but tracks water availability, *Glob. Chang. Biol.*, *22*(4), 1666–1676, doi:10.1111/gcb.13151.

Eagleson, P. S. (1982), Ecological optimality in water-limited natural soil vegetation systems: 1. Theory and hypothesis, *Water Resour. Res.*, *18*(2), 325–340.

Eamus, D., and P. G. Jarvis (1989), The Direct Effects of Increase in the Global Atmospheric $CO_2$ Concentration on Natural and Commercial Temperate Trees and Forests, in *Advances in Ecological Research*, vol. 19, pp. 1–55.

Eamus, D., G. A. Duff, and C. A. Berryman (1995), Photosynthetic responses to temperature, light flux-density, $CO_2$ concentration and vapour pressure deficit in *Eucalyptus tetrodonta* grown under $CO_2$ enrichment, *Environ. Pollut.*, *90*(1), 41–49, doi:10.1016/0269-7491(94)00088-U.

Eamus, D., D. T. Taylor, C. M. O. Macinnis-Ng, S. Shanahan, and L. De Silva (2008), Comparing model predictions and experimental data for the response of stomatal conductance and guard cell turgor to manipulations of cuticular conductance, leaf-to-air vapour pressure difference and temperature: Feedback mechanisms are able to account

for all observations, *Plant, Cell Environ.*, *31*(3), 269–277, doi:10.1111/j.1365-3040.2007.01771.x.

Ellis, T. W., and T. J. Hatton (2008), Relating leaf area index of natural eucalypt vegetation to climate variables in southern Australia, *Agric. Water Manag.*, *95*(6), 743–747, doi:10.1016/j.agwat.2008.02.007.

Ellsworth, D. S., R. Thomas, K. Y. Crous, S. Palmroth, E. Ward, C. Maier, E. Delucia, and R. Oren (2012), Elevated $CO_2$ affects photosynthetic responses in canopy pine and subcanopy deciduous trees over 10 years: A synthesis from Duke FACE, *Glob. Chang. Biol.*, *18*(1), 223–242, doi:10.1111/j.1365-2486.2011.02505.x.

Ellsworth, D. S., Anderson, I. C., Crous, K. Y., Cooke, J., Drake, J. E., Gherlenda, A. N., Gimeno, T. E., Macdonald, C. A., Medlyn, B. E., Powell, J. R., Tjoelker, M. G. and Reich, P. B. (2017), Elevated $CO_2$ does not increase eucalypt forest productivity on a low-phosphorus soil, *Nat. Clim. Chang.*, *7*(4), 279–282, doi:10.1038/nclimate3235.

Elser, J. J., M. E. S. Bracken, E. E. Cleland, D. S. Gruner, W. S. Harpole, H. Hillebrand, J. T. Ngai, E. W. Seabloom, J. B. Shurin, and J. E. Smith (2007), Global analysis of nitrogen and phosphorus limitation of primary producers in freshwater, marine and terrestrial ecosystems, *Ecol. Lett.*, *10*(12), 1135–1142, doi:10.1111/j.1461-0248.2007.01113.x.

Evaristo, J., S. Jasechko, and J. J. McDonnell (2015), Global separation of plant transpiration from groundwater and streamflow, *Nature*, *525*, 91–94, doi:10.1038/nature14983.

Fang, H. Fang, H., Jiang, C., Li, W., Wei, S., Baret, F., Chen, J. M., Garcia-Haro, J., Liang, S., Liu, R., Myneni, R. B., Pinty, B., Xiao, Z. and Zhu, Z. (2013), Characterization and intercomparison of global moderate resolution leaf area index (LAI) products: Analysis of climatologies and theoretical uncertainties, *J. Geophys. Res. Biogeosciences*, *118*(2), 529–548, doi:10.1002/jgrg.20051.

Fang, H., S. Wei, and S. Liang (2012), Validation of MODIS and CYCLOPES LAI products using global field measurement data, *Remote Sens. Environ.*, *119*, 43–54, doi:10.1016/j.rse.2011.12.006.

Farquhar, G. D., S. Caemmerer, and J. A. Berry (1980), A biochemical model of photosynthetic $CO_2$ assimilation in leaves of C3 species, *Planta*, *149*(1), 78–90, doi:10.1007/BF00386231.

Farquhar, G. (1978), Feedforward Responses of Stomata to Humidity, *Aust. J. Plant Physiol.*, *5*(6), 787, doi:10.1071/PP9780787.

Fatichi, S., and S. Leuzinger (2013), Reconciling observations with modeling: The fate of water and carbon allocation in a mature deciduous forest exposed to elevated $CO_2$, *Agric. For. Meteorol.*, *174–175*, 144–157, doi:10.1016/j.agrformet.2013.02.005.

Fatichi S, Vivoni ER, Ogden FL, Ivanov VY, Mirus B, Gochis D, Downer CW, Camporese M, Davison JH, Ebel B, Jones N, Kim J, Mascaro G, Niswonger R, Restrepo P, Rigon R, Shen C, Sulis M, Tarboton D (2016) An overview of current applications, challenges,

and future trends in distributed process-based models in hydrology. *J Hydrol* 537:45–60. http://dx.doi.org/10.1016/j.jhydrol.2016.03.026

Feng, S., and Q. Fu (2013), Expansion of global drylands under a warming climate, *Atmos. Chem. Phys.*, *13*(19), 10081–10094, doi:10.5194/acp-13-10081-2013.

Finzi, A. C., E. H. DeLucia, J. G. Hamilton, D. D. Richter, and W. H. Schlesinger (2002), The nitrogen budget of a pine forest under free air $CO_2$ enrichment, *Oecologia*, *132*(4), 567–578, doi:10.1007/s00442-002-0996-3.

Flexas, J., M. Ribas-Carbó, A. Diaz-Espejo, J. Galmés, and H. Medrano (2008), Mesophyll conductance to CO2: Current knowledge and future prospects, *Plant, Cell Environ.*, *31*(5), 602–621, doi:10.1111/j.1365-3040.2007.01757.x.

Franklin, O. (2007), Optimal nitrogen allocation controls tree responses to elevated $CO_2$, *New Phytol.*, 174(4), 811–822, doi:10.1111/j.1469-8137.2007.02063.x, 2007.

Franklin, O., J. Johansson, R. C. Dewar, U. Dieckmann, R. E. McMurtrie, A. K. Brännström, and R. Dybzinski (2012), Modeling carbon allocation in trees: A search for principles, *Tree Physiol.*, *32*(6), 648–666, doi:10.1093/treephys/tpr138.

Franks, P. J., I. R. Cowan, and G. D. Farquhar (1997), The apparent feedforward response of stomata to air vapour pressure deficit: information revealed by different experimental procedures with two rainforest trees, *Plant. Cell Environ.*, *20*(1), 142–145, doi:10.1046/j.1365-3040.1997.d01-14.x.

Franks, P. J. (2004), Stomatal control and hydraulic conductance, with special reference to tall trees, *Tree Physiol.*, *24*(8), 865–878, doi:10.1093/treephys/24.8.865.

Franks, P. J., J. A. Berry, D. L. Lombardozzi, and G. B. Bonan (2017), Stomatal Function across Temporal and Spatial Scales: Deep-Time Trends, Land-Atmosphere Coupling and Global Models, *Plant Physiol.*, *174*(2), 583–602, doi:10.1104/pp.17.00287.

Garrigues, S., Lacaze, R., Baret, F., Morisette, J. T., Weiss, M., Nickeson, J. E., Fernandes, R., Plummer, S., Shabanov, N. V., Myneni, R. B., Knyazikhin, Y. and Yang, W. (2008), Validation and intercomparison of global Leaf Area Index products derived from remote sensing data, *J. Geophys. Res. Biogeosciences*, *113*(2), doi:10.1029/2007JG000635.

Gimeno, T. E., K. Y. Crous, J. Cooke, A. P. O'Grady, A. Ósvaldsson, B. E. Medlyn, and D. S. Ellsworth (2016), Conserved stomatal behaviour under elevated $CO_2$ and varying water availability in a mature woodland, *Funct. Ecol.*, *30*(5), 700–709, doi:10.1111/1365-2435.12532.

Gimeno, T. E., T. R. McVicar, A. P. O'Grady, D. T. Tissue, and D. S. Ellsworth (2018), Elevated $CO_2$ did not affect the hydrological balance of a mature native Eucalyptus woodland, *Glob. Chang. Biol.*, *33*(0), 0–2, doi:10.1111/gcb.14139.

Goll, D. S., Vuichard, N., Maignan, F., Jornet-Puig, A., Sardans, J., Violette, A., Peng, S., Sun, Y., Kvakic, M., Guimberteau, M., Guenet, B., Zaehle, S., Penuelas, J., Janssens, I. and Ciais, P. (2017), A representation of the phosphorus cycle for ORCHIDEE (revision 4520), *Geosci. Model Dev.*, *10*(10), 3745–3770, doi:10.5194/gmd-10-3745-2017.

Gunderson, C. A., and S. D. Wullschleger (1994), Photosynthetic acclimation in trees to rising atmospheric $CO_2$: A broader perspective, *Photosynth. Res.*, *39*(3), 369–388, doi:10.1007/BF00014592.

Hamerlynck, E. P., T. E. Huxman, T. N. Charlet, and S. D. Smith (2002), Effects of elevated $CO_2$ (FACE) on the functional ecology of the drought-deciduous Mojave Desert shrub, *Lycium andersonii*, *Environ. Exp. Bot.*, *48*(2), 93–106, doi:10.1016/S0098-8472(02)00012-6.

Haxeltine, A., I. C. Prentice, and I. D. Creswell (1996), A coupled carbon and water flux model to predict vegetation structure, *J. Veg. Sci.*, *7*(5), 651–666, doi:10.2307/3236377.

Heskel, M. A., O'Sullivan, O. S., Reich, P. B., Tjoelker, M. G., Weerasinghe, L. K., Penillard, A., Egerton, J. J. G., Creek, D., Bloomfield, K. J., Xiang, J., Sinca, F., Stangl, Z. R., Martinez-de la Torre, A., Griffin, K. L., Huntingford, C., Hurry, V., Meir, P., Turnbull, M. H. and Atkin, O. K. (2016), Convergence in the temperature response of leaf respiration across biomes and plant functional types, *Proc. Natl. Acad. Sci.*, *113*(14), 201520282, doi:10.1073/pnas.1520282113.

Hill, M. J., U. Senarath, A. Lee, M. Zeppel, J. M. Nightingale, R. (Dick) J. Williams, and T. R. McVicar (2006), Assessment of the MODIS LAI product for Australian ecosystems, *Remote Sens. Environ.*, *101*(4), 495–518, doi:10.1016/j.rse.2006.01.010.

Huang, L. F., J. H. Zheng, Y. Y. Zhang, W. H. Hu, W. H. Mao, Y. H. Zhou, and J. Q. Yu (2006), Diurnal variations in gas exchange, chlorophyll fluorescence quenching and light allocation in soybean leaves: The cause for midday depression in $CO_2$ assimilation, *Sci. Hortic. (Amsterdam).*, *110*(2), 214–218, doi:10.1016/j.scienta.2006.07.001.

Humphrey, V., J. Zscheischler, P. Ciais, L. Gudmundsson, S. Sitch, and S. I. Seneviratne (2018), Sensitivity of atmospheric $CO_2$ growth rate to observed changes in terrestrial water storage, *Nature*, *560*(7720), 628–631, doi:10.1038/s41586-018-0424-4.

Iio, A., K. Hikosaka, N. P. R. Anten, Y. Nakagawa, and A. Ito (2014), Global dependence of field-observed leaf area index in woody species on climate: A systematic review, *Glob. Ecol. Biogeogr.*, *23*(3), 274–285, doi:10.1111/geb.12133.

IPCC, 2014: Climate Change 2014: Synthesis Report. Contribution of Working Groups I, II and III to the Fifth Assessment Report of the Intergovernmental Panel on Climate Change [Core Writing Team, R.K. Pachauri and L.A. Meyer (eds.)]. *IPCC*, Geneva, Switzerland, 151 pp.

Jarvis, P. G. (1995), Scaling processes and problems, *Plant. Cell Environ.*, *18*(10), 1079–1089, doi:10.1111/j.1365-3040.1995.tb00620.x.

Jin, Y., and M. L. Goulden (2014), Ecological consequences of variation in precipitation: separating short- versus long-term effects using satellite data, *Glob. Ecol. Biogeogr.*, *23*(3), 358–370, doi:10.1111/geb.12135.

Joos, F., and R. Spahni (2008), Rates of change in natural and anthropogenic radiative forcing over the past 20,000 years, *Proc. Natl. Acad. Sci.*, *105*(5), 1425–1430, doi:10.1073/pnas.0707386105.

Kamakura, M., Y. Kosugi, S. Takanashi, K. Matsumoto, M. Okumura, and E. Philip (2011), Patchy stomatal behaviour during midday depression of leaf $CO_2$ exchange in tropical trees, *Tree Physiol.*, *31*(2), 160–168, doi:10.1093/treephys/tpq102.

Keenan, T. F., D. Y. Hollinger, G. Bohrer, D. Dragoni, J. W. Munger, H. P. Schmid, and A. D. Richardson (2013), Increase in forest water-use efficiency as atmospheric carbon dioxide concentrations rise, *Nature*, *499*(7458), 324–327, doi:10.1038/nature12291.

Keenan, T., S. Sabate, and C. Gracia (2010), Soil water stress and coupled photosynthesis-conductance models: Bridging the gap between conflicting reports on the relative roles of stomatal, mesophyll conductance and biochemical limitations to photosynthesis, *Agric. For. Meteorol.*, *150*(3), 443–453, doi:10.1016/j.agrformet.2010.01.008.

Kelly, J. W. G., R. A. Duursma, B. J. Atwell, D. T. Tissue, and B. E. Medlyn (2015), Drought × $CO_2$ interactions in trees: a test of the low-intercellular $CO_2$ concentration (Ci) mechanism, *New Phytol.*, n/a-n/a, doi:10.1111/nph.13715.

Kergoat L. (1998), A model for hydrological equilibrium of leaf area index on a global scale, *J. Hydrol.*, *212–213*, 268–286, doi:10.1016/S0022-1694(98)00211-X.

Kergoat, L. (2002), Impact of doubled $CO_2$ on global-scale leaf area index and evapotranspiration: Conflicting stomatal conductance and LAI responses, *J. Geophys. Res.*, *107*(D24), 4808, doi:10.1029/2001JD001245.

Kimball, B. A., J. R. Mauney, F. S. I. Nakayama, and S. B. Idso (1993), Effects of increasing atmospheric $CO_2$ on vegetation, *Vegetatio*, *104/105*(June), 65–75.

Klein, T., M. K. F. Bader, S. Leuzinger, M. Mildner, P. Schleppi, R. T. W. Siegwolf, and C. Körner (2016), Growth and carbon relations of mature Picea abies trees under 5 years of free-air $CO_2$ enrichment, edited by E. Lines, *J. Ecol.*, *104*(6), 1720–1733, doi:10.1111/1365-2745.12621.

Knauer, J., C. Werner, and S. Zaehle (2015), Evaluating stomatal models and their atmospheric drought response in a land surface scheme: A multibiome analysis, *J. Geophys. Res. Biogeosciences*, *120*(10), 1894–1911, doi:10.1002/2015JG003114.

Knauer, J., S. Zaehle, M. Reichstein, B. E. Medlyn, M. Forkel, S. Hagemann, and C. Werner (2017), The response of ecosystem water-use efficiency to rising atmospheric $CO_2$ concentrations: sensitivity and large-scale biogeochemical implications, *New Phytol.*, *213*(4), 1654–1666, doi:10.1111/nph.14288.

Knyazikhin, Y., Myneni, R. B., Privette, J. L., Running, S. W., Nemani, R., Zhang, Y., Tian, Y., Wang, Y., Morissette, J. T., Glassy, J. and Votava, P. (1999), MODIS Leaf Area Index (LAI) And Fraction Of Photosynthetically Active Radiation Absorbed By Vegetation (FPAR) Product, *Modis Atbd*, *Version 4*.(4.0), 130, doi:http://eospso.gsfc.nasa.gov/atbd/modistables.html.

Kool, D., N. Agam, N. Lazarovitch, J. L. Heitman, T. J. Sauer, and A. Ben-Gal (2014), A review of approaches for evapotranspiration partitioning, *Agric. For. Meteorol.*, *184*, 56–70, doi:10.1016/j.agrformet.2013.09.003.

Korner, C., R. Asshoff, O. Bignucolo, S. Hattenschwiler, S. G. Keel, S. Pelaez-Riedl, S. Pepin, R. T. W. Siegwolf, and G. Zotz (2005), Carbon flux and growth in mature deciduous forest trees exposed to elevated $CO_2$, *Science (80-. ).*, *309*(5739), 1360–1362.

Kowalczyk, E. A., Y. P. Wang, and R. M. Law (2006), The CSIRO Atmosphere Biosphere Land Exchange (CABLE) model for use in climate models and as an offline model, *CSIRO Mar. Atmos. Res. Pap.*, *13*(November 2015), 42, doi:1921232390.

Kumarathunge, D.P., B. E. Medlyn, J. E. Drake, M. G. Tjoelker, M. J. Aspinwall, M. Battaglia, F. J. Cano1, K. R. Carter, M. A. Cavaleri, L. A. Cernusak, J. Q. Chambers, Kr. Y. Crous, M. G. De Kauwe, D. N. Dillaway, E. Dreyer, D. S. Ellsworth, O. Ghannoum, Q. Han, K. Hikosaka, A. M. Jensen, J. W. G. Kelly, E. L. Kruger, L. M. Mercado, Y. Onoda, P. B. Reich, A. Rogers, M. Slot, N. G Smith, L. Tarvainen, D. T. Tissue1, H. F. Togashi, E. S.Tribuzy, J. Uddling, A. Vårhammar, G. Wallin, J. M. Warren, D. A. Way (2018), Acclimation and adaptation components of the temperature dependence of plant photosynthesis at the global scale, *New Phytol.*, accepted.

Lawlor, D. W., and G. Cornic (2002), Photosynthetic carbon assimilation and associated metabolism in relation to water deficits in higher plants., *Plant. Cell Environ.*, *25*(2), 275–294, doi:10.1046/j.0016-8025.2001.00814.x.

Lawlor, D. W., and W. Tezara (2009), Causes of decreased photosynthetic rate and metabolic capacity in water-deficient leaf cells: A critical evaluation of mechanisms and integration of processes, *Ann. Bot.*, *103*(4), 561–579, doi:10.1093/aob/mcn244.

Le Quéré, C., Andrew, R. M., Friedlingstein, P., Sitch, S., Pongratz, J., Manning, A. C., Korsbakken, J. I., Peters, G. P., Canadell, J. G., Jackson, R. B., Boden, T. A., Tans, P. P., Andrews, O. D., Arora, V. K., Bakker, D. C. E., Barbero, L., Becker, M., Betts, R. A., Bopp, L., Chevallier, F., Chini, L. P., Ciais, P., Cosca, C. E., Cross, J., Currie, K., Gasser, T., Harris, I., Hauck, J., Haverd, V., Houghton, R. A., Hunt, C. W., Hurtt, G., Ilyina, T., Jain, A. K., Kato, E., Kautz, M., Keeling, R. F., Klein Goldewijk, K., Körtzinger, A., Landschützer, P., Lefèvre, N., Lenton, A., Lienert, S., Lima, I., Lombardozzi, D., Metzl, N., Millero, F., Monteiro, P. M. S., Munro, D. R., Nabel, J. E. M. S., Nakaoka, S., Nojiri, Y., Padín, X. A., Peregon, A., Pfeil, B., Pierrot, D., Poulter, B., Rehder, G., Reimer, J., Rödenbeck, C., Schwinger, J., Séférian, R., Skjelvan, I., Stocker, B. D., Tian, H., Tilbrook, B., van der Laan-Luijkx, I. T., van der Werf, G. R., van Heuven, S., Viovy, N., Vuichard, N., Walker, A. P., Watson, A. J., Wiltshire, A. J., Zaehle, S. and Zhu, D. (2017), Global Carbon Budget 2017, *Earth Syst. Sci. Data Discuss.*, (November), 1–79, doi:10.5194/essd-2017-123.

Le Quéré, C., Raupach, M. R., Canadell, J. G., Marland, G., Bopp, L., Ciais, P., Conway, T. J., Doney, S. C., Feely, R. A., Foster, P., Friedlingstein, P., Gurney, K., Houghton, R. A., House, J. I., Huntingford, C., Levy, P. E., Lomas, M. R., Majkut, J., Metzl, N., Ometto, J. P., Peters, G. P., Prentice, I. C., Randerson, J. T., Running, S. W., Sarmiento, J. L., Schuster, U., Sitch, S., Takahashi, T., Viovy, N., Van Der Werf, G. R. and Woodward, F. I. (2009), Trends in the sources and sinks of carbon dioxide, *Nat. Geosci.*, *2*(12), 831–836, doi:10.1038/ngeo689.

Leuning, R. (1995), A critical appraisal of a combined stomatal - photosynthesis model for C3 plants, *Plant. Cell Environ.*, *18*, 339–355, doi:10.1111/j.1365-3040.1995.tb00370.x.

Lin, Y. S., Medlyn, B. E., Duursma, R. A., Prentice, I. C., Wang, H., Baig, S., Eamus, D., de Dios, V. R., Mitchell, P., Ellsworth, D. S., de Beeck, M. O., Wallin, G., Uddling, J., Tarvainen, L., Linderson, M.-L., Cernusak, L. A., Nippert, J. B., Ocheltree, T. W., Tissue, D. T., Martin-StPaul, N. K., Rogers, A., Warren, J. M., De Angelis, P., Hikosaka, K., Han, Q., Onoda, Y., Gimeno, T. E., Barton, C. V. M., Bennie, J., Bonal, D., Bosc, A., Löw, M., Macinins-Ng, C., Rey, A., Rowland, L., Setterfield, S. A., Tausz-Posch, S., Zaragoza-Castells, J., Broadmeadow, M. S. J., Drake, J. E., Freeman, M., Ghannoum, O., Hutley, L. B., Kelly, J. W., Kikuzawa, K., Kolari, P., Koyama, K., Limousin, J.-M., Meir, P., Lola da Costa, A. C., Mikkelsen, T. N., Salinas, N., Sun, W. and Wingate, L. (2015), Optimal stomatal behaviour around the world, *Nat. Clim. Chang.*, 1–14, doi:10.1038/nclimate2550.

Liu, B., H. Guan, W. Zhao, Y. Yang, and S. Li (2017), Groundwater facilitated water-use efficiency along a gradient of groundwater depth in arid northwestern China, *Agric. For. Meteorol.*, *233*, 235–241, doi:10.1016/j.agrformet.2016.12.003.

Lohammar, T., S. Larsson, S. Linder, and S. O. Falk (1980), FAST: Simulation Models of Gaseous Exchange in Scots Pine, *Ecol. Bull.*, (32), 505–523, doi:10.2307/20112831.

Lu, Y., R. A. Duursma, and B. E. Medlyn (2016), Optimal stomatal behaviour under stochastic rainfall, *J. Theor. Biol.*, *394*, 160–171, doi:10.1016/j.jtbi.2016.01.003.

Luo, Y., B. Medlyn, D. Hui, D. Ellsworth, J. Reynolds, and G. Katul (2001), Gross primary productivity in duke forest: Modeling synthesis of $CO_2$ experiment and eddy-flux data, *Ecol. Appl.*, *11*(1), 239–252, doi:10.2307/3061070.

Luo, Y., Su, B., Currie, W. S., Dukes, J. S., Finzi, A., Hartwig, U., Hungate, B., Mc MURTRIE, R. E., Oren, R., Parton, W. J., Pataki, D. E., Shaw, M. R., Zak, D. R. and Field, C. B. (2004), Progressive Nitrogen Limitation of Ecosystem Responses to Rising Atmospheric Carbon Dioxide, *Bioscience*, 54(8), 731.

Ma, X., Huete, A., Cleverly, J., Eamus, D., Chevallier, F., Joiner, J., Poulter, B., Zhang, Y., Guanter, L., Meyer, W., Xie, Z. and Ponce-Campos, G. (2016), Drought rapidly diminishes the large net $CO_2$ uptake in 2011 over semi-arid Australia, *Sci. Rep.*, *6*(November), 1–9, doi:10.1038/srep37747.

Macfarlane, C., D. A. White, and M. A. Adams (2004), The apparent feed-forward response to vapour pressure deficit of stomata in droughted, field-grown Eucalyptus globulus Labill, *Plant, Cell Environ.*, *27*(10), 1268–1280, doi:10.1111/j.1365-3040.2004.01234.x.

Mahowald, N., F. Lo, Y. Zheng, L. Harrison, C. Funk, D. Lombardozzi, and C. Goodale (2016), Projections of leaf area index in earth system models, *Earth Syst. Dyn.*, *7*(1), 211–229, doi:10.5194/esd-7-211-2016.

Maier-Maercker, U. (1983), The role of peristomatal transpiration in the mechanism of stomatal movement, *Plant. Cell Environ.*, *6*(5), 369–380, doi:10.1111/j.1365-3040.1983.tb01269.x.

Manzoni, S., G. Vico, S. Palmroth, A. Porporato, and G. Katul (2013), Optimization of stomatal conductance for maximum carbon gain under dynamic soil moisture, *Adv. Water Resour.*, *62*, 90–105, doi:10.1016/j.advwatres.2013.09.020.

Matusick, G., K. X. Ruthrof, N. C. Brouwers, B. Dell, and G. S. J. Hardy (2013), Sudden forest canopy collapse corresponding with extreme drought and heat in a mediterranean-type eucalypt forest in southwestern Australia, *Eur. J. For. Res.*, *132*(3), 497–510, doi:10.1007/s10342-013-0690-5.

McMurtrie, R. E., R. J. Norby, B. E. Medlyn, R. C. Dewar, D. A. Pepper, P. B. Reich, and C. V. M. Barton (2008), Why is plant-growth response to elevated $CO_2$ amplified when water is limiting, but reduced when nitrogen is limiting? A growth-optimisation hypothesis, *Funct. Plant Biol.*, *35*(6), 521–534, doi:10.1071/FP08128.

McMurtrie, R. E., and R. C. Dewar (2013), New insights into carbon allocation by trees from the hypothesis that annual wood production is maximized, *New Phytol.*, *199*(4), 981–990, doi:10.1111/nph.12344.

Medlyn, B. E., Dreyer, E., Ellsworth, D., Forstreuter, M., Harley, P. C., Kirschbaum, M. U. F., Le Roux, X., Montpied, P., Strassemeyer, J., Walcroft, A., Wang, K. and Loustau, D. (2002), Temperature response of parameters of a biochemically based model of photosynthesis. II. A review of experimental data, *Plant, Cell Environ.*, *25*(9), 1167–1179, doi:10.1046/j.1365-3040.2002.00891.x.

Medlyn, B. E., Badeck, F.-W., De Pury, D., Barton, C., Broadmeadow, M., Ceulemans, R., De Angelis, P., Forstreuter, M., Jach, M., Kellomäki, S., Laitat, E., Marek, M., Philippot, S., Rey, A., Strassemeyer, J., Laitinen, K., Liozon, R., Portier, B., Robertntz, P., Wang, K. and Jarvis, P. (1999), Effects of elevated [$CO_2$] on photosynthesis in European forest species: a meta-analysis of model parameters, *Plant Cell Environ.*, *22*, 1475–1495.

Medlyn, B. E., De Kauwe, M. G., Lin, Y.-S., Knauer, J., Duursma, R. A., Williams, C. A., Arneth, A., Clement, R., Isaac, P., Limousin, J.-M., Linderson, M.-L., Meir, P., Martin-StPaul, N. and Wingate, L. (2017), How do leaf and ecosystem measures of water-use efficiency compare?, *New Phytol.*, *216*(3), 758–770, doi:10.1111/nph.14626.

Medlyn, B. E., De Kauwe, M. G., Zaehle, S., Walker, A. P., Duursma, R. A., Luus, K., Mishurov, M., Pak, B., Smith, B., Wang, Y. P., Yang, X., Crous, K. Y., Drake, J. E., Gimeno, T. E., Macdonald, C. A., Norby, R. J., Power, S. A., Tjoelker, M. G. and Ellsworth, D. S. (2016), Using models to guide field experiments: a priori predictions for the $CO_2$ response of a nutrient- and water-limited native Eucalypt woodland, *Glob. Chang. Biol.*, *22*(8), 2834–2851, doi:10.1111/gcb.13268.

Medlyn, B. E., R. A. Duursma, D. Eamus, D. S. Ellsworth, I. C. Prentice, C. V. M. Barton, K. Y. Crous, P. De Angelis, M. Freeman, and L. Wingate (2011), Reconciling the optimal and empirical approaches to modelling stomatal conductance, *Glob. Chang. Biol.*, *17*(6), 2134–2144, doi:10.1111/j.1365-2486.2010.02375.x.

Medlyn, B. E., D. a Pepper, A. P. O'Grady, and H. Keith (2007), Linking leaf and tree water use with an individual-tree model., *Tree Physiol.*, *27*(12), 1687–1699, doi:10.1093/treephys/27.12.1687.

Medlyn, B. E., Zaehle, S., De Kauwe, M. G., Walker, A. P., Dietze, M. C., Hanson, P. J., Hickler, T., Jain, A. K., Luo, Y., Parton, W., Prentice, I. C., Thornton, P. E., Wang, S., Wang, Y. P., Weng, E., Iversen, C. M., Mccarthy, H. R., Warren, J. M., Oren, R. and Norby, R. J. (2015), Using ecosystem experiments to improve vegetation models, *Nat. Clim. Chang.*, *5*(6), 528–534, doi:10.1038/nclimate2621.

Mehran, A., A. AghaKouchak, and T. J. Phillips (2014), Evaluation of CMIP5 continental precipitation simulations relative to satellite-based gauge-adjusted observations, *J. Geophys. Res. Atmos.*, *119*(4), 1695–1707, doi:10.1002/2013JD021152.

Méndez-Toribio, M., G. Ibarra-Manríquez, A. Navarrete-Segueda, and H. Paz (2017), Topographic position, but not slope aspect, drives the dominance of functional strategies of tropical dry forest trees, *Environ. Res. Lett.*, *12*(8), 085002, doi:10.1088/1748-9326/aa717b.

Miller, J. M., R. J. Williams, and G. D. Farquhar (2001), Carbon isotope discrimination by a sequence of eucalyptus species along a subcontinental rainfall gradient in Australia, *Funct. Ecol.*, *15*(2), 222–232, doi:10.1046/j.1365-2435.2001.00508.x.

Mitchell, P. J., E. Veneklaas, H. Lambers, and S. S. O. Burgess (2009), Partitioning of evapotranspiration in a semi-arid eucalypt woodland in south-western Australia, *Agric. For. Meteorol.*, *149*(1), 25–37, doi:10.1016/j.agrformet.2008.07.008.

Monteith, J. L. (1995), A reinterpritation of stomatal responses to humidity, *Plant, Cell Environ.*, *18*(1991), 357–364.

Morison, J. I. L. (1985), Sensitivity of stomata and water use efficiency to high $CO_2$, *Plant, Cell Environ.*, *8*, 467–474.

Mott, K. A., and T. N. Buckley (1998), Stomatal heterogeneity, *J. Exp. Bot.*, *49*(Special), 407–417, doi:10.1093/jxb/49.Special_Issue.407.

Mott, K. A., and D. F. Parkhurst (1991), Stomatal responses to humidity in air and helox, *Plant. Cell Environ.*, *14*(5), 509–515, doi:10.1111/j.1365-3040.1991.tb01521.x.

Murray-Tortarolo, G. et al. (2013), Evaluation of land surface models in reproducing satellite-derived LAI over the high-latitude northern hemisphere. Part I: Uncoupled DGVMs, *Remote Sens.*, *5*(10), 4819–4838, doi:10.3390/rs5104819.

Naumburg, E., D. C. Housman, T. E. Huxman, T. N. Charlet, M. E. Loik, and S. D. Smith (2003), Photosynthetic responses of Mojave Desert shrubs to free air $CO_2$ enrichment

are greatest during wet years, *Glob. Chang. Biol.*, *9*(2), 276–285, doi:10.1046/j.1365-2486.2003.00580.x.

Neilson, R. P. (1995), A Model for Predicting Continental-Scale Vegetation Distribution and Water Balance, *Ecol. Appl.*, *5*(2), 362–385.

Nemani, R. R., and S. W. Running (1989), Testing a theoretical climate-soil-leaf area hydrologic equilibrium of forests using satellite data and ecosystem simulation, *Agric. For. Meteorol.*, *44*(3–4), 245–260, doi:10.1016/0168-1923(89)90020-8.

Nicholls, N. (2006), Detecting and attributing Australian climate change: a review, *Aust. Meteorol. Mag.*, *55*(3), 199–211.

Niinemets, Ü., T. F. Keenan, and L. Hallik (2015), A worldwide analysis of within-canopy variations in leaf structural, chemical and physiological traits across plant functional types, *New Phytol.*, *205*(3), 973–993, doi:10.1111/nph.13096.

Norby, R. J. (1996), Forest canopy productivity index, *Nature*, *381*(6583), 564–564, doi:10.1038/381564a0.

Norby, R. J. DeLucia, E. H., Gielen, B., Calfapietra, C., Giardina, C. P., King, J. S., Ledford, J., McCarthy, H. R., Moore, D. J. P., Ceulemans, R., De Angelis, P., Finzi, A. C., Karnosky, D. F., Kubiske, M. E., Lukac, M., Pregitzer, K. S., Scarascia-Mugnozza, G. E., Schlesinger, W. H. and Oren, R. (2005), Forest response to elevated $CO_2$ is conserved across a broad range of productivity, *Proc. Natl. Acad. Sci.*, *102*(50), 18052–18056, doi:10.1073/pnas.0509478102.

Norby, R. J., J. M. Warren, C. M. Iversen, B. E. Medlyn, and R. E. McMurtrie (2010), $CO_2$ enhancement of forest productivity constrained by limited nitrogen availability, *Proc. Natl. Acad. Sci.*, *107*(45), 19368–19373, doi:10.1073/pnas.1006463107.

Norby, R. J., L. Gu, I. C. Haworth, A. M. Jensen, B. L. Turner, A. P. Walker, J. M. Warren, D. J. Weston, C. Xu, and K. Winter (2016), Informing models through empirical relationships between foliar phosphorus, nitrogen and photosynthesis across diverse woody species in tropical forests of Panama, *New Phytol.*, doi:10.1111/nph.14319.

Norby, R. J., S. D. Wullschleger, C. A. Gunderson, D. W. Johnson, and R. Ceulemans (1999), Tree responses to rising $CO_2$ in field experiments: Implications for the future forest, *Plant, Cell Environ.*, *22*(6), 683–714, doi:10.1046/j.1365-3040.1999.00391.x.

Norby, R. J., and D. R. Zak (2011), Ecological Lessons from Free-Air $CO_2$ Enrichment (FACE) Experiments, *Annu. Rev. Ecol. Evol. Syst.*, *42*(1), 181–203, doi:10.1146/annurev-ecolsys-102209-144647.

Novick, K. A., Ficklin, D. L., Stoy, P. C., Williams, C. A., Bohrer, G., Oishi, A. C., Papuga, S. A., Blanken, P. D., Noormets, A., Sulman, B. N., Scott, R. L., Wang, L. and Phillips, R. P. (2016), The increasing importance of atmospheric demand for ecosystem water and carbon fluxes, *Nat. Clim. Chang.*, *1*(September), 1–5, doi:10.1038/nclimate3114.

Ogle, K., J. J. Barber, C. Willson, and B. Thompson (2009), Hierarchical statistical modeling of xylem vulnerability to cavitation: Methods, *New Phytol.*, *182*(2), 541–554, doi:10.1111/j.1469-8137.2008.02760.x.

Onoda, Y., I. J. Wright, J. R. Evans, Hikosaka, K., Kitajima, K., Niinemets, ??lo, Poorter, H., Tosens, T. and Westoby, M. (2017), Physiological and structural tradeoffs underlying the leaf economics spectrum, *New Phytol.*, 1447–1463, doi:10.1111/nph.14496.

Pan, Y. Birdsey, R. A., Fang, J., Houghton, R., Kauppi, P. E., Kurz, W. A., Phillips, O. L., Shvidenko, A., Lewis, S. L., Canadell, J. G., Ciais, P., Jackson, R. B., Pacala, S. W., McGuire, A. D., Piao, S., Rautiainen, A., Sitch, S. and Hayes, D. (2011), A Large and Persistent Carbon Sink in the World's Forests, *Science (80 ).*, *333*(6045), 988–993, doi:10.1126/science.1201609.

Pappas, C., S. Fatichi, and P. Burlando (2016), Modeling terrestrial carbon and water dynamics across climatic gradients: Does plant trait diversity matter?, *New Phytol.*, *209*(1), 137–151, doi:10.1111/nph.13590.

Parton, W. J., Scurlock, J. M. O., Ojima, D. S., Gilmanov, T. G., Scholes, R. J., Schimel, D. S., Kirchner, T., Menaut, J.-C., Seastedt, T., Garcia Moya, E., Kamnalrut, A. and Kinyamario, J. I. (1993), Observations and modeling of biomass and soil organic matter dynamics for the grassland biome worldwide, *Global Biogeochem. Cycles*, *7*(4), 785–809, doi:10.1029/93GB02042.

Parton, W. J., P. J. Hanson, C. Swanston, M. Torn, S. E. Trumbore, W. Riley, and R. Kelly (2010), ForCent model development and testing using the Enriched Background Isotope Study experiment, *J. Geophys. Res. Biogeosciences*, *115*(4), 1–15, doi:10.1029/2009JG001193.

Peñuelas, J., J. G. Canadell, and R. Ogaya (2011), Increased water-use efficiency during the 20th century did not translate into enhanced tree growth, *Glob. Ecol. Biogeogr.*, *20*(4), 597–608, doi:10.1111/j.1466-8238.2010.00608.x.

Piao, S. et al. (2013), Evaluation of terrestrial carbon cycle models for their response to climate variability and to $CO_2$ trends, *Glob. Chang. Biol.*, *19*(7), 2117–2132, doi:10.1111/gcb.12187.

Pitman, A. J. (2003), The evolution of, and revolution in, land surface schemes designed for climate models, *Int. J. Climatol.*, *23*(5), 479–510, doi:10.1002/joc.893.

Prentice, I. C., N. Dong, S. M. Gleason, V. Maire, and I. J. Wright (2014), Balancing the costs of carbon gain and water transport: testing a new theoretical framework for plant functional ecology, *Ecol. Lett.*, *17*(1), 82–91, doi:10.1111/ele.12211.

Reichstein, M., Bahn, M., Ciais, P., Frank, D., Mahecha, M. D., Seneviratne, S. I., Zscheischler, J., Beer, C., Buchmann, N., Frank, D. C., Papale, D., Rammig, A., Smith, P., Thonicke, K., Van Der Velde, M., Vicca, S., Walz, A. and Wattenbach, M. (2013), Climate extremes and the carbon cycle, *Nature*, *500*(7462), 287–295, doi:10.1038/nature12350.

Renchon, A., A. Griebel, A., Metzen, D., Williams, C. A., Medlyn, B., Duursma, R. A., Barton, C. V. M., Maier, C., Boer, M. M., Isaac, P., Tissue, D., Resco De DIos, V. and Pendall, E. (2018), Upside-down fluxes Down Under: $CO_2$ net sink in winter and net source in summer in a temperate evergreen broadleaf forest, *Biogeosciences*, *15*(12), 3703–3716, doi:10.5194/bg-15-3703-2018.

Rey, A., and P. G. Jarvis (1998), Long-term photosynthetic acclimation to elevated atmospheric $CO_2$ in birch (*Betula pendula Roth.*), *Impacts Glob. Chang. Tree Physiol. For. Ecosyst.*, *52*(1996), 87–91.

Risbey, J. S. (2011), Dangerous climate change and water resources in Australia, *Reg. Environ. Chang.*, *11*(SUPPL. 1), 197–203, doi:10.1007/s10113-010-0176-7.

Roderick, M. L., and G. D. Farquhar (2004), Changes in Australian pan evapouration from 1970 to 2002, *Int. J. Climatol.*, *24*(9), 1077–1090, doi:10.1002/joc.1061.

Roderick, M. L., P. Greve, and G. D. Farquhar (2015), On the assessment of aridity with changes in atmospheric $CO_2$, *Water Resour. Res.*, *51*(7), 5450–5463, doi:10.1002/2015WR017031.

Rogers, A., Medlyn, B. E., Dukes, J. S., Bonan, G., von Caemmerer, S., Dietze, M. C., Kattge, J., Leakey, A. D. B., Mercado, L. M., Niinemets, ??lo, Prentice, I. C., Serbin, S. P., Sitch, S., Way, D. A. and Zaehle, S. (2017), A roadmap for improving the representation of photosynthesis in Earth system models, *New Phytol.*, *213*(1), 22–42, doi:10.1111/nph.14283.

Roy, J., Picon-Cochard, C., Augusti, A., Benot, M.-L., Thiery, L., Darsonville, O., Landais, D., Piel, C., Defossez, M., Devidal, S., Escape, C., Ravel, O., Fromin, N., Volaire, F., Milcu, A., Bahn, M. and Soussana, J.-F. (2016), Elevated $CO_2$ maintains grassland net carbon uptake under a future heat and drought extreme, *Proc. Natl. Acad. Sci.*, *113*(22), 6224–6229, doi:10.1073/pnas.1524527113.

Running, S. W., and R. R. Nemani (1988), Relating seasonal patterns of the AVHRR vegetation index to simulated photosynthesis and transpiration of forests in different climates, *Remote Sens. Environ.*, *24*(2), 347–367, doi:10.1016/0034-4257(88)90034-X.

Ryan, E. M., Ogle, K., Peltier, D., Walker, A. P., De Kauwe, M. G., Medlyn, B. E., Williams, D. G., Parton, W., Asao, S., Guenet, B., Harper, A., Lu, X., Luus, K. A., Zaehle, S., Shu, S., Werner, C., Xia, J. and Pendall, E. (2016), Gross primary production responses to warming, elevated $CO_2$ , and irrigation:quantifying the drivers of ecosystem physiology in a semiarid grassland, *Glob. Chang. Biol.*, *38*(1), 42–49, doi:10.1111/gcb.13602.

Sands, P. J. (1995), Modelling Canopy Production II. From Single-leaf Photosynthetic Parameters to Daily Canopy Photosynthesis, *Aust. J. Plant Physiol.*, *22*(4), 603–14, doi:dx.doi.org/10.1071/PP9950603.

Sands, P. J. (1996), Modelling Canopy Production. III. Canopy Light-Utilisation Efficiency and Its Sensitivity to Physiological and Environmental Variables, *Funct. Plant Biol.*, *23*(1), 103–114, doi:doi:10.1071/PP9960103.

Sawada, Y., and T. Koike (2016), Ecosystem resilience to the Millennium drought in southeast Australia (2001-2009), *J. Geophys. Res. Biogeosciences*, *121*(9), 2312–2327, doi:10.1002/2016JG003356.

Saxe, H., D. S. Ellsworth, and J. Heath (1998), Tree and forest functioning in an enriched $CO_2$ atmosphere, *New Phytol.*, *139*(3), 395–436, doi:10.1046/j.1469-8137.1998.00221.x.

Schimel, D. S., House, J. I., Hibbard, K. A., Bousquet, P., Ciais, P., Peylin, P., Braswell, B. H., Apps, M. J., Baker, D., Bondeau, A., Canadell, J., Churkina, G., Cramer, W., Denning, A. S., Field, C. B., Friedlingstein, P., Goodale, C., Heimann, M., Houghton, R. A., Melillo, J. M., Moore, B., Murdiyarso, D., Noble, I., Pacala, S. W., Prentice, I. C., Raupach, M. R., Rayner, P. J., Scholes, R. J., Steffen, W. L. and Wirth, C. (2001), Recent patterns and mechanisms of carbon exchange by terrestrial ecosystems, *Nature*, *414*(6860), 169–172, doi:10.1038/35102500.

Schymanski, S. J., M. Sivapalan, M. L. Roderick, L. B. Hutley, and J. Beringer (2009), An optimality-based model of the dynamic feedbacks between natural vegetation and the water balance, *Water Resour. Res.*, *45*(1), doi:10.1029/2008WR006841.

Schymanski, S. J., M. L. Roderick, and M. Sivapalan (2015), Using an optimality model to understand medium and long-term responses of vegetation water use to elevated atmospheric $CO_2$ concentrations, *AoB Plants*, *7*(1), plv060, doi:10.1093/aobpla/plv060.

Sitch, S., Smith, B., Prentice, I. C., Arneth, A. C., Bondeau, A., Cramer, W., Kaplan, J. O., Levis, S., Lucht, W., Sykes, M. T., Thonicke, K., and Venevsky, S. (2003), Evaluation of ecosystem dynamics, plant geography and terrestrial carbon cycling in the LPJ dynamic global vegetation model , *Glob. Chang. Biol.*, *9*(2), 161–185, doi:10.1046/j.1365-2486.2003.00569.x.

Smith, I. (2004), An assessment of recent trends in Australian rainfall, *Aust. Meteorol. Mag.*, *53*(3), 163–173.

Smith, N. G., Rodgers, V. L., Brzostek, E. R., Kulmatiski, A., Avolio, M. L., Hoover, D. L., Koerner, S. E., Grant, K., Jentsch, A., Fatichi, S. and Niyogi, D. (2014), Toward a better integration of biological data from precipitation manipulation experiments into Earth system models, *Rev. Geophys.*, *52*(3), 412–434, doi:10.1002/2014RG000458.

Specht, R. L., and A. Specht (1989), Canopy structure in Eucalyptus-dominated communities in Australia along climatic gradients, *Acta Oecologica. Oecologia Plant.*, *10*(2), 191–213.

Sperry, J. S., Y. Wang, B. T. Wolfe, D. S. Mackay, W. R. L. Anderegg, N. G. McDowell, and W. T. Pockman (2016), Pragmatic hydraulic theory predicts stomatal responses to climatic water deficits, *New Phytol.*, doi:10.1111/NPH.14059.

Sutanto, S. J., J. Wenninger, A. M. J. Coenders-Gerrits, and S. Uhlenbrook (2012), Partitioning of evaporation into transpiration, soil evapouration and interception: A comparison between isotope measurements and a HYDRUS-1D model, *Hydrol. Earth Syst. Sci.*, *16*(8), 2605–2616, doi:10.5194/hess-16-2605-2012.

Swann, A. A. L. S., F. M. Hoffman, C. D. Koven, and J. T. Randerson (2016), Plant responses to increasing $CO_2$ reduce estimates of climate impacts on drought severity, *Proc. Natl. Acad. Sci.*, *113*(36), 10019–10024, doi:10.1073/pnas.1604581113.

Tezara, W., V. J. Mitchell, S. D. Driscoll, and D. W. Lawlor (1999), Water stress inhibits plant photosynthesis by decreasing coupling factor and ATP, *Nature*, *401*(6756), 914–917, doi:10.1038/44842.

Thomas, D. S., and D. Eamus (1999), The influence of predawn leaf water potential on stomatal responses to atmospheric water content at constant $C_i$ and on stem hydraulic conductance and foliar ABA concentrations, *J. Exp. Bot.*, *50*(331), 243–251, doi:10.1093/jxb/50.331.243.

Timbal, B. (2004), Southwest Australia past and future rainfall trends, *Clim. Res.*, *26*(3), 233–249, doi:10.3354/cr026233.

Tuzet, A., A. Perrier, and R. Leuning (2003), A coupled model of stomatal conductance, photosynthesis and transpiration, *Plant, Cell Environ.*, *26*(7), 1097–1116, doi:10.1046/j.1365-3040.2003.01035.x. van Dijk, A. I. J. M., H. E. Beck, R. S. Crosbie, R. A. M. De Jeu, Y. Y. Liu, G. M. Podger, B. Timbal, and N. R. Viney (2013), The Millennium Drought in southeast Australia (2001-2009): Natural and human causes and implications for water resources, ecosystems, economy, and society, *Water Resour. Res.*, *49*(2), 1040–1057, doi:10.1002/wrcr.20123.

Verhoef, A., and G. Egea (2014), Modeling plant transpiration under limited soil water: Comparison of different plant and soil hydraulic parameterizations and preliminary implications for their use in land surface models, *Agric. For. Meteorol.*, *191*, 22–32, doi:10.1016/j.agrformet.2014.02.009.

Villar, R., and J. Merino (2001), Comparison of leaf construction costs in woody species with differing leaf life-spans in contrasting ecosystems, *New Phytol.*, *151*(1), 213–226, doi:10.1046/j.1469-8137.2001.00147.x.

von Caemmerer, S., and J. R. Evans (2015), Temperature responses of mesophyll conductance differ greatly between species, *Plant, Cell Environ.*, *38*(4), 629–637, doi:10.1111/pce.12449.

Walker, A. P., Hanson, P. J., De Kauwe, M. G., Medlyn, B. E., Zaehle, S., Asao, S., Dietze, M., Hickler, T., Huntingford, C., Iversen, C. M., Jain, A., Lomas, M., Luo, Y., McCarthy, H., Parton, W. J., Prentice, I. C., Thornton, P. E., Wang, S., Wang, Y.-P., Warlind, D., Weng, E., Warren, J. M., Woodward, F. I., Oren, R. and Norby, R. J. (2014), Comprehensive ecosystem model-data synthesis using multiple data sets at two temperate forest free-air $CO_2$ enrichment experiments: Model performance at ambient $CO_2$ concentration, *J. Geophys. Res. Biogeosciences*, *119*(5), 937–964, doi:10.1002/2013JG002553.

Wang, K., and R. E. Dickinson (2012), A review of global terrestrial evapotranspiration: observation, modelling, climatology, and climatic variability, *Rev. Geophys.*, *50*(2011), 1–54, doi:10.1029/2011RG000373.1.

Wang, L., K. K. Caylor, J. C. Villegas, G. A. Barron-Gafford, D. D. Breshears, and T. E. Huxman (2010), Partitioning evapotranspiration across gradients of woody plant cover: Assessment of a stable isotope technique, *Geophys. Res. Lett.*, *37*(9), 1–7, doi:10.1029/2010GL043228.

Wang, L., S. P. Good, and K. K. Caylor (2014), Global synthesis of vegetation control on evapotranspiration partitioning, *Geophys. Res. Lett.*, *41*(19), 6753–6757, doi:10.1002/2014GL061439.

Wang, Y. P., A. Rey, and P. G. Jarvis (1998), Carbon balance of young birch trees grown in ambient and elevated atmospheric $CO_2$ concentrations, *Glob. Chang. Biol.*, *4*(8), 797–807, doi:10.1046/j.1365-2486.1998.00170.x.

Wang, Y., Ciais, P., Goll, D., Huang, Y., Luo, Y., Wang, Y. P., Bloom, A. A., Broquet, G., Hartmann, J., Peng, S., Penuelas, J., Piao, S., Sardans, J., Stocker, B. D., Wang, R., Zaehle, S. and Zechmeister-Boltenstern, S. (2018), GOLUM-CNP v1.0: A data-driven modeling of carbon, nitrogen and phosphorus cycles in major terrestrial biomes, *Geosci. Model Dev.*, *11*(9), 3903–3928, doi:10.5194/gmd-11-3903-2018.

Warren, C. R.: Soil water deficits decrease the internal conductance to $CO_2$ transfer but atmospheric water deficits do not, *J. Exp. Bot.*, 59(2), 327–334, doi:10.1093/jxb/erm314, 2008.

Whitley, R., Beringer, J., Hutley, L., Abramowitz, G., De Kauwe, M. G., Duursma, R., Evans, B., Haverd, V., Li, L., Ryu, Y., Smith, B., Wang, Y.-P., Williams, M. and Yu, Q. (2015), A model inter-comparison study to examine limiting factors in modelling Australian tropical savannas, *Biogeosciences Discuss.*, *12*(23), 18999–19041, doi:10.5194/bgd-12-18999-2015.

Whitley, R., D. Taylor, C. Macinnis-Ng, M. Zeppel, I. Yunusa, A. O'Grady, R. Froend, B. Medlyn, and D. Eamus (2013), Developing an empirical model of canopy water flux describing the common response of transpiration to solar radiation and VPD across five contrasting woodlands and forests, *Hydrol. Process.*, *27*(8), 1133–1146, doi:10.1002/hyp.9280.

Wild, A. (1958), The phosphate content of Australian soils, *Aust. J. Agric. Res.*, *9*(2), 193–204, doi:10.1071/AR9580193.

Will, R. E., S. M. Wilson, C. B. Zou, and T. C. Hennessey (2013), Increased vapour pressure deficit due to higher temperature leads to greater transpiration and faster mortality during drought for tree seedlings common to the forest-grassland ecotone, *New Phytol.*, *200*(2), 366–374, doi:10.1111/nph.12321.

Wolf, A., W. R. L. Anderegg, and S. W. Pacala (2016), Optimal stomatal behaviour with competition for water and risk of hydraulic impairment, *Proc. Natl. Acad. Sci. U. S. A.*, *113*(46), E7222–E7230, doi:10.1073/pnas.1615144113.

Woodward, F. I. (1987), Climate and Plant Distribution, *Cambridge University Press*, *154*(2), 174, doi:10.2307/633873.

Woodward, F. I., and M. R. Lomas (2004), Vegetation dynamics--simulating responses to climatic change., *Biol. Rev. Camb. Philos. Soc.*, *79*(3), 643–670, doi:10.1017/s1464793103006419.

Wright, I. J., Reich, P. B., Westoby, M., Ackerly, D. D., Baruch, Z., Bongers, F., Cavender-Bares, J., Chapin, T., Cornelissen, J. H. C., Diemer, M., Flexas, J., Garnier, E., Groom, P. K., Gulias, J., Hikosaka, K., Lamont, B. B., Lee, T., Lee, W., Lusk, C., Midgley, J. J., Navas, M.-L., Niinemets, Ü., Oleksyn, J., Osada, N., Poorter, H., Poot, P., Prior, L., Pyankov, V. I., Roumet, C., Thomas, S. C., Tjoelker, M. G., Veneklaas, E. J. and Villar, R. (2004), The worldwide leaf economics spectrum., *Nature*, *428*(6985), 821–827, doi:10.1038/nature02403.

Wright, J. K., M. Williams, G. Starr, J. McGee, and R. J. Mitchell (2013), Measured and modelled leaf and stand-scale productivity across a soil moisture gradient and a severe drought, *Plant Cell Environ.*, *36*(2), 467–483, doi:10.1111/j.1365-3040.2012.02590.x.

Xu, X., D. Medvigy, S. Joseph Wright, K. Kitajima, J. Wu, L. P. Albert, G. A. Martins, S. R. Saleska, and S. W. Pacala (2017), Variations of leaf longevity in tropical moist forests predicted by a trait-driven carbon optimality model, *Ecol. Lett.*, doi:10.1111/ele.12804.

Yang, J., B. E. Medlyn, M. G. De Kauwe, and R. A. Duursma (2018), Applying the Concept of Ecohydrological Equilibrium to Predict Steady State Leaf Area Index, *J. Adv. Model. Earth Syst.*, *10*(8), 1740–1758, doi:10.1029/2017MS001169.

Yang, Y., R. J. Donohue, T. R. McVicar, M. L. Roderick, and H. E. Beck (2016), Long-term $CO_2$ fertilization increases vegetation productivity and has little effect on hydrological partitioning in tropical rainforests, *J. Geophys. Res. Biogeosciences*, *121*(8), 2125–2140, doi:10.1002/2016JG003475.

Yepez, E. A., T. E. Huxman, D. D. Ignace, N. B. English, J. F. Weltzin, A. E. Castellanos, and D. G. Williams (2005), Dynamics of transpiration and evaporation following a moisture pulse in semiarid grassland: A chamber-based isotope method for partitioning flux components, *Agric. For. Meteorol.*, *132*(3–4), 359–376, doi:10.1016/j.agrformet.2005.09.006.

Zaehle, S., and D. Dalmonech (2011), Carbon-nitrogen interactions on land at global scales: Current understanding in modelling climate biosphere feedbacks, *Curr. Opin. Environ. Sustain.*, *3*(5), 311–320, doi:10.1016/j.cosust.2011.08.008.

Zaehle, S., Medlyn, B. E., De Kauwe, M. G., Walker, A. P., Dietze, M. C., Hickler, T., Luo, Y., Wang, Y. P., El-Masri, B., Thornton, P., Jain, A., Wang, S., Warlind, D., Weng, E., Parton, W., Iversen, C. M., Gallet-Budynek, A., Mccarthy, H., Finzi, A., Hanson, P. J., Prentice, I. C., Oren, R. and Norby, R. J. (2014), Evaluation of 11 terrestrial carbon-nitrogen cycle models against observations from two temperate Free-Air $CO_2$ Enrichment studies, *New Phytol.*, *202*(3), 803–822, doi:10.1111/nph.12697.

Zeppel, M., C. MacInnis-Ng, A. Palmer, D. Taylor, R. Whitley, S. Fuentes, I. Yunusa, M. Williams, and D. Eamus (2008), An analysis of the sensitivity of sap flux to soil and plant variables assessed for an Australian woodland using a soil-plant-atmosphere model, *Funct. Plant Biol.*, *35*(6), 509–520, doi:10.1071/FP08114.

Zhang, L., W. R. Dawes, and G. R. Walker (2001), Response of Mean Annual Evapotranspiration to Vegetationchanges at Catchment Scale, *Water Resour.*, *37*(3), 701–708.

Zhang, L., Z. Hu, J. Fan, D. Zhou, and F. Tang (2014), A meta-analysis of the canopy light extinction coefficient in terrestrial ecosystems, *Front. Earth Sci.*, *8*(4), 599–609, doi:10.1007/s11707-014-0446-7.

Zhou, S., B. Medlyn, S. Sabate, D. Sperlich, and I. C. Prentice (2014), Short-term water stress impacts on stomatal, mesophyll and biochemical limitations to photosynthesis differ consistently among tree species from contrasting climates, *Tree Physiol.*, *34*(10), 1035–1046, doi:10.1093/treephys/tpu072.

Zhou, S., R. A. Duursma, B. E. Medlyn, J. W. G. Kelly, and I. C. Prentice (2013), How should we model plant responses to drought? An analysis of stomatal and non-stomatal responses to water stress, *Agric. For. Meteorol.*, *182–183*, 204–214, doi:10.1016/j.agrformet.2013.05.009.

Zhu, Z., Piao, S., Myneni, R. B., Huang, M., Zeng, Z., Canadell, J. G., Ciais, P., Sitch, S., Friedlingstein, P., Arneth, A., Liu, R., Mao, J., Pan, Y., Peng, S., Peñuelas, J. and Poulter, B. (2016), Greening of the Earth and its drivers, *Nat. Clim. Chang.*, (April), 1–6, doi:10.1038/nclimate3004.